ADVANCED OXYGEN REDUCTION REACTION CATALYSTS/MATERIAL FOR DIRECT METHANOL FUEL CELL (DMFC) APPLICATION

BY

Rapelang Gloria Motsoeneng

Student Number: 2766546

A thesis submitted in fulfilment of the requirements for the degree of Magister Scientiae in the
Department of Chemistry, University of the Western Cape.

Supervisor : Dr L. Khotseng
Co-supervisors : Dr R.M. Modibedi

November 2014

DECLARATION

I declare that "*Advanced oxygen reduction reaction catalysts/material for Direct Methanol Fuel Cell (DMFC) application*" is my own work, that it has not been submitted for any degree or examination in any other university, and that all the sources I have used or quoted have been indicated and acknowledged by complete references.

Rapelang Gloria Motsoeneng November 2014

Signature……..

DEDICATION

I dedicate this work first to God Almighty for his protection, guidance, love and provision throughout my Masters studies and to all my family members, especially my mother, Mrs Motsoeneng, my sisters, Bonolo Motsoeneng, Keiso Motsoeneng and my brothers, Tebello Motsoeneng, Lawrence Thibedi and Teboho Motsoeneng for always believing in me.

"Glory belongs to God, honour to my parents and the privilege was mine"

ACKNOWLEDGEMENTS

- I would like to thank the Lord Jesus Christ for giving me the strength to continue with my work and finish it, because it is all by His grace that managed to be where I am today.

- Greatest thanks to my family and friends for the love, support and encouragement throughout my studies.

- Huge thanks to my supervisors, Supervisor: Dr L. Khotseng and Cosupervisor: Dr R.M Modibedi for equipping/mentoring me to get the knowledge I needed.

- I would also like to pass my gratitude to the staff of the South African Institute for Advanced materials (SAIAMC) and Material Science and Manufacturing (MSM) group at the Centre for Scientific and Industrial Research (CSIR) for giving me the opportunity to conduct my research in the institute.

- Great thanks to NRF, ESKOM and CSIR for fundings.

- Lastly, I would like to thank Dr Cummings for helping me with (Scanning Electron microscopy unit, Department of physics, University of the Western Cape)

PRESENTATIONS AND PUBLICATIONS

The results obtained from this work have been presented in regional and national conferences

Conferences

- R.G.Motsoeneng, L.Khotseng, G.M.Modibedi. Limited redox-replacement reaction for oxygen reduction reaction. 225th ECS Meeting, Orlando, USA, 14 May 2014. Oral presentation.

- R.G.Motsoeneng, L.Khotseng, G.M.Modibedi. Limited redox-replacement reaction for oxygen reduction reaction. CARISMA, Cape Town, 1-3 December 2014. Postal presentation.

Publications

- R.M. Modibedi, M. K. Mathe, E. K. Louwa, K. I. Ozoemena, Lindiwe E. Khotseng, Rapelang G. Motsoeneng, Electro-deposition of Pd on Carbon paper and Ni foam via surface limited redox-replacement reaction for oxygen reduction reaction. *Electrochem Acta*.**128** (2013): p.406-411

ABSTRACT

Fuel cells are widely considered to be efficient and non-polluting power source offering much higher energy density. This study is aimed at developing oxygen reduction reactions (ORR) catalysts with reduced platinum (Pt) loading. In order to achieve this aim, monometallic Pd and Pt nanostructured catalysts were electrodeposited on a substrate (carbon paper) by surface limited redox replacement using electrochemical atomic layer deposition (ECALD) technique. Pd:Pt bimetallic nanocatalysts were also deposited on carbon paper. Pd:Pt ratios were (1:1, 2.1 and 3:1). The prepared mono and bimetallic catalysts were characterized using electrochemical methods for the ORR in acid electrolyte.

The electrochemical characterization of these catalysts includes: Cyclic Voltammetry (CV) and linear sweep voltammetry (LSV). The physical characterization includes: scanning electron microscopy (SEM) and energy dispersive spectroscopy (EDS) for Morphology and elemental composition, respectively.

The deposition of copper (Cu) on carbon paper was done by applying a potential of -0.05 V at 60s, 90s and 120s. 8x cycles of Pt or Pd showed better electrochemical activity towards hydrogen oxidation reaction. Multiples of eight were used in this work to deposit Pt: Pd binary catalyst. Cyclic voltammetry showed high electroactive surface area for Pt24Pd24/Carbon-paper while LSV showed high current density and positive onset potential. HRSEM also displayed small particle size compared to other Pt:Pd ratios.

TABLE OF CONTENTS

LIST OF FIGURES

LIST OF TABLES

LIST OF ABBREVIATIONS

AFC	Alkaline fuel cell
CVD	Chemical vapour deposition
CNT	Carbon nanotubes
CV	Cyclic voltammetry
DMFC	Direct methanol fuel cell
EC-ALD	Electrochemical atomic layer deposition
ECSA	Electrochemical surface area
HRTEM	Higher resolution transmission microscopy
LSV	Linear sweep voltammetry
MCFC	Molten carbonates fuel cell
MOR	Methanol oxidation reaction
ORR	Oxygen reduction reaction
PAFC	Phosphoric acid fuel cell
PEMFC	Proton Exchange Membrane fuel cell
PVD	Physical vapour deposition
RDE	Rotating disk electrode
HRSEM	High resolution scanning electron microscopy
XRD	X-ray diffraction

KEY WORDS

Direct methanol fuel cell

Cathode

Oxidation reduction reactions

Binary catalysts

CHAPTER 1

INTRODUCTION

1.1 BACKGROUND OF THE RESEARCH

The world's ever increasing energy requirements, rapid and continuous depletion of fossil fuels (e.g. coal, oil or any hydrocarbon fuel) along with shocking increase of greenhouse gases concentration have directed large scale research into the development of alternative and greener energy sources. Consequently, due to their very low or zero emission of harmful greenhouse gases (e.g. CO_2, NO_x, SO_x, etc.) fuel cells have generated a lot of interest amongst the scientific and engineering communities [1, 2]. Fuel cells are considered widely to be efficient power source, offering high energy densities and energy efficient compared to other conventional systems. A fuel cell is an electrochemical device that converts the chemical energy of a fuel (e.g. hydrogen, methanol, etc.) and oxidant in the presence of a catalyst into electricity, heat and water [3, 4]. Fuel cells may lead to an innovatory increase in energy production and before long they could become the next world energy resources, because they have a greater impact which is related to the current petroleum and oil markets [5]. Attributes of fuel cell that makes their use more beneficial are as follows:

Quiet operation: Fuel cells, due to their nature of operation, are extremely quiet in operation. This allows fuel cells to be used in residential or built-up areas where the noise pollution is undesirable [6].

Low temperature operation: The fuel cell systems that are suitable for motorized applications, operates at low temperatures. This is one of the key advantages of fuel cells, which is they require slight warm-up time, harmful temperature is reduced, and the thermodynamic efficiency of the electrochemical reaction is fundamentally better that of conventional combustion-based technologies.

Environmentally friendly: due to low emission of harmful greenhouse gases, the imagined use of fuel cells in the automobile industry can replace the use of combustion

engines. They can be used for electricity provision to the rural areas without a connection to a national electricity supply [7-9].

High power densities: A high power density allows fuel cells to be relatively solid source of electric power beneficial in application with space restrictions. The power is generated at a distant location using an electrical transmission & distribution (T&D) infrastructure to deliver the power to the end user [9].

Highly efficient: Unlike thermal engines, which uses combustion to generate electricity, fuel cell uses less fuel to produce the same amount of electricity. Thus showing a high efficiency that does not drop as the power plant decreases [10].

Safety: Fuel cell is very safe because it uses hydrogen (H_2) as the fuel. Hydrogen is a safe fuel as long the safety precautions are followed.

Clean energy: Pure hydrogen and oxygen are used in fuel cells and this produces water as a by-product. The carbon dioxide that is produced in some fuel cells can be readily recaptured in order to prevent it from being emitted into the atmosphere [10].

1.2 RATIONALE TO THE RESEARCH

Among liquid fuels direct methanol fuel cell (DMFC), is found to have a large number of advantages and has considerately brought attention for portable application. Liquid fuel is considered to be more essential due to the fact that it is easy to be stored and transported. Furthermore, liquid fuel has less safety concerns and fairly small investment needed for placing the relevant support infrastructure. Although DMFC has many advantages, methanol crossover from the anode to the cathode is one of the key challenges. This challenge can be conquered by developing the cathode catalysts that cannot be easily corroded in the presence of methanol [11].

Many studies are being made for more active electrocatalysts and ways to enhance the distribution of such catalysts. Pt is known as one of the best ORR catalyst, but its high costs in the market resulted in a broad research for substituting it with other noble metals. Furthermore, studies showed that Ru-based catalysts have some promising properties, which are high activity for oxygen reduction reactions and high methanol tolerant [12-14]. However, another possible candidate to substitute platinum (Pt) is palladium (Pd) [5].

Palladium has a four-electron pathway for the oxygen reduction reaction and it is considered as a cathode catalyst because of its high activity towards oxygen reduction in a direct methanol fuel cell [7-9].

For methanol crossover reduction, development of new proton conducting polymers and modification of Nafion membranes have been considered. Therefore, great research is done on development of high methanol tolerance and low catalyst content as well as the alternatives for electrocatalyst with high oxygen reduction reaction activity [15, 16]. These catalysts can be achieved by using materials with high surface area e.g. nanocomposite, as supports for the catalyst metal. Normally the supports materials for these catalysts are regularly carbon black such as Vulcan XC 72, carbon film and carbon nanotubes, which are relatively new types of support material that poses high quality and improve catalysts properties.

Developing fuel cells and electrolysers that maintain their performance is still a challenge, although they are more affordable. High costs are due to membranes required for their operation as well as the expensive electrocatalysts. Reducing material costs is very important for future commercialization of fuel cell technologies; hence the research focus is in development of electrocatalysts that will increase the slow kinetics in the cathode electrode [16]. To lower the costs and increase the performance, eletrocatalysts particle sizes are reduced to the nanoscale (10^{-9}) in order to enhance their electroactive surface area. Wide research has focused on development of high performance nanophase electrocatalysts to advance the efficiency of fuel cells. To further increase the activity of the catalyst, important physical and chemical properties of nanophase electrocatalysts need to be identified and characterised. Basically, the characterization of nanophase electrocatalyst plays the major role in identifying the importance of the methods used to prepare the catalyst.

1.3 RESEARCH PROBLEM STATEMENT

During the previous years, chemical deposition techniques have played an extremely important role in the design and manufacture of new advanced devices. Physical deposition techniques, such as molecular beam epitaxy (MBE), physical vapour deposition (PVD) or

sputtering, have been used for these applications [17]. However, they suffer from limitation such as poor conformality, low throughput, restricted directional variation, and reduced compositional control. All of these issues can and have been addressed using electrochemical atomic layer deposition techniques (ECALD) which offer additional advantages such as: ambient temperature, use of a small precursor solution, and an increase in potential. ECALD also offers atomic layer control, which is fundamental for controlled growth processes [17-20].

1.4 OBJECTIVES OF THE STUDY

The study is aimed at advancing the oxygen reduction reaction catalysts/ material for direct methanol fuel cell applications. The objectives of the study are as follows:

- Determine the deposition potential of copper on carbon paper (gas diffusion layer – GDL - used in fuel cells) using cyclic voltammetry.

- Synthesize the monometallic and bimetallic catalyst nanoparticles on carbon paper using electrochemical atomic layer deposition (ECALD) technique with copper as a sacrificial metal.

- Determine the electrochemical activity of the prepared catalyst towards the oxygen reduction reaction (ORR) in acid electrolyte.

- Investigate the methanol tolerance of the nanocatalyst in acid electrolyte in the presence of oxygen

- Study the morphological structure of the catalyst on carbon paper utilizing Scanning Electrode Microscopy (SEM) coupled to Energy Dispersive X-ray spectroscopy (EDX).

- Prepare bimetallic catalyst nanoparticles on carbon paper and determine the electrochemical activity of the prepared catalyst towards ORR in acid electrolyte, using EC-ALD technique at the CSIR.

1.5 FRAME WORK OF THE STUDY

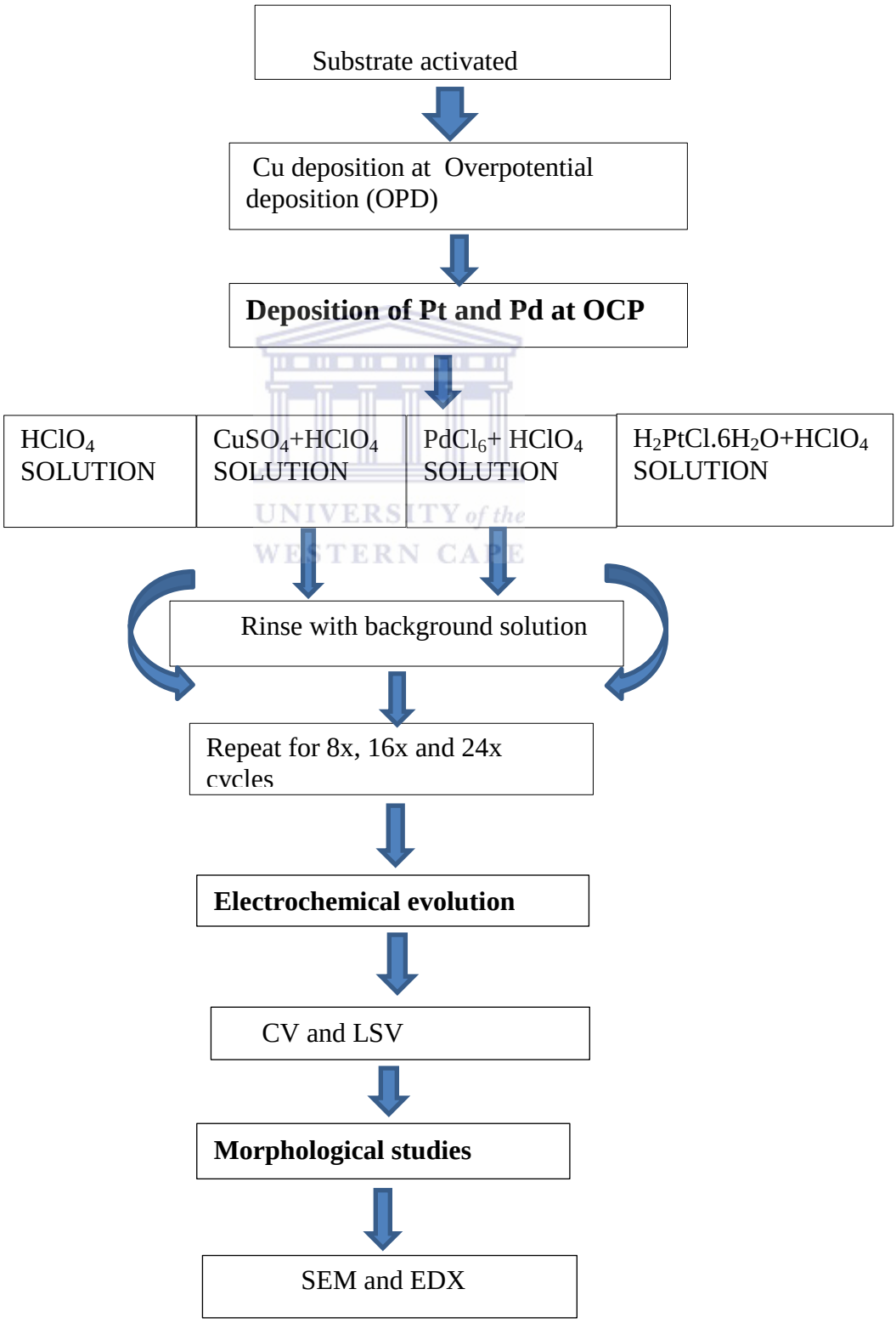

1.6 RESEARCH OUTLINE

Chapter 1: Introduction

In chapter 1, the introductions to fuel cell and the attributes of fuel cells are discussed.

Chapter 2: Literature review -background

This chapter discuss the detailed summary of fuel cells as well as the various types of fuel cells. The oxygen reduction reaction and various deposition methods that are used in fuel cells are explained.

Chapter 3: Methodology

Chapter 3 describes the chemicals that were used, preparation methods and techniques that were used throughout this study. Short basic information about the characterization techniques used in the study follows after the introduction to the chapter.

Chapter 4: Results and Discussion

The Physical and electrochemical Characterization of the used electrocatalysts will be shown and discussed.

Chapter 5: Conclusion and Recommendations

The ultimate conclusion on the ideal method for preparation of the best active catalyst drawn from the results acquired during characterization after comparing all the material and the properties are stated in this chapter. Future recommendations are also described in this chapter.

CHAPTER 2

LITERATURE REVIEW

2.1 THE OVERVIEW OF FUEL CELLS

Fuel cell was initially discovered in 1939 by a Welsh physicist, Sir William Grove [21]. He revealed that when immersing two ends of platinum electrodes in sulphuric acid and each of the ends be placed in two isolated containers containing oxygen and hydrogen, a constant current flow would result. This led to an invention of what is called a battery. Consequently, several innovations in fuel cell technologies have taken this study further and there have been major developments when comparing the current status with the previous years. Fuel cells, convert the chemical energy of fuel and oxidant, in the presence of a catalyst, to electrical energy. Fuel cells are similar to batteries in many aspects except that the fuel and oxidant are continually fed in the devise's electrode and that the electrodes do not undergo chemical changes [22].

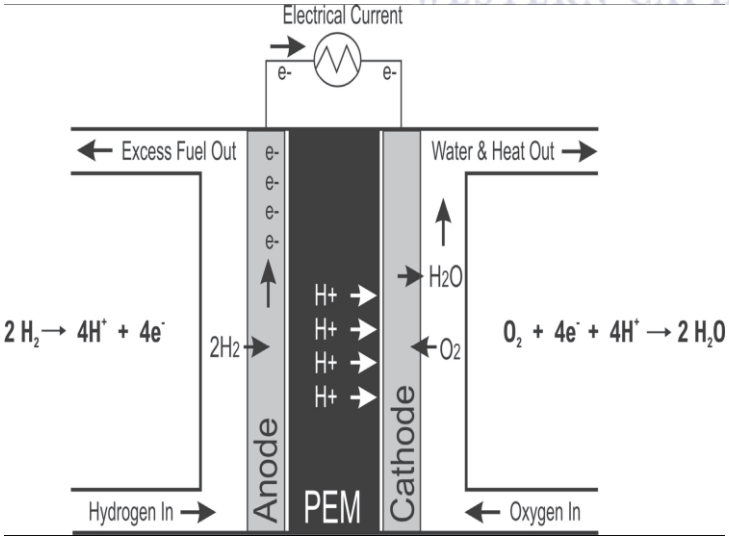

Figure 2.1: Shows the schematic diagram of a basic fuel cell [22].

The above diagram (figure 2.1) demonstrates the general functioning principle of a basic fuel cell. In its simplest form, a single fuel cell consists of two electrodes, an anode and a

cathode, with an electrolyte between them. At the anode, hydrogen splits, creating a positively charged ion and a negatively charged electron. The proton passes through the electrolyte, while the electron travels through a circuit, creating a current. At the cathode, oxygen reacts with the hydrogen (H) ion and electron, forming water and useful heat [23].

The main characteristic of a fuel cell is its ability to convert chemical energy directly into electrical energy giving much higher conversion efficiency than any other conversional thermo-mechanical systems. Thus extracting more electricity from the same amount of fuel, operates without combustion so they are almost pollution free and have quiet operation since there are no moving parts [23, 24].

The figure 2.2 below shows a simple energy conversion in fuel cells versus the combustion engines. In combustion engines, fuel is burned inside the engine to ignite it to mechanical energy then to electrical energy, whereas chemical energy in fuel cells is directly converted to electrical energy [25].

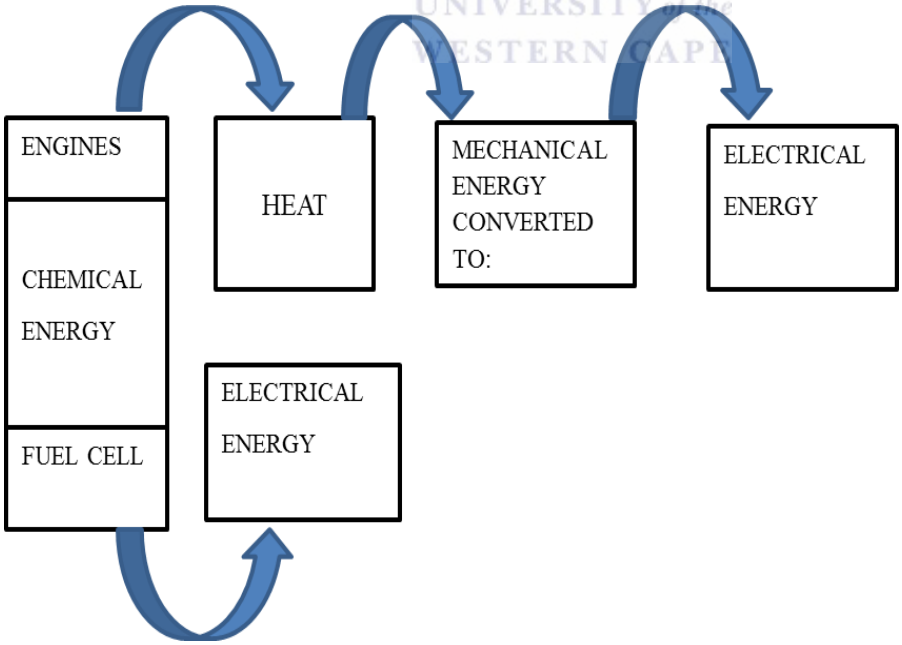

Figure 2.2: Energy conversion routes corresponding to combustion engines and fuel cell.

2.2 COMPONENTS OF FUEL CELL

Since fuel cell consists of two electrodes i.e. anode and cathode, electrolyte and catalyst, each part is very important and independent on the other. The main function of the electrode is to bring about reaction between the reactants (fuel or oxygen) without itself being used up or corroded. It must also bring into contact the three phase i.e. gaseous fuel, liquid and solid electrode and the electrode itself. The anode, used as the negative post of the fuel cell, separates the hydrogen gas equally over the whole surface of the catalyst and conducts the electrons that are freed from hydrogen molecule, to be used as a useful power in an external circuit. The cathode, the positive post of the fuel cell, distributes the oxygen fed to it onto the surface of the catalyst and conducts the electrons back from the external circuit where they can recombine with hydrogen ions, passed across the electrolyte and oxygen to form water [26].

2.3 DIFFERENT TYPES OF FUEL CELLS

There are several types of fuel cell technologies that have been developed for different applications. All these fuel cells have an amount of interest in terms of research throughout the world. They are divided into high temperature fuel cell system (molten carbonate fuel cell (MCFC), phosphoric acid fuel cell (PAFC), and solid oxide fuel cell (SOFC) and low temperature fuel cell system (alkaline fuel cell (AFC), proton exchange membrane (PEM) fuel cell, direct methanol fuel cell (DMFC). A number of these fuel cell types are commercially available today. These types of fuel cells are classified by the various types of electrolyte; temperature, catalysts and fuel as shown in Table 2.1. This causes the ineffectiveness of the internal energy to be reduced to the lowest standards to ensure that the electrodes are not over-powered [27, 28].

Table 2.1: Types of fuel cells and their technical characteristics [29].

Types	Electrolyte	Operating T (°C)	Fuel
Alkaline (AFC)	Potassium hydroxide (KOH)	50-200	Pure hydrogen or hydrazine
Direct methanol (DMFC)	Polymer	60-200	Liquid methanol
Phosphoric acid (SAFC)	Phosphoric acid	160-210	Hydrogen from hydrocarbons and alcohol
Proton-exchange membrane (PEMFC)	Polymer, PEM	50-80	Less pure hydrogen from hydrocarbons or methanol
Molten carbonate (MCFC)	Carbonates, nitrate and sulphate	630-650	Hydrogen, carbon monoxide, natural gas,propane,marine diesel
Solid oxide (SOFC)	Stabilized zirconia and doped perovskite	600-1000	Natural gas or propane

2.3.1 High temperature fuel cells

Phosphoric fuel cell (PAFC): PAFC operates under high temperature and a concentrated phosphoric acid (approximately 100%) is used as an electrolyte [30]. This fuel cell is mostly used for stationary power generation, but some have been applied in large vehicles such as city buses and trucks. It is said to be the first fuel cell to be commercially available.

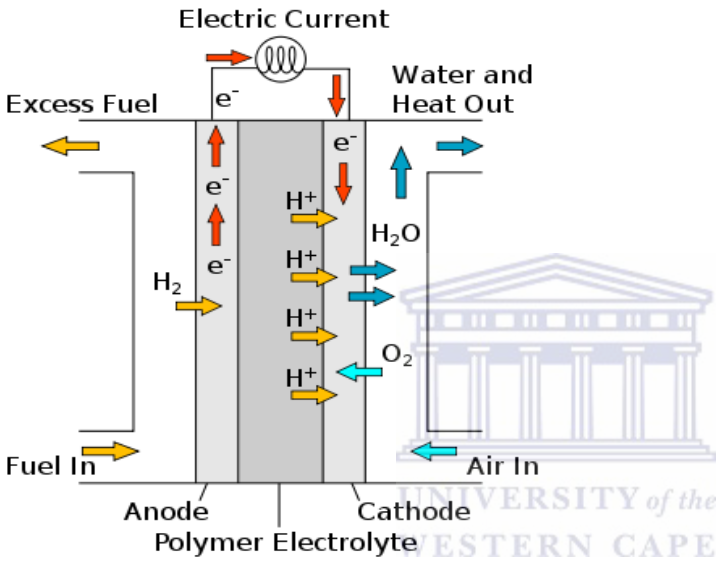

Figure 2.3: Principle operation of Phosphoric Acid Fuel Cell [42].

The figure 2.3 above shows a basis operation of a phosphoric fuel cell. PAFC consists of a pair of porous electrodes (the fuel electrode and air electrode) formed from mainly carbon material, between which an electrolyte layer consisting of a matrix filled with highly concentrated phosphoric acid solution is placed. The catalytic layer of the electrodes where reactions take place consists of the carbon material and metal catalyst particles [31]. The PAFC does not suffer from carbon dioxide-induced electrolyte degeneration seen in other types of fuel cells, and so can use reformed gas derived from fossil fuels, though expensive platinum catalyst is necessary in order to promote the electrode reactions. Thus it can make use of city gas (natural gas-based) and other existing fuel infrastructure. However, when CO exists at high concentrations, as in coal-gasified gas, the platinum catalyst used in electrodes is poisoned, leading to a decrease in performance. Therefore the use of such fuels is impractical without effective means of eliminating CO. [32].

Solid Oxide Fuel Cell (SOFC): Solid oxide fuel cells are fuel cells that are primarily made up of ceramic materials. The cell is made with two porous electrodes that sandwich an electrolyte (figure. 2.4). At the cathode side, oxygen molecules combine with electrons from the anode and become oxygen ions at the cathode. SOFC operates under high temperature, usually from 600 to 1000 °C, which allows the electrolyte (typically made of yttria-stablized- zirconia) to function as an ionic conductor to transport oxygen ions from the cathode to the anode. This high temperature allows SOFC to reform fossil fuels into hydrogen (H) and carbon monoxide (CO) gases in order to oxidise them at the anode. At the anode side, the gaseous fuel is oxidized by oxygen ions and refers the electrons to the external circuit [33].

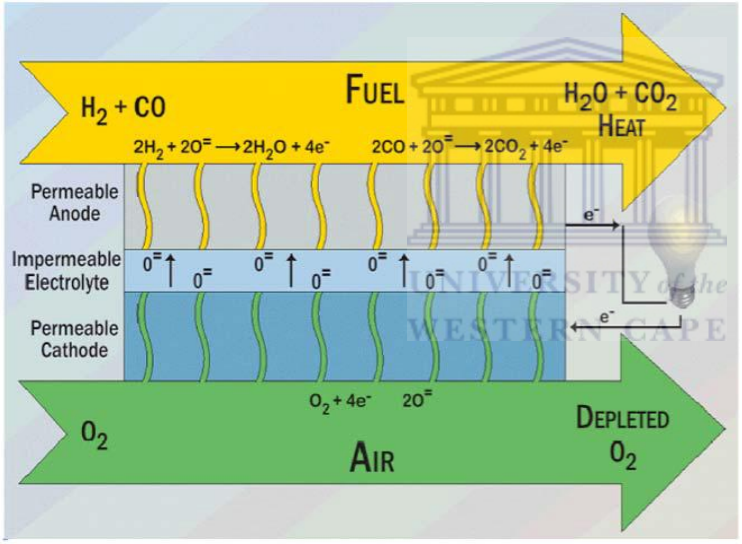

Figure 2.4: The standard functioning of a solid oxide fuel cell (SOFC) [33].

At both electrodes, the reactions take place at a triple-phase boundary (TPB) where an electronic conductor, ionic conductor, and the gas phase meet. The products of the anode reaction include water, carbon dioxide, heat, and electrons. The electrons transport through the external circuit to produce electricity. The disadvantage of this fuel cell is the high temperature that is used to operate it. The cell takes time to start up and reach operation temperature; it must be strongly constructed, and be shielded to prevent heat lost [34].

2.3.2 Low temperature fuel cell

Alkaline fuel cell AFC: AFC are amongst the most matured and low temperature ($23^{o}C$-$70^{o}C$) operating fuel cell technologies. They have been used since the mid 1960's by national aeronautics and space administration (NASA) in the Apollo and space shuttle programs [35-37]. AFC are typically defined according to the substance used as an electrolyte. Alkaline fuel cell uses an alkaline electrolyte. This fuel cell consists of two electrodes separated by a liquid, alkaline based electrolyte (typically KOH) [38, 39].

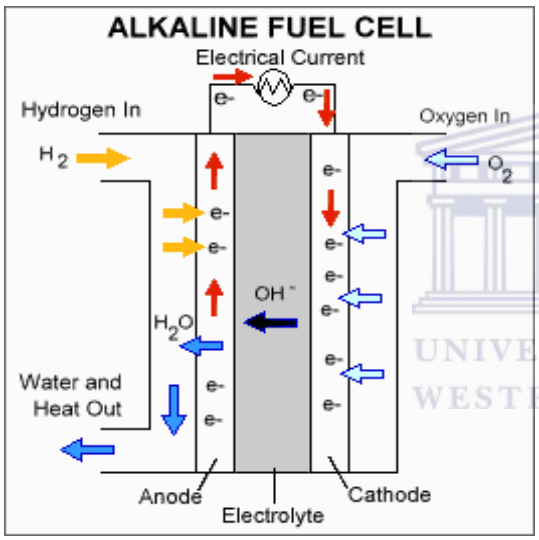

Figure 2.5: Schematic diagram of an alkaline fuel cell [37]

In an alkaline fuel cell, the electrodes perform the most important and demanding task. At both electrodes, a triple phase boundary forms, which is a curve in three dimension where the gas (fuel or oxidant), liquid and solid catalyst assemble as shown in figure 2.5. This is the place where the electrochemical reactions occur. In order for the reactions to be sustainable, the reactant gases and the reaction products require to be transported to and from the reaction sites and an electrical connection must be present through which the electric charges can be transported [39]. This is commonly achieved by using a gas diffusion layer (GDL) which is porous, hydrophobicity and electrically conductive. The hydrophobicity ensures that the liquid electrolyte does not flood the gas diffusion paths.

Mechanical support of the fuel cell is usually achieved using nickel material which is resistant to corrosion by the alkaline electrolyte [40, 41]. However, a major disadvantage of AFCs is that alkaline electrolytes, such as sodium hydroxide (NaOH) or potassium hydroxide (KOH), turn to react with CO_2 to precipitate carbonates. The other limitation of AFC is that, their electrolyte is retained in asbestos conditions, which is harmful for human health [41].

Anion Exchange Membrane Fuel Cell

Anion exchange membrane fuel cells (AEMFCs) are a type of alkaline fuel cell which operate at 90^0C and are currently bringing a renewed attention. The AEMFC functions the same way as alkaline fuel cell, the difference being AEMFC uses a solid polymer electrolyte. In an AEMFC, the fuel (hydrogen or methanol) is supplied at the anode and oxygen through air and water are supplied at cathode. Fuel is oxidized at anode and oxygen is reduced at cathode. At cathode, oxygen reduction produces hydroxides ions (OH-) or carbonate ions that migrate through the electrolyte towards the anode. At anode, hydroxide ions react with the fuel to produce water and electrons. Electrons go through the circuit producing current. The challenge of this type of fuel cell is achieving OH^- ion conductivity comparable to H^+ conductivity observed in PEMFCs [42].

The electrochemical reactions when hydrogen is the fuel

Anode: $2H_2 + 4OH^- \rightarrow 4H_2O + 4e^-$ (1)

Cathode: $O_2 + 2H_2O + 4e^- \rightarrow 4OH$

The electrochemical reactions when methanol is the fuel

Anode: $CH_3OH + 6OH^- \rightarrow CO_2 + 5H_2O + 6e$- (2) [42]

Cathode: $3/2O_2 + 3H_2O + 6e^- \rightarrow 6OH^-$

The most important advantage of AEMFCs is that under alkaline conditions, electrode reaction kinetics are much more facile, allowing use of low-cost, non-noble metal catalysts such as nickel for the fuel electrode and silver, etc. for the cathode. Corrosion problems are

also greatly reduced under alkaline conditions. Methanol has an advantage of being easy to store, transport and has higher energy density compared to hydrogen. Also, methanol crossover from anode to cathode is reduced in AEMFCs compared to PEMFCs, due to the opposite direction of ion passing through the membrane from cathode to anode. In addition, use of higher alcohols such as ethanol and propanol is possible in AEMFCs, since anode potential in AEMFCs is sufficient to oxidize C-C bonds present in alcohols [43, 44]. The biggest challenge of AEMFCs is to fabricate anion exchange membranes (AEM) with high OH- ion conductivity and mechanical stability without chemical corrosion at raised pH and temperatures [45].

Proton exchange membrane fuel cell (PEMFC): PEMFC, which is also known as the polymer electrolyte membrane is a type of a fuel cell that uses a stable polymeric electrolyte, in which water dissolves, but itself is not soluble in water [46].

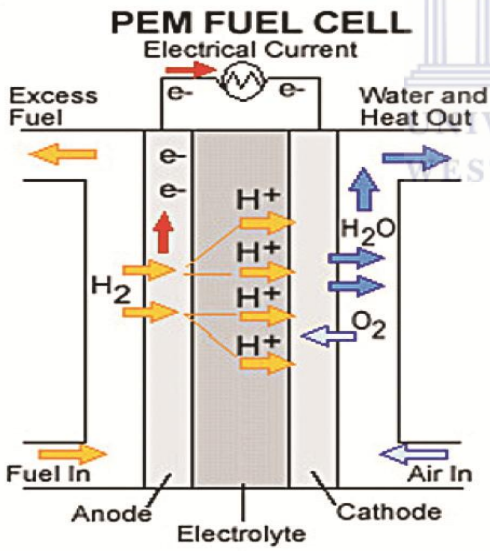

Figure 2.6: Schematic diagram for Proton exchange membrane fuel cell [42]

Anode: $H \rightarrow 2H + 2e^-$ (3)

Cathode: $1/2O_2 + 2H + 2e^- \rightarrow H_2O$

Overall: $H_2 + 1/2O_2 \rightarrow H_2O$

In this fuel cell, the anode electrode is catalytically separated into protons and electrons. The proton passes through the selective permeable membrane whereas the electrons are passed through an external circuit, which is representing the current. On that same movement, after passing through the membrane the protons become reduced in the presence of oxygen at the cathode end to form water. PEMFC operates silently and under low temperatures (80^{o}C). Fuel cell temperature above 100^{o} C is a highly desirable goal [47, 48]. The CO which is produced from hydrocarbon reforming process is a poison factor in PEMFC. It adsorbs at Pt surface and blocks the access of new reactant molecules to the surface active centres. Thus, CO is a severe poison to Pt catalyst in PEM fuel cells [49, 50].

Direct methanol fuel cell: DMFC is a fuel cell that operates directly on methanol without having to convert those fuels to hydrogen gas. The system has been widely proposed since the early 1990s as a replacement for batteries in civilian or military portable power applications [41].The direct methanol fuel cell has several advantages that make it more suitable for applications: it removes the requirement for fuel reforming, it is a simpler system designed with the potential for low capacity and lightweight packaging. These advantages allow DMFCs to be improved for use in portable electronic devices such as cell phones, laptops and cameras [51]. Equation (4) describes anodic and cathodic reactions occurring in a direct methanol fuel cell.

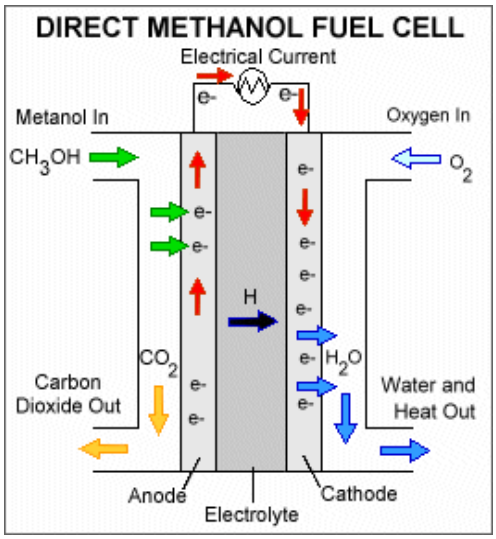

Figure 2.7: The schematic diagram of a direct methanol fuel cell [42].

Anode reaction is $CH_3OH + H_2O \rightarrow CO_2 + 6H^+ + 6e^-$ (4)

Cathode reaction is $1.5O_2 + 6H^+ + 6e^- \rightarrow 3H_2O$

Reaction Formula is $CH_3OH + 1.5O_2 \rightarrow CO_2 + 2H_2O$

DMFC consists of two catalytic electrodes where the methanol oxidation at the anode and the oxygen reduction at the cathode are separated by a membrane, which conducts the proton from the anode to the cathode. The practical term for these polymer electrolyte membrane (PEM) used in DMFCs today is Nafion^{TM}. The methanol that is fed at the anode side passes through the diffusion layer to the catalytic layer where it is electrochemically oxidised into mostly carbon dioxide, protons and electrons. The protons that are formed during this reaction diffuse through the membrane to the cathode catalytic layer. They participate in oxygen reduction to form excess water at the cathode side [51].

DMFC challenges

The major challenges that are facing this fuel cell are the cost of Pt catalyst and methanol cross over. PtRu catalyst in DMFC is used at the anode and Pt on the cathode side to speed up the slow reaction electrokinetics without itself being consumed. On the other hand, methanol cross over is the permeation of methanol from the anode through the electrolyte membrane to the cathode compartment where the fed oxygen turns to react with methanol to form methanol oxidation reaction (MOR). This depresses cathode performance and reduces fuel efficiency [52, 53]. The schematic diagram in figure 2.8 below shows a methanol crossover.

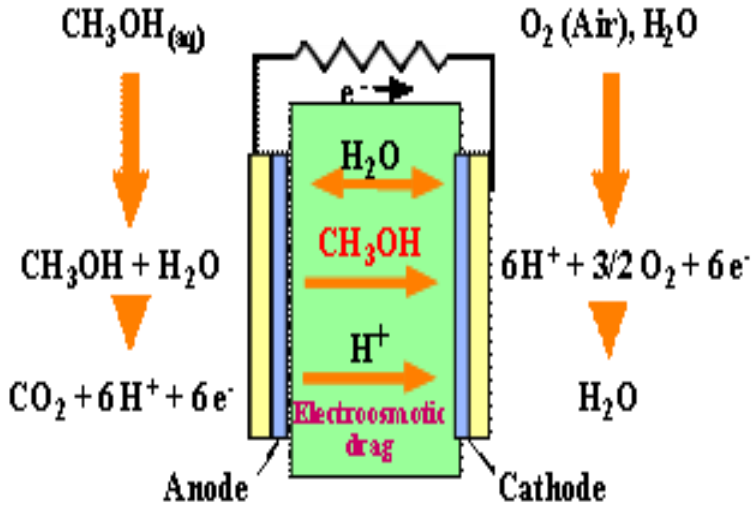

Figure 2.8: The schematic diagram of the methanol crossover [53].

The crossover reactions at the cathode is given as

$$CH_3OH + 3/2\ O_2 \rightarrow CO_2 + 3H_2O \quad (5)$$

To avoid mixed potentials in the cathode electrode, caused by the simultaneous methanol oxidation and oxygen reduction reactions taking place, a possible solution would be using a selective cathode electrocatalyst for the oxygen reduction reaction. Previous studies showed that precious metals have some promising properties, which have reasonably high activity for oxygen reduction and high methanol tolerance [54-56].

2.4 KINETICS IN DIRECT METHANOL FUEL CELLS

2.4.1 Oxygen reduction reactions (ORR)

Oxygen in the Earth's crust is the most excessive element. The oxygen reduction reaction (ORR) is the most significant reaction in life processes such as, energy converting systems in fuel cells [57-59]. There are two processes in ORR that involve parallel reaction pathways in acid medium. A direct four-electron reaction path way in which O_2 reduced to water is given in figure 2.9:

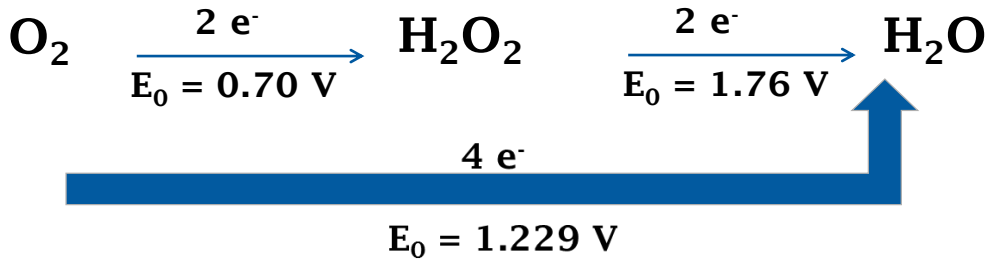

Figure 2.9: The 4e$^-$ free pathways for fuel cell application [44].

The mechanism shown in figure 2.9 indicated that O_2 can be reduced either directly to water (direct four-electron reduction) electrochemically with the standard potential (E_0) of 1.229 V or to adsorb hydrogen peroxide (H_2O_2) with the standard potential (E_0) of 0.70V. The H_2O_2 can be further reduced to water with E_0= 2.76 V. This ORR mechanism has also been investigated on Pt by theoretical calculation based on the electronic structure, using density functional theory [60-62].

In direct methanol fuel cell (DMFC) and proton exchange membrane (PEM), ORR occurs at the cathode. Normally, the ORR kinetics is very slow. In order to speed up the ORR kinetics for a better working level in a fuel cell, a cathode ORR catalysts with a high performance is needed. Currently in technology, Pt-based material is the most applied catalysts [59]. Research over the past several years has focused on developing alternative catalysts in order to control the cross over problem and to reduce the amount of Pt that is used, by developing binary catalysts. These electrocatalysts include noble metals and alloys, carbon material, transition metal chalcogenides and transition metal carbides [58, 59]. The present study focuses on O_2 reduction reaction and various ways of deposition methods in order to increase the catalyst performance.

2.4.2 Methanol oxidation reactions (MOR)

DMFC liquid methanol is the most promising and preferable fuel cell than gaseous hydrogen, due to its advantages such as fuel storage, transportation and cost effective. In DMFC, the methanol oxidation reaction (MOR) occurs at the anode electrode producing the protons and electrons and the kinetic reaction is slow. Even using Pt as a catalyst, MOR is still much slower [52, 53].

$$CH_3OH \rightarrow Pt - CH_3OH_{ads} \quad (6)$$

$$Pt\text{-}CH_3OH_{ads} \rightarrow Pt\text{-}CO_{ads} + 4H^+ + 4e^-$$

$$M + H_2O \rightarrow M\text{-}H_2O_{ads} \quad (7)$$

$$M\text{-}H_2O_{ads} \rightarrow M\text{-}OH_{ads} + H^+ + e^-$$

$$Pt\text{-}CO_{ads} + M\text{-}OH \rightarrow Pt + M + CO_2 + H^+ + e^-$$

Methanol is electrochemically oxidised on the Pt surface at the anode producing carbon monoxide (CO) which is a by-product of the methanol oxidation reaction. The intermediate of MOR including CO easily poisons the Pt active sites causing large anode overpotential and the sluggish kinetics [54-56]. This can be solved by developing a catalyst that can easily form M $(OH)_{ads}$ (M being the metal) species at a low electrode potential oxidising the CO to carbon dioxide (CO_2). This resulted to a great amount of research towards the study of Pt-Ru alloy, in which Pt-Ru/C has been reported as the best binary catalyst towards methanol oxidation [53].

2.5 CATALYST

Figure 2.10 show that unanalyzed reactions require higher activation energy than catalyst reactions. Catalysts are classified in two different ways: heterogeneous and homogeneous catalyst. In heterogeneous catalyst, both catalyst and reactants are in different phases (e.g. a mixture of oil and water); while in homogeneous catalyst the reactants and the catalyst are in the same phase [63, 64]. A catalyst is the most essential component in fuel cells. Basically a catalyst is a substance that participates in electrochemical reactions to modify and speed up the rate of reaction without itself being consumed. It also provides a different pathway to the electrochemical reaction with less activation energy [63].

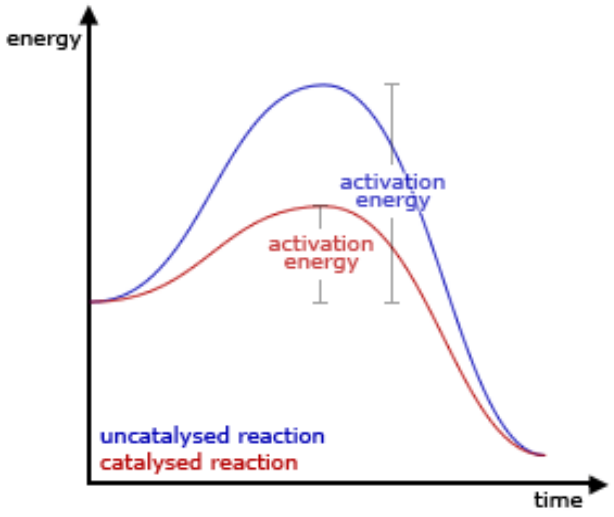

Figure 2.10: Diagram displaying the activation energy with and without a catalyst.

The performance of a fuel cell depends strongly on the activity of the anode and cathode catalysts [64]. The anode catalyst is usually used to oxidise the methanol fuel, while the cathode catalyst is used to reduce oxygen to water. All catalysts function by the same general principle, that is, the activation energy of the rate-determining step must be lowered in order for an increase in the rate or reaction to occur [24].

2.5.1 ORR catalyst for DMFC

In DMFC, the ORR catalyst material must be stable under the extremely corrosive conditions yet chemically active enough to be able to activate O_2. The main characteristics that are important for ORR catalyst in DMFC are:

Activity: the catalyst must adsorb species with enough strength to allow chemical bonds to break but be weak enough to release the product when the reaction has occurred. If the binding between the metal and oxygen is too weak, the substrate will not be able to adsorb well on the catalyst and that will result in a slow reaction or the reaction will not take place at all; if the binding interaction is too strong, the catalytic surface will quickly become blocked by the substrate, intermediate or product and the reaction will stop. The Sabatier principle describes the model of interaction between the substrate and catalyst [65]. *Balandin volcano's plot* which is shown in figure 2.11 also illustrates the principle of binding between a single O atom and various metals [66].

Selectivity: The catalyst must progress the reaction to make the desired product whereas it is minimizing the production of unwanted intermediates and side products. The ORR reactions at the cathode can follow one or two pathways and the adsorption of O_2 (first step) is determined by the selectivity of the catalyst [67].

Stability: For any metal to be suitable as a fuel cell electrocatalyst, it must not only have appropriate catalytic activity and selectivity, but it must also be able to tolerate the harsh chemical environment within a fuel cell. The presence of strong oxidants, extreme re-activities, low pH, and rapid potential fluctuations, especially on the cathode, rules out the use of most transition metals in their pure forms [68].

Poisoning resistance: A good catalyst must be resistant to poisoning by impurities likely to be found in the fuel cell itself an in the feed gases. Impurities in both the methanol and the air streams may have a negative impact upon the workings of a DMFC. All catalysts are susceptible to poisoning but there are so many different poisons and poisoning mechanisms that it is very difficult to make any meaningful complete ranking [69].

DMFC has been dependent on Pt based electrocatalyst as seen in figure 2.11. However, Pd is a promising candidate to substitute Pt. Pd like Pt, has a four-electron pathway for oxygen reduction reactions (ORR), although its ORR activity in acid medium is surpassed by Pt [69, 70]. Extensive research have been made and several groups have reported the increased activity of Pd-Pt catalyst towards selective ORR compared to pure Pt in the presence of methanol [71-73]. Therefore, Pd is considered as one of the best candidates for cathode catalyst, due to its high activity towards oxygen reduction in DMFCs [71].

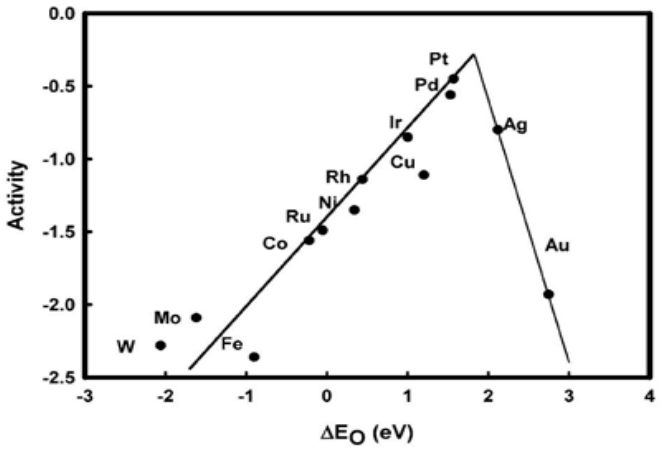

Figure 2.11: Oxygen reduction activity on various transition metal electrodes as a function of the oxygen binding energy from density functional theory (DFT) calculations [44].

2.5.2 Binary catalysts as cathode electrocatalysts for DMFC

The poisoning of the cathode electrode due to the crossover problem reduce the performance of fuel cell. This problem may be solved by using electrolytes (i.e. Polymer membrane) with lower methanol permeability or by developing new cathode electrocatalysts with high methanol tolerance and higher activity for oxygen reduction than pure platinum. One of the studies investigated the activity of Pt alloys towards oxygen reduction in the presence of methanol and used them as direct methanol fuel cell cathode catalysts [74, 75].

Many studies showed that Pt is the most active ORR catalyst for DMFC but it is limited by the costs hence there is a desire to develop less Pt ORR catalysts. One of the best methods to lower the use of Pt is alloying it with low costs metals without compromising the fuel cell performance [76]. *Tsivadze et al* [77] described the catalysts that are insufficiently tolerant to alcohols and enhanced their activity by using them with phosphorus and sulphur to improve methanol tolerance. These electrocatalyst are termed improved binary catalysts. A lot of research has been done on Pt binary catalysts and they have been found to give improved catalytic activity [78]. Several metals including; Ru, Pt, Ag, Ir, Rh, Au, Re, Os as well as Co have been discovered to be used as binary catalysts [79].

Previous studies showed that Ru has some promising properties that are the strong physicochemical interaction between the catalysts particles and the other metal generates a bi-functional mechanism for catalyst reaction that improves the reaction kinetics. For an example, when Pt is combined with ruthenium (Ru) to form an alloy catalyst, the activity of the alloy catalyst towards methanol or the oxidation of carbon monoxide (CO) becomes faster. This resulted to a great amount of research towards the study of Pt-Ru alloy, in which Pt-Ru/C has been reported as the best binary catalyst towards methanol oxidation since from 1990's [80-82]. However, current reports have shown palladium (Pd) as a possible candidate for ORR catalysts because it has lower reactivity towards methanol oxidation [83].

The ORR of Pt, Pd and Pd alloys in the presence of methanol was studied by *Lee et al* [70]. They found that Pt electrode showed large anodic current above 0.75V versus NHE due to methanol oxidation. This methanol oxidation led to an onset potential of 200mV lower that that observed without methanol in the electrolyte, which was credited to the formation of a mixed potential on the Pt surface. A lot of research have been made with regards to the improved activity of Pd_XPt_X binary catalyst towards the ORR compared to pure Pt in the presence of methanol [71-73]. *Wang at al* [84] studied the carbon supported Pd-Pt alloy electrocatalysts of different Pd/Pt atomic ratios. They found that the Pd-Pt/C catalysts showed much higher ORR activity than Pt/C in the presence of methanol.

2.6 COMPLEXING AGENT

Complexing agents are mostly used to reduce the free ions activity and allow the exchange rate relative to the solution introduction, which advances the deposit uniformity. In the previous studies citrate was used as a complexing agent, the same principle was applied in the study of Pd [86, 87], where ethylenediamine tetraacetic acid (EDTA) was used to form Pd^{2+} ions. Those Pd showed enhanced uniformity, but at the expense of two-third of their thickness. The majority Pd^{2+} ions Currently, the studies describe the use of Cl^- ions as an substitute complexing agent for Pt^{2+} through ECALD formation of Pd nanofilms via surface limited redox reactions (SLRR).

2.7 SUPPORT MATERIALS USED IN DMFC

Support materials play a significant role on the performances of electrocatalysts for fuel cells. A great amount of research has been done to lower the electrocatalyst cost in order to commercialize fuel cells. The aim is to develop supports that will be able to increase the electro conductivity, activate the metal particles, improve the electrocatalyst dispersion and enhance the stability of the electrocatalyst [88]. A support material is supposed to have a high surface area to improve the catalytic dispersion, be thermal and electrical conductive, should be adequately chemically or electrochemically stable in the electrolyte conditions and should be porous enough to allow the reactants to flow in order to be considered as a support material for a fuel cell electrocatalyst [89]. The support materials used include; calcium carbonate ($CaCo_3$), metal oxide such as alumina (Al_2O_3), porous carbon black (Vulcan XC-72) [90, 91] and carbon nanotubes (CNTs) [88, 92& 93]. Carbon nanotubes and carbon black possess better support properties hence are considered as the best electrocatalyst supports [94].

2.7.1 Carbon black

There are various types of carbon blacks, such as Acetylene black, Vulcan XC-72, and Ketjen black. The physical and chemical properties, such as specific surface area, electrical conductivity, porosity and surface functionality are reported to have an effect on the performance of the carbon black supported catalysts but the parameter that has a major effect on the catalytic performance is the specific surface area [95, 96]. The Carbon blacks are now commercially available at low costs. Pt or other Pt based alloy electro-catalysts are prepared by using Vulcan XC-72 carbon black as support. It was reported that the pre-treatment of the carbon black before preparing the catalyst can enhance the catalytic performance [97-103].

Figure 2.12: A picture of carbon Black support material [104].

In current studies the catalytic performance was associated with the surface area of the supporting materials and the size of the active metal. There are some disadvantages concerning the use of Vulcan XC-72 carbon. Carbon black have pores which are too small to be filled by the electrolyte polymer therefore, many Pt particles are trapped in the microspores of the carbon black that are not involved in the electrochemical reactions on electrodes due to the absence of the triple-phase boundaries (gas-electrolyte-electrode) [105-112].

2.8 CATALYST PREPARATION METHODS

There are various methods used for catalyst synthesis, which include; spray pyrolysis, sol-gel method, impregnation method, precipitation method, colloidal method and Bonnemann method. A good method for making electro-catalysts should provide, a preferred crystallite structure, narrow particle size distribution, uniform particle composition and allow the catalyst to disperse on support material.

2.8.1 Spray pyrolysis

Spray pyrolysis is a process in which thin and thick films or metals are deposited by spraying a solution on a heated surface, where the components react to form a chemical compound. The process of deposition through this technique is particularly useful for the deposition of metal-oxides [113]. However, metal films can also be deposited by the spray

pyrolysis technique [114]. Spray pyrolysis possesses many advantages, such as low processing temperature, high homogeneity and purity of products etc. This deposition technique offers a very simple method for preparing films of any composition. Spray pyrolysis does not need high-quality substrates or chemicals .Unlike many other film deposition techniques; spray pyrolysis represents a very simple and reasonable cost-effective processing method (particularly with regard to equipment costs). The method has been used for the deposition of porous films, solid films, and for production of powder. Even multi-layered films can be easily prepared using this multipurpose technique. Spray pyrolysis has been used for last decades in the solar cell production and in glass industry. Basic spray pyrolysis equipment consists of an atomizer, precursor solution, substrate heater, and temperature controller. However, the key challenges of this technique: are control over the morphology and composition of product particles. Another disadvantage that is found in spray pyrolysis is that the coatings are not uniform in thickness [115].

2.8.2 Sol gel method

Sol gel method was developed in the 1960's, primarily due to the need of new synthesis methods. The idea behind this method is to dissolve a compound in a liquid in order to produce a solid material that is in a well-ordered manner. Sol gel is generally used to prepare the material with different shapes such as porous structure, powders and thin film material. In this method metal salt, reducing agents and aged gel are used. Sol gel technique can produce thin bond-coating to convey excellent connection between the metallic substrate and the top coat. It can also produce thick coating to provide corrosion protection performance and shaped materials are easily formed into complex geometries in a gel state. Despite its advantages, sol-gel technique has never reached its full industrial potential due to some limitations, e.g. low wear-resistance, weak bonding, high permeability, and the absorbency which is difficult to control [116].

The sol-gel method used to synthesize Pt–RuO_2 deposits on a carbon black substrate and the catalysts activity towards methanol electro oxidation was evaluated by *H. B. Suffrendini* and co-workers [117]. *Hua et al* [118] studied the effect of metal precursor and calcination on the synthesized catalysts using the sol-gel method. *M.L. Calegaro* and co-

workers [119] showed that the sol-gel method is an attractive way of synthesizing catalysts by incorporating different metal oxides on a substrate composed of platinum dispersed on carbon.

2.8.3 Impregnation reduction method

The impregnation method is perceived as one of the most common and simplest methods for the preparation of catalysts in fuel cell. The method mostly involves the impregnation of a metal salt solution onto a support material at certain time intervals. In the impregnation method the metallic catalyst precursor is soaked into a support before it is reduced into metallic nanoparticles. There are two possible reduction steps such as chemical and electrochemical reduction and these reduction steps can be conducted in a liquid phase or gas phase. The slurry is then heated to remove the solvent and the residue is successively reduced at elevated temperatures to decompose the salt and give rise to the desired catalyst. The metallic catalyst precursors that are mostly used in this method are chloride salts (H_2PtCl_6 and $RuCl_3$) because they are simply available [120].

The challenge facing this method is the use of the chloride precursors that might lead to chloride poisoning, resulting in lower catalytic activity and stability of the chloride-salt derived catalyst. The investigation of the impregnation methods that could use chloride free precursors have been done using metal nitrate/nitrite salts such as Pt $(NH_3)_2(NO_2)_2$ and RuNO $(NO_3)_x$ [121], metal sulphite salts such as $Na_6Pt\ (SO_3)_4$, carbonyl complexes such as $Ru_3\ (CO)_{12}$ [122] and $Na_6Ru(SO_3)_4$ [123] as metal precursors in the impregnation method, respectively. These chloride-free routes give higher dispersion and better catalytic activity as compared to the conventional Cl-containing route.

2.9 DEPOSITION METHOD

During the last several decades, deposition methods of catalysts have brought down a lot of attention, mainly due to their functional advantages over bulk materials, processing flexibility, and cost considerations [124].Thin film deposition techniques have been divided into two major processes: physical deposition and chemical deposition processes

[125]. Physical methods include physical vapor deposition (PVD), laser ablation, molecular beam epitaxy (MBE), and sputtering. The chemical methods comprise of gas phase deposition methods and solution techniques. The gas phase methods include chemical vapor deposition (CVD) and atomic layer deposition (ALD), while in solution techniques spray pyrolysis, sol-gel, spin coating and dip coating methods deposition of precursor solutions is also employed.

2.9.1 Physical vapor deposition (PVD)

PVD is a process that is used to deposit thin layers of material [126]. This deposition method is environmentally friendly and it occurs under vacuum deposition technique using three important steps. The first step is vaporization of the solid phase material supported by high temperature vacuum. The second step involves the vapor transportation onto the surface of the substrate. The last step is condensation that normally occurs on the substrate to form thin films. Different PVD technologies use these three vital steps to generate and deposit material. Thermal evaporation and sputtering are the two most important processes [127].

PVD can be used in different applications, including batteries, fuel cell electrodes, and fabrication of micro-electronic devises, optical and conductive coatings and surface modification. There are quite a few advantages that make PVD to be one of the recognized deposition methods. This technique has the ability to use almost any type of organic and inorganic material on the substrate surface using a variety of finishes. PVD coating are harder and more resistant to corrosion. High temperature coating produces good impact strength and strong durability. However, PVD suffer from a lot of limitations such as high capital costs, selection of the best PVD technology and high temperature operation need some experience. A cooling water system is required to dissolve large heat loads. Another disadvantage is that, the specific technologies can impose limitations; for example, line-of-sight transfer makes annular coating shapes practically impossible [128-130].

2.9.2 Chemical vapor deposition (CVD)

CVD is a process that is used for the production of high purity and high performance solid material. This process is normally used in the semiconductors to produce thin films. In a general CVD process, a substrate is exposed to one or more volatile precursors, which decompose or react on the substrate surface to produce the desired deposits. Regularly, volatile by-products are also produced and they are removed by gas flow through the reaction chamber. This technique can also be used in microfabrication process to deposit material in different forms including: monocrystalline, polycrystalline, unstructured and epitaxial. The material that include: silicon, carbon nanofibers, carbon fiber, carbon nanotubes and filaments, are also included. CVD have several advantages on depositing thin films. One of the major advantages is that, films are regularly quite conformal, i.e. the film thickness on the sidewalls of the structures is comparable to the thickness on the top with high aspect ratios. This means that films can be applied to elaborately shaped pieces, including the interiors and undersides of structures. Additionally, CVD can deposit a wide variety of materials with very high purity. The impurities that may be formed are removed from gaseous precursors using distillation technique [131].

Another advantage is that, the equipment does not usually require ultrahigh vacuum and mostly can be adapted to many process variations. Its flexibility is such that it allows several changes in composition throughout deposition and the codeposition of compounds or elements can be readily achieved. However, CVD possesses a lot of disadvantages. The primary disadvantage lies in the properties of the precursors. Possibly the precursors at almost room temperature needs to be volatile. CVD precursors can also be highly corrosive, toxic, and explosive. Some of these precursors are very costly and the by-products are also hazardous [131-133]. One of the major disadvantages of CVD is the fact that the deposition of the film is usually at high temperature. This puts some limitations on the type of substrate that can be coated. More essentially, it courses tress on deposited films more especially on material that have various thermal expansion coefficients, which can result in mechanical instability in the deposited film [134].

2.9.3 Electrochemical Atomic layer deposition method (ECALD)

In 1970s, electrochemical atomic layer deposition (ECALD) was developed to deposit thin films chemically from a vapor phase. The research continued until the first ECALD that was used for noble metal thin films growth reported in 2003 [135]. Since then, more attention on the process development has been growing due to the importance of these materials in different application.

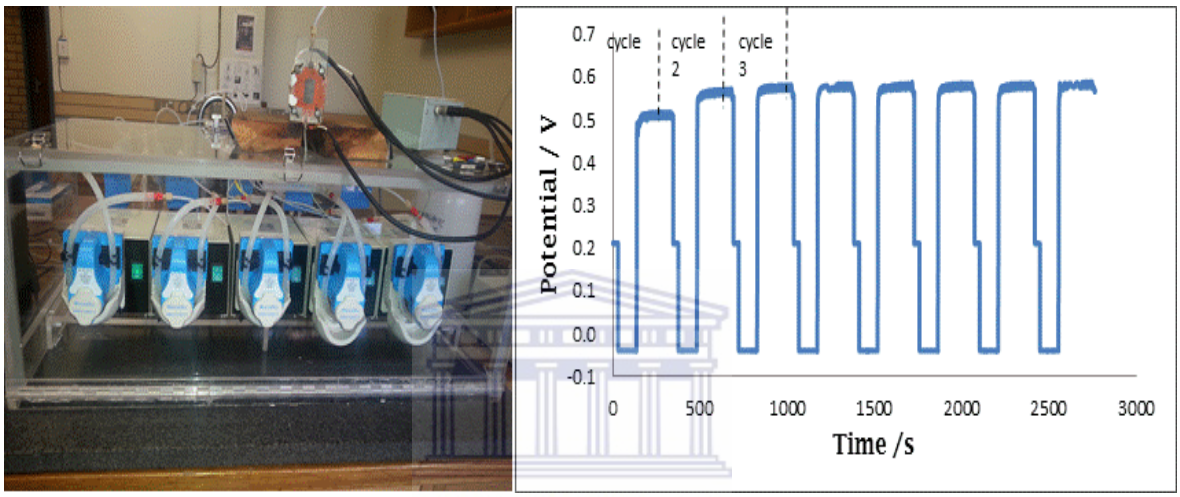

Figure 2.14: A picture taken at CSIR lab (Pretoria, SA) for electrochemical atomic layer (ECALD) and the experimented results for deposited sequential cycles.

Electrochemical atomic layer deposition (ECALD) is a method that is used to form conformal nanofilms, by allowing one atomic layer at a time using surface limited reactions (SLR). Compared to other deposition methods ECALD remain on the top, due its quality operations. For example, chemical reactants are alternatively pulsed in a reaction chamber simultaneously and they are chemisorbed on to the surface of the substrate in order to form the monolayer as shown in the figure (2.14) above. This allows the reaction set up to be very easy and it doesn't necessarily require many restrictions over the reactants, allowing the use of different materials. ECALD cycles are defined by the set of successive pulses of two or more precursors divided by a purge period. The surface is exposed to the first precursor which saturates the surface. The adsorbed layer of the first precursor is then exposed to and reacted with the second precursor. The sacrificial metal (often known as Cu) and excess of the second precursor are eliminated from the reactor

during open circuit [136-138]. The rate of the film growth on the surface of the substrate is measured by the film thickness during each cycle [139].

ECALD can be used in different application areas, such as in batteries, catalysis, semiconductors and electronics fuel cells [140]. In this study, ECALD was recognised as a potential technique for catalyst fabrication. This technique include an alternated electrodeposition of atomic layers of elements on a substrate surface applying under potential deposition (UPD),where one element deposits to another element at the potential prior to that required to deposits the first element to itself [141]. Generally, these deposition processes use small concentration of precursors and they are also carried out at low temperature. Various solutions are used separately to deposit each element. ECALD possesses advantages such as sequential electrochemical deposition with self-limiting of growth deposits, fine-tuning of catalytic properties in relation to ratios of constituent elements, by discontinuing the growth of deposits at appropriate points [142].

2.10 THE PHYSICAL CHARACTERIZATION

2.10.1 Scanning electron microscopy (SEM)

SEM is an important technique that is used to produce the images of a sample by scanning it with a focused beam of electrons. In this study SEM was use to observe the quantitative and qualitative information concerning particles morphology, size, shape and agglomeration on the surface of the substrate. The electron beam was focused into a fine analyzer which detects over the sample surface. The dispersed electrons are collected by a detector, controlled, and enlarged to produce precise elementary analysis on the sample surface and particle distribution [143, 144-148]. The elemental structure of the catalysts was investigated using energy dispersive spectroscopic (EDX) emission analysis. Every sample was scanned in order to obtain the average wait percentage (wt. %) of the metal.

2.11 ELECTROCHEMICAL CHARACTERIZATION

The electrochemical characterization was used to investigate behavior of the prepared catalysts in acid medium. An electrochemical experimental set up consists of a

potentiostat, an interface card and a computer. During electrochemical measurements, an electrochemical cell was used. This cell was connected to the potentiostat by three electrodes named working electrode (WE), counter electrode (CE) and reference electrode (RE) [149]. Each electrode has its functions as follows:

(i) **Working electrode**

A working electrode is an electrode in an electrochemical system on which the reaction of interest occurs [150]. Normally, a WE is often used in combination with the counter and reference electron in a three electrode system. This depends on whether the reaction is a reduction or an oxidation [151].

(ii) **Counter electrode**

The function of the counter electrode is simply to generate an equal and opposite current to that flowing to or from the working electrode, in order for the reference electrode to remain in the steady state. Pt is mostly used as a counter electrode material, because it is inert and it does not easily decompose to damage the electrolyte. In this study gold wire (Au) was used as a counter electrode. For ORR experiments in $HClO_4$ it is very important to minimise the polarization of the counter electrode in order to avoid contamination of the electrolyte by unwanted reactions such as:

ClO^{4-} (aq) + $8H^+$ +$7e^-$ ↔ ½ Cl_2 (g) +4 H_2O (aq) E^{Φ} = 1.42 V [150] (5)

(iii) **Reference electrode.**

Reference electrode is used to measure the function of the potential applied on the working electrode (WE). In this study the most common and simplest reference system of silver / silver chloride (Ag/AgCl) was used. This usually consists of a cylindrical glass tube containing a 3 Molar solution of potassium chloride (KCl) saturated with AgCl [149].

2.11.1 Cyclic voltammetry

Cyclic voltammetry is an electrochemistry technique that is used to provide the information about catalysts and electrochemical reactions which includes; the activity of the catalysts with respect to electrochemical reactions that occurs on the surface of the substrate [152]. It consists of three electrodes namely, counter electrode, working electrode

and the reference electrode. This technique can also offer a fast position of redox potential for electro active catalysts. The initial (E_i) and final (E_f) potentials are set before scanning the working electrode. The potential of the working electrode is then scanned linearly to the final potential. The scan's direction is reversed when the final potential is reached, moving towards the initial value forming a cyclic voltammetry. Cyclic voltammetry provides a plot of current versus potential; the plot is normally used to determine the reactions that are occurring at the surface of the working electrode. After scanning the WE potential, anodic and cathodic peaks are observed as it can be seen from figure 2.15 below. Furthermore, the forward scan (that shows a hydrogen adsorption and catalyst oxidation peak) is known as the anodic scan. The reverse scan (that shows the catalyst reduction peak and hydrogen desorption peak) is known as the cathode scan [153].

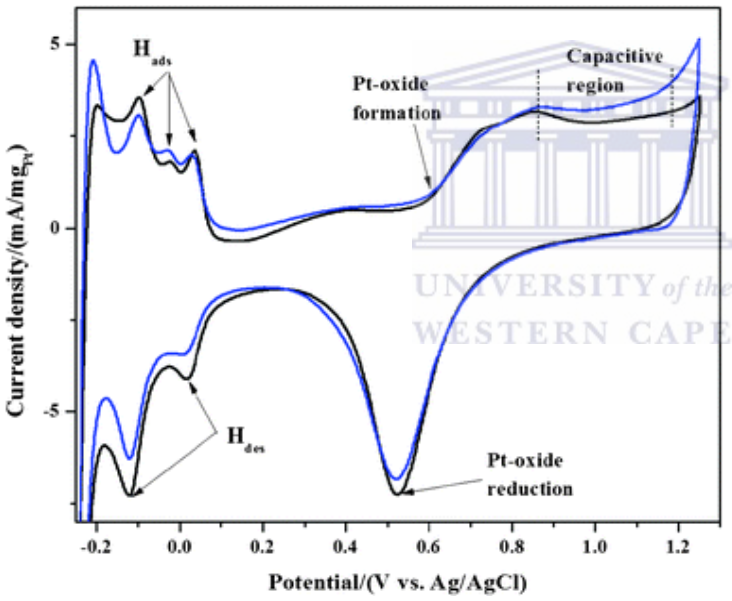

Figure 2.15: The overview of a basic cyclic voltammetry of Pt/C

2.11.2 Linea sweep voltammetry (LSV)

LSV is an electrochemical technique that is used to measure the current at the working electrode (WE) as a function of time. This technique was used in order to study the reversed (cathode) scan of a cyclic voltammetry. The onset potential and an onset current were obtained by this technique. LSV and CV might look relatively the same, but the main difference is the way their potential is measured. In a LSV the potential is not reversibly, while in CV a cycled potential is observed. However, an analyte species can either be

oxidized or reduced as the potential between WE and RE is linearly swept resulting in a current response to a WE [154].

CHAPTER 3

EXPERIMENTAL METHODOLOGY

3.1 EXPERIMENTAL PROCEDURE

3.1.1 Materials and methods

Chemical and instruments that were used in this study for deposition. The chemicals used for catalyst preparation

Table 3.1: The chemicals used for catalyst preparation and their supplier.

Reagent	**Supplier**
Hydrogen hexachlorohydroxyplatinate ($H_2PtCl_6.6H_2O$)	SA Precious metals
Palladium Chloride ($PdCl_2$)	SA Precious metals
Copper sulphate pentahydrate ($CuSO_4.5H_2O$)	Merck
70% Perchloric acid ($HClO_4$)	Merck
32% Hydrochloric acid(HCl)	Sigma Aldrich
Carbon Paper Toray TGPH090	E-TEK

*Gases (N_2 and O_2) were supplied by Air Liquid with at least 99.99 % purity.

Deionised water of sensitivity not less than 18.2 MΩ cm was used. All chemicals were received without any further purification.

The catalysts preparation were as follows; Pd solution (1 mM $PdCl_2$ pH=1), copper sulphate solution (1 mM $CuSO_4.5H_2O$, pH = 1) and platinum solution (1mM H_2PtCl_6 , pH = 1), were prepared in perchloric acid (0.1 M $HClO_4$). A complexing agent (50 mM HCl) was used during Pd deposition in order to slow the rate of replacement to produce uniform distribution of Pt and Pd on the substrate as described by *Modibedi et al*[155] and *Mkhwizu et al* [156].

The formation of Pt and Pd nanostructured was performed using a custom developed lab-view (national instrument, TX) programs (virtual instrument) as elaborated in [157].All the pumps, five-valve ways and the Potentiostat were computer controlled using a standard RS-232 and USB interfaces. A maximum of four solutions could be carried independently to the flow-cell by the outlet channel of the five-way valve. Nitrogen gas was purged into all the solutions for 1hour before the measurements and this atmosphere was maintained throughout the experiments. At 25^{o}C, three electrodes were used for the electrochemical depositions. The flow-cell used was defined by a thick silicon rubber gasket (0.255 cm and 0.46 cm thicknesses) for sealing purposes and also consists of two perplex blocks for holding of the reference, counter (8.4 cm thick Au wire) and the working electrodes. The reference electrode (Ag/AgCl,3M KCl) was placed at the outlet channel of the cell. The carbon paper connected by the copper foil was used as the working electrode and the exposed surface area for deposition was 4.06 cm^2. After the cell was assembled, 0.1M $HClO_4$ was used for electrochemical cleaning by applying 1.00 V for 5 minutes. Before an electrochemical deposition, underpotential deposition (UPD) on carbon paper (TGPH090) was not observed, because it is less noble than the copper adlayer. Therefore, a small overpotential deposition (OPD) of 0.05 V versus Ag/AgCl was used for Cu deposition on substrate as it was discussed by *Mkwizu et al* [157].

The electrodeposition of the nanostructured materials was carried as shown in *figure 3.1*: Firstly, solutions (1 mM $CuSO_4$, 1 mM H_2PtCl_6, 1 mM $PdCl_2$ and the background electrolyte (0.1M $HClO_4$) were delivered by a sequential cycle. Each cycle involved (i) rinsing the cell with the BE, followed by filling the cell with 0.1 mM Cu^{2+} solution at selected applied potential E_{appl}, (ii) Cu deposition at E_{dep}, followed by rinsing the cell with the background electrode (BE) at E_{dep}, (iii) filling the cell with the Pt $^{4+}$ solution at open circuit (OC), followed by the OC surface limited redox reactions (SLRR) reaction of Cu adlayers conditions, (iv) rinsing with BE and filling the cell with the Cu^{2+} solution at E_{appl}, (v) Cu deposition at E_{dep}, followed by rinsing the cell with the BE at E_{dep} and (vi) rinsing with the Pd^{2+} solution at OC, followed by OC SLRR reaction of Cu adlayers by Pd at low temperatures. 8x cycles for Pd Pt deposition were used furthermore; the maximum cycles of 24 in different ratios were performed.

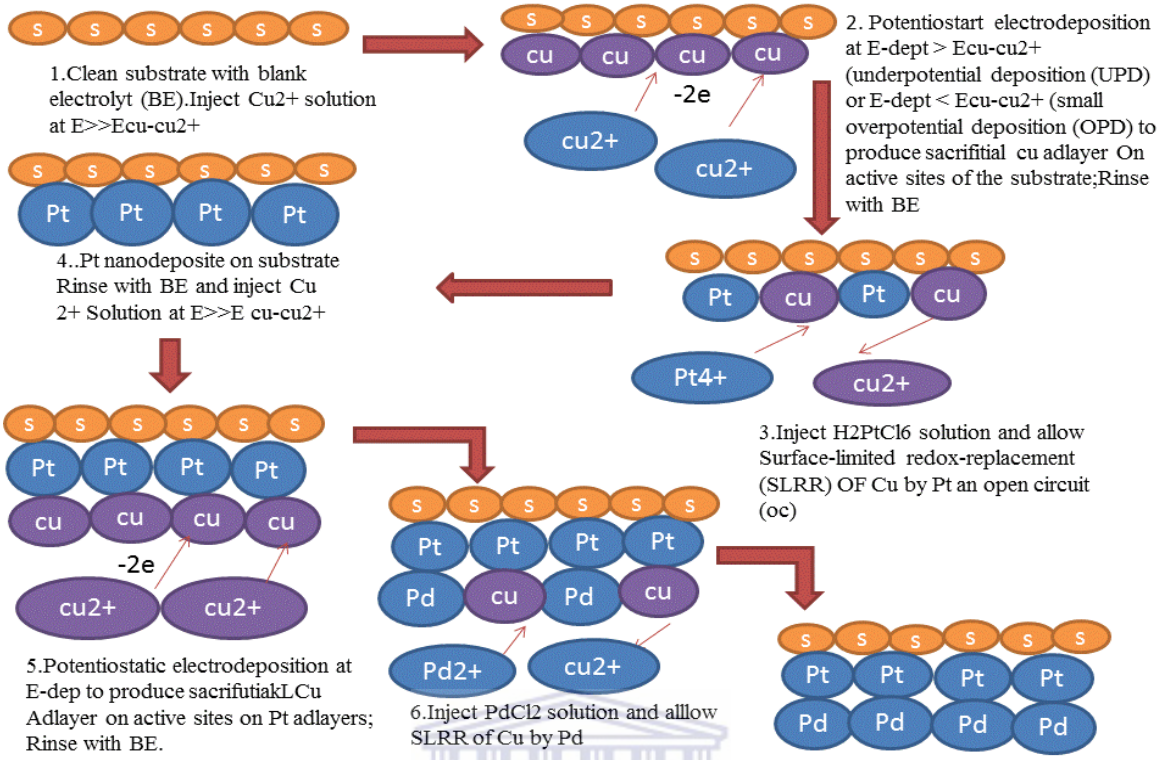

Figure 3.1: A sequential layer by layer electrodeposition of PtPd using Cu as a sacrificial metal [157].

Physical characterisation was done usingthe scanning electrode microscopy (SEM), mapping and Energy dispersive X-Ray spectroscopy (EDX) in order to observe the morphological structure and thickness of the catalysts on the surface of the substrate,. Electrochemical characterization by cyclic voltammetry (CV) and linear sweep voltammetry (LSV) were also done in order to observe the electrochemical reaction on the surface of the substrate.

3.2 THE PHYSICAL CHARACTERISATION

3.2.1 Scanning electron microscopy (SEM)

A high resolution scanning electron microscopy (HRSEM) was used to observe the quantitative and qualitative information concerning morphology, size, shape and agglomeration on the surface of the substrate. The substrate was focused on the beam of electron into a fine analyser which detects over the surface of the carbon paper. The

dispersed electrons were collected by a detector, controlled, and enlarged to produce precise elementary analysis on the sample surface and particle distribution. The elemental composition of the catalysts was investigated using energy dispersive spectroscopic (EDX) emission analysis. Every sample was scanned in order to obtain the average weight percentage (wt. %) of the metal.

3.3 THE ELECTROCHEMICAL CHARACTERISATION OF PdPt NANOSTRUCTURES

Electrochemical characterization was carried out using Autolab potentiostat.Linear sweep voltammetry (LSV) technique was used in order to obtain the onset potential and a current density. The LSV's were recorded at the scan rate of 5 mV in different flow rates. 0.1M $HClO_4$ was used as the electrolyte, saturated with oxygen. The Koutecky–Levich (K-L) plots were also extracted using LSV. On the other hand, Cyclic Voltammograms were employed in order to determine the electrochemical surface area of each catalyst at a constant scan rate of 50 mV using 0.1 M $HClO_4$ as an electrolyte saturated with nitrogen and oxygen.

3.3.1 Electrochemical surface area measurements

The electrochemical surface area (ECSA) of an electrode is an important property which must be determined in order to calculate and compare the current densities measured for different catalysts and catalyst loading. For Platinum (Pt) electrode, the combined hydrogen adsorption and desorption peaks gives a total charge passed during H^+ adsorption. However, the equation is given by:

$$Q_H = Q_{adsorption} + Q_{desorption}/2 \quad (8)$$

The ECSA equation for Pt is given as:

$$ECSA = QH \times 100/210\mu C \times \text{Area of electrode} \quad (9)$$

For palladium (Pd) electrodes, in comparable with platinum, the charge of a monolayer of adsorbed hydrogen is difficult to determine due to the ability of palladium lattice structure to absorb hydrogen [158, 159]. Therefore, the electrochemical surface area was calculated

from the charge of the monolayer of chemisorbed oxygen, which was estimated from the area of the palladium oxide reduction peak (Q_{PdO}). The charge of the oxygen monolayer (Q_O) for a smooth palladium electrode is twice as large as the hydrogen monolayer (Q_H) in platinum, the equation is given as

$$Q_H = 1/2\ Q_O \quad (10)$$

$$Q_H = 210\ \mu C\ cm^{-2}\ [158] \quad (11)$$

The electrochemically surface area of Pt and Pd can then be calculated assuming a relating value of 210μC/cm^2 which is a theoretical charge given for full monolayer coverage of the two combined peaks [160-162].

After calculating the electrochemical surface area, LSV plots are used in correlation with ECSA values to determine the K-L plot which will make it easier to determine the catalyst that undergoes a 4e$^-$ direct pathway. The analysis to extract the K-L plots for ORR involved the following expression:

$$\frac{-1}{i} = \frac{1}{k} + \frac{1}{nAFZ_{O2}C_{O2}v^{-1/3}} \quad (12)$$

Where *i* is the current measure at the applied potential *E*, *v* is the linear velocity (m s^{-1}), C_O is the saturation concentration of O_2 (1.22 x10^{-6} mol cm^{-3}), *n* is the number of electrons transferred and A is the surface area of the electrode.

CHAPTER 4

RESULTS AND DISCUSSION

4.1 PREPARATION METHOD

4.1.1 Copper deposition potential

The deposition potential of Cu on carbon paper in perchloride ($HClO_4$) was determined following the procedure by *Mkwizu et al* [155] and *Modibedi et al* [156, 163]. The Cu UPD peak was not observed on the carbon paper substrate as shown in figure 4.1 since the substrate is less noble than the Cu adlayer [164]. Therefore the small overpotential Deposition (OPD) voltage of -0.05V vs Ag/AgCl was used to deposit Cu on carbon paper.

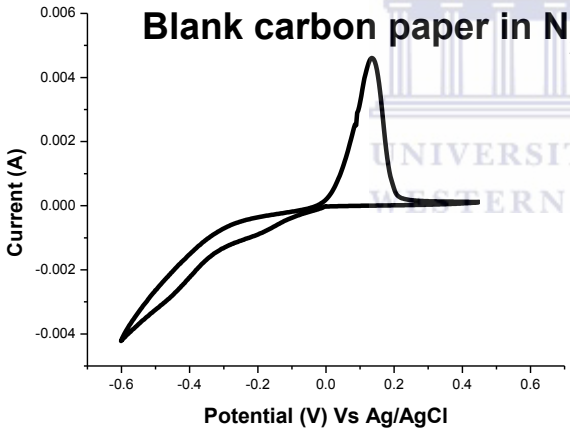

Figure 4.1: Cyclic Voltammogram of carbon paper substrate in 0.1mM $CuSO_4$ + 0.1M $HClO_4$ Scan rate = 50 mV/s.

4.1.2 Copper deposition time

The amount of copper deposited on the substrate depends on the deposition time [165]. Copper was deposited on the carbon paper by applying a potential of -0.05 V at 60s, 90s and 120s. Cyclic voltammograms were recorded by sweeping the potential from -0.05 to 0.7 V. Figure 4.2 confirms the effect of deposition time on the Cu oxidation at -0.05 V. The stripping current reaches a plateau after 90s, indicating that the deposition process is saturated and there is no further increase in the oxidation charge with time. Therefore, an applied potential of -0.05 V and deposition time of 90 s was chosen as the optimal values for Cu deposition and all the deposition in this report used these parameters .

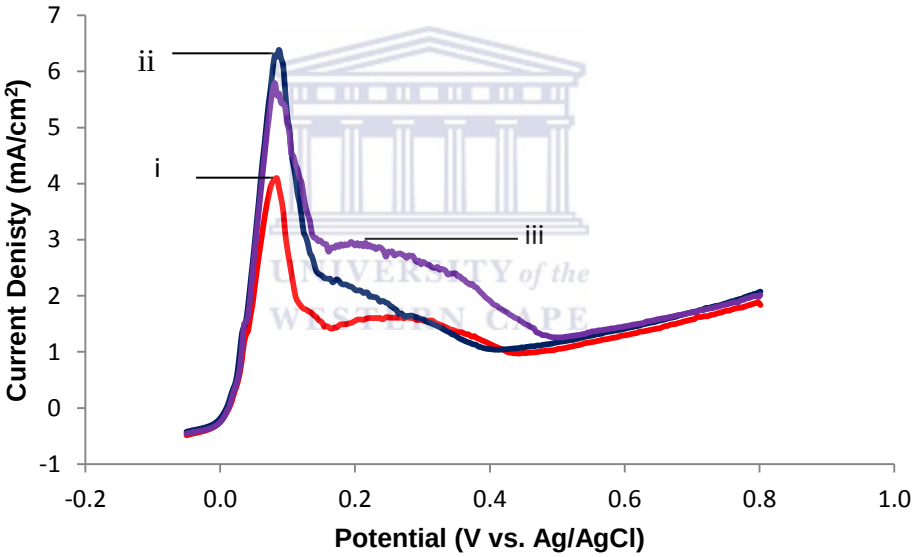

Figure 4.2: Cyclic voltammagram of Cu deposition on carbon paper in 0.1 M HClO4 + 1 mM CuSO4.5H2O at 60s (i), 90s (ii) and 120s (iii). Scan rate 50mV/s

4.1.3 Deposition cycles

Various deposition cycles were investigated and 8x cycles showed better electrochemical activity of Pt or Pd towards hydrogen oxidation reaction. Figure 4.3 illustrates the time-potential curve recorded during Pd electrodeposition on carbon paper substrate. Multiples of eight will be used in this report to deposit PtPd binary catalyst. Various Pt: Pd ratio (1:1, 2:1, 3:1) as well as the changing between Pt and Pd as the first metal to be deposited. The

nanostructured catalysts will be characterized and evaluated for the electrochemical reduction of oxygen in acid electrolyte.

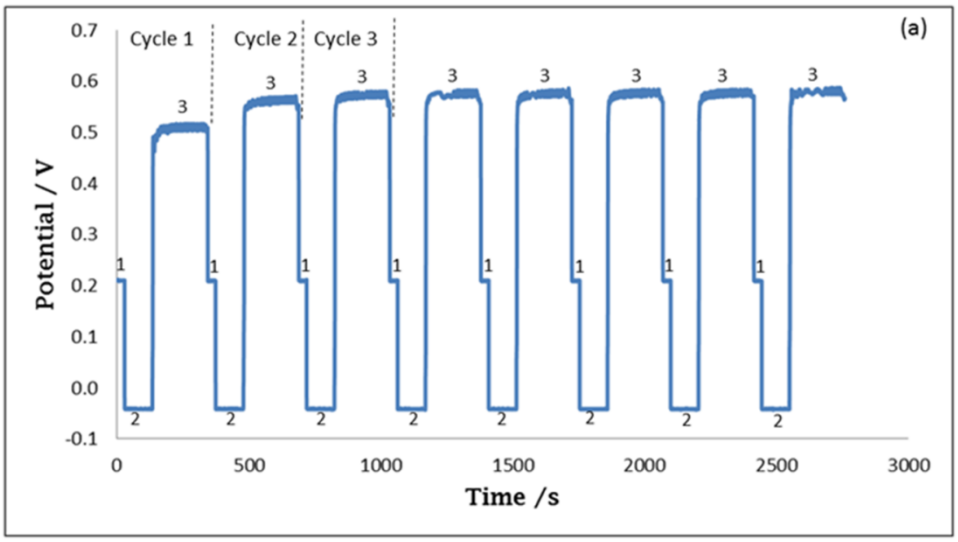

Figure 4.3: Time-potential curves recorded during sequential layer-by-layer electrodeposition of Pd on Carbon paper.

4.2 CHARACTERISATION

4.2.1 SEM and EDX results

The morphology, particle size distribution and element analysis of all prepared electrocatalysts were investigated using Scanning Electron Microscopy (SEM) with Energy dispersive X-ray spectroscopy (EDX). Figure 4.4 below shows the morphological structure of a blank carbon paper at (a) 500X and (b) 5.00 KX magnification. The Carbon paper (TGHP060) is made up of fibers that have a tube like structure as it can be seen clear at 5.00 KX magnification (figure 4.4b). The surface area of 4.06cm^2 was the area that was exposed for catalyst deposition. When the catalyst is well deposited, it gets absorbed by the fibers and covers the whole exposed surface area of the carbon paper. This depends on the optimum number of cycles that were used during each deposition.

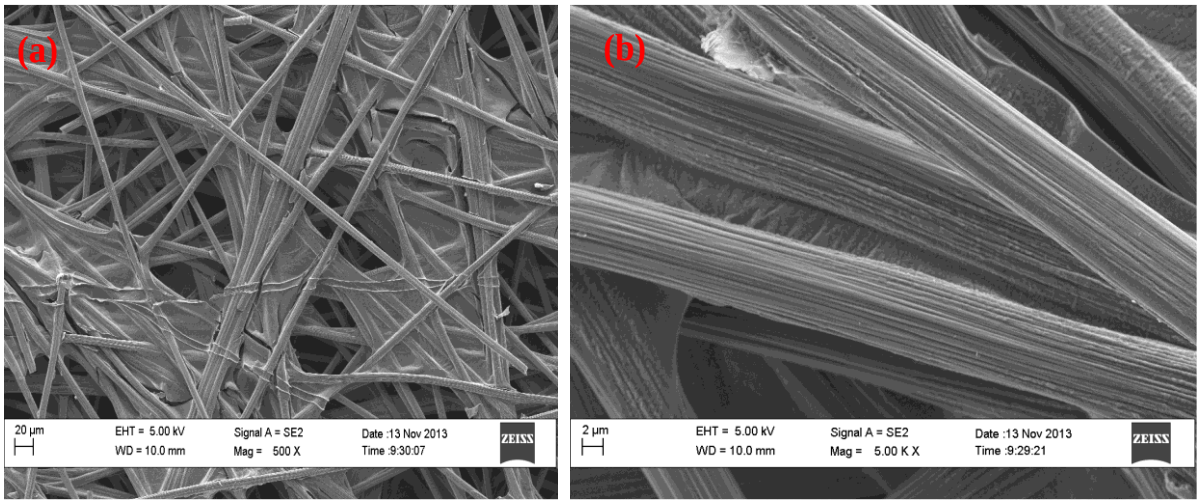

Figure 4.4: HRSEM images for blank carbon paper (TGHP060) at a low and high magnification.

Figure 4.5 below illustrate SEM images and particle size distribution of (a) Pd/Carbon-paper and (b) Pt/Carbon-paper after 8x deposition at low magnification and the corresponding particle size distribution, respectively. The results obtained revealed that during deposition of palladium into the Carbon-paper, Pd particles have agglomerated and formed a star-like shape. While during the platinum deposition, the cube-like shaped particles are observed for Pt electrocatalyst. In addition, both Pd and Pt particles did not completely cover the surface of the substrate. The histogram shows that Pd/Carbon-paper and Pt/Carbon-paper have normal bell-shaped particle size distribution. However, the distribution of Pd/Carbon-paper is broader than that of Pt/Carbon-paper, which resulted in a bigger particle size as can be seen in Table 4.1. The particle size of Pd/Carbon-paper is 6.5 nm and Pt/Carbon-paper is 4.25 nm. The particle size was obtained as the mean for all catalysts without any further change. *Álvarez et al* [166] also obtained approximately the same particle size for Pt and Pd on carbon (Vulcan XC-72R), using reduction of metals precursors. The particle size was obtained as the mean for all catalysts without any further change.

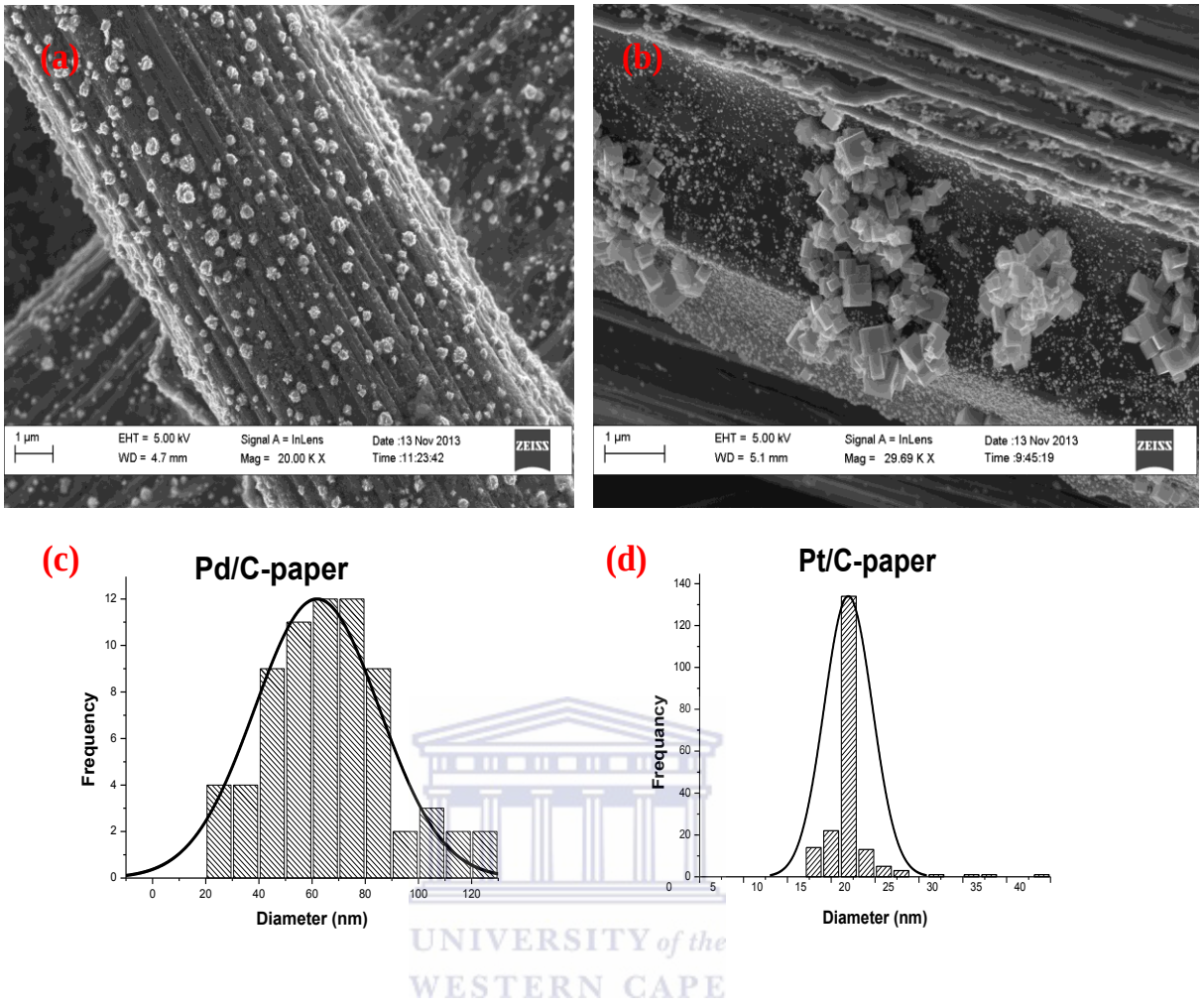

Figure 4.5: HRSEM images after 8x cycles of (a) palladium on carbon paper (Pd/Carbon-paper) and (b) platinum on carbon paper (Pt/Carbon-paper) in high magnifications. The Histogram images (c) and (d) of Pd/Carbon-paper and Pt/Carbon-paper, respectively.

Table 4.1: Represent the particle size and Pd: Pt ratio of the prepared electrocatalysts.

Catalyst	**Particle size (nm)**	**Ratio**
Pd/C-paper	6.5	1:0
Pt/C-paper	4.25	1:0
Pd8Pt8/C-paper	37.1	Pd:Pt 1:1
Pt8Pd8/C-paper	35.7	Pt:Pd 1:1
Pd16Pt16/C-paper	25	Pd:Pt 1:1
Pt16Pd16/C-paper	16	Pt:Pd 1:1
Pt24Pd24/C-paper	10	Pt:Pd 1:1
Pd24Pt24/C-paper	-	Pd:Pt 1:1
Pd16Pt8/C-paper	22	Pd:Pt 2:1
Pd24Pt16/C-paper	13	Pd:Pt 2:1
Pd24Pt8/C-paper	20	Pd:Pt 3:1
Pd16Pt16/C-paper Co-deposition	17.5	Pd:Pt 1:1
Pd24Pt24/C-paper Co-deposition	11	Pd:Pt 1:1

As it can be seen from SEM images (figure 4.6 (a and b) below, the particles of Pd8Pt8/Carbon-paper are uniformly distributed and do not show any agglomeration.

However, some particles are smaller and others and have a spherical shape, which is quite different from the particle shape observed for nanostructures of Pd/Carbon-paper and Pt/Carbon-paper in (figure 4.5). EDX confirmed the presence of Pd and Pt (figure 4.6c) which are represented by an intense peak observed at 0.3 keV. In addition, carbon peak is also observed in the same peak range as Pd-Pt which indicates that the substrate is made up of carbon.

At 8 deposition cycles, Pd8Pt8 homogenous catalyst was formed. There is no intense peak of an individual element observed, instead Pd8Pt8 is observed at 0.3 keV and 2.9 keV. Histogram image in figure 4.6 d shows a normal particle distribution. A big range particle distribution is also observed, between small and big particles. Pd8Pt8/Carbon-paper obtained a large particle diameter of 37.1 nm as represented in table 4.1. Same observations were observed by Jayashree et al [167].

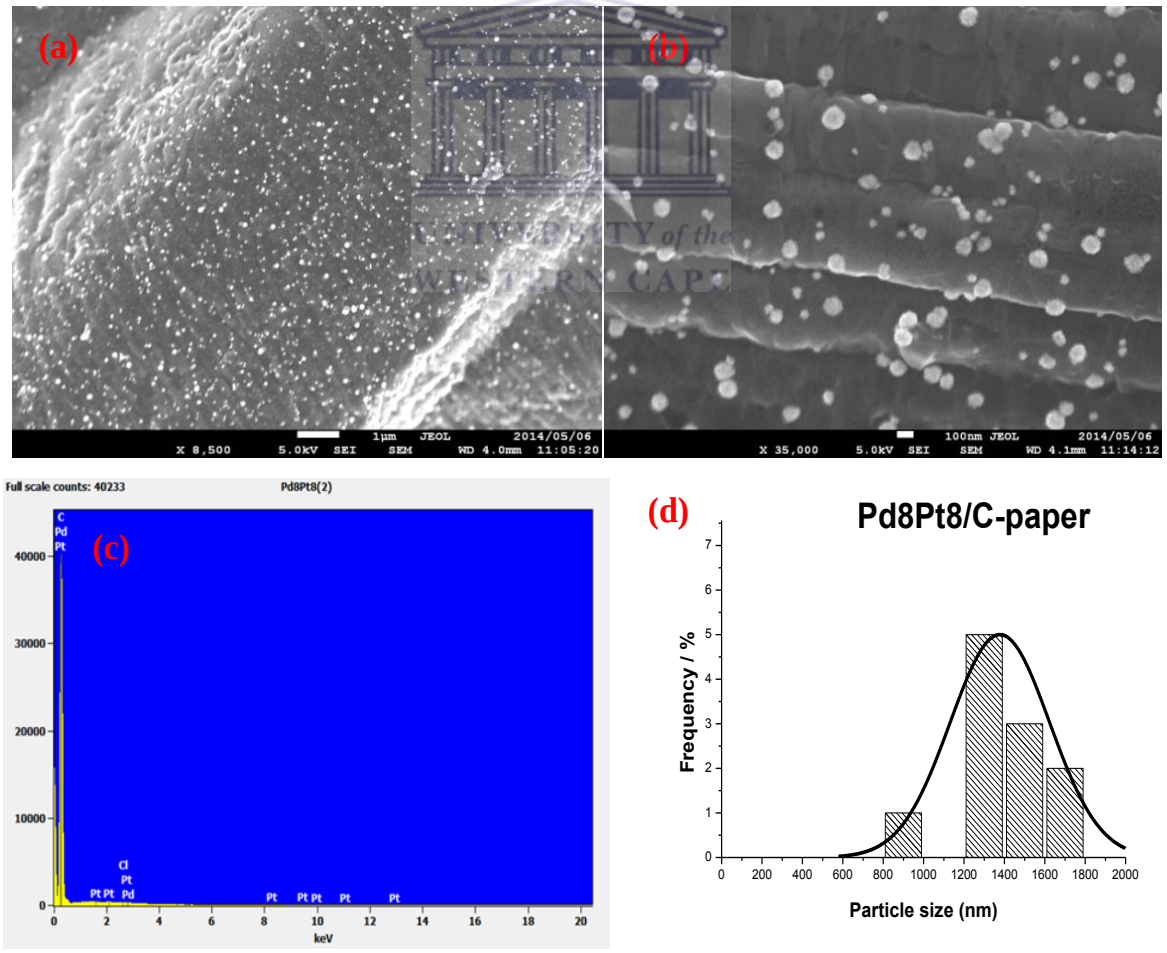

Figure 4.6: SEM images after 8x cycles of palladium-platinum on carbon paper (Pd8Pt8/Carbon-paper) in (a) low and (b) high magnification, (c) EDX for Pd8Pt8/Carbon-

paper and (d) histogram of Pd8Pt8/Carbon-paperFigure 4.7 (a) and (b) below shows the distributed particles of Pt8Pd8/Carbon-paper, which is randomly dispersed on the substrate surface and not much of agglomeration, is observed. A spherical shape of Pd8Pt8/Carbon-paper can be seen in (b), while monostructures of Pd/Carbon-paper and Pt/Carbon-paper in figure 4.5 has less defined spherical shapes that are similar to figure 4.7 (a). In (b) the presence of both Pt and Pd is shown by an intense peak at 0.3keV and another visible peak is also shown at 2.1 keV.

There is an element of inhomogeneity in Pd8Pt8/Carbon-paper, because (b) shows an excess Pt in certain areas of carbon paper. Histogram image (d) shows a normal particle distribution, although the particles are far away from each other and also there are small and very big particles. The particle size of Pt8Pd8/Carbon-paper is 35.67 nm. Same observations were observed by Jayashree et al [167].

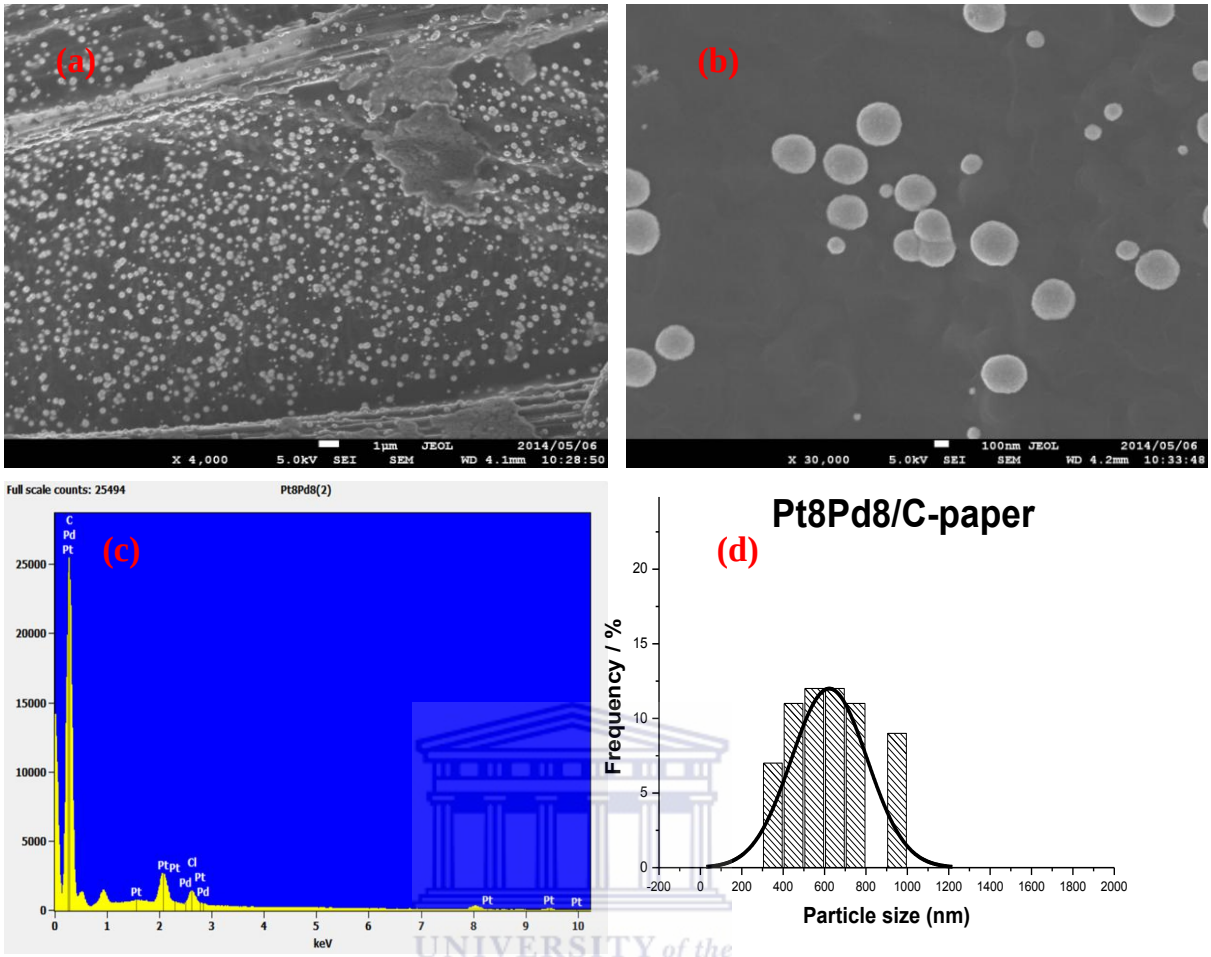

Figure 4.7: SEM images after 8 cycles of platinum-palladium on carbon paper (Pt8Pd8/Carbon-paper) in (a) low and (b) high magnifications, (c) EDX for Pt8Pd8/Carbon-paper and (d) histogram ofPt8Pd8/Carbon-paper.

Figure 4.8 shows the morphology of the Pd16Pt16 deposited on carbon paper. The fibres of the carbon paper are uniformly covered with Pt and Pd particles. Agglomeration of binary Pd16Pt16/Carbon-paper particles is observed. A cube-like shape is observed in (b) as was observed in figure 4.5 (b). The presence of Pd and Pt are confirmed by EDX in (c), where an intense peak is observed at 0.3keV. Another intense peak for Pt is observed at 2.1keV.

The intense peak at 2 keV suggests that excess Pt was deposited at certain areas of the substrate. Histogram image (d) also shows a broad particle distribution of Pd16Pt16/Carbon-paper which makes it inaccurate to measure the 100 maximum amounts of particles required as it is skewed to the right. The particle size of Pd16Pt16/Carbon-

paper is 25 nm, which is also a large particle size. *Wang et al* [168] also obtained such agglomeration in the ration of 1:1 for Pd: Pt/Carbon-paper.

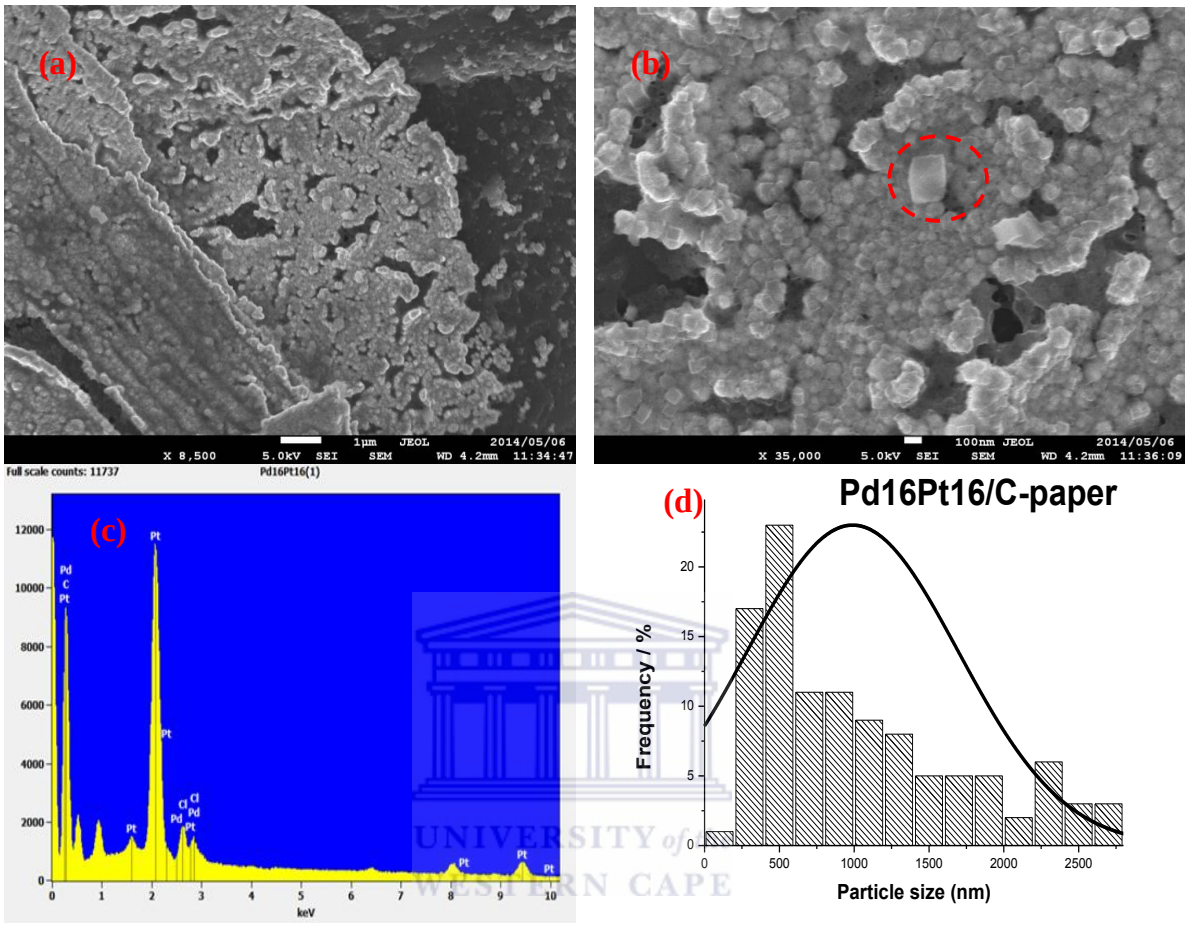

Figure 4.8: SEM morphological structure after 16 cycles of palladium-platinum on carbon paper (Pd16Pt16/Carbon-paper) in (a) low and (b) high magnification, (c) EDX for Pd16Pt16/Carbon-paper and (d) histogram of Pd16Pt16/Carbon-paper.

Figure 4.9 shows Pt16Pd16/Carbon-paper in different magnifications with some few agglomerations in the areas of the carbon paper. Spherical particles are observed. The particles are uniformly distributed and they cover the carbon fibres. The presence of Pd and Pt are confirmed by EDX in (c), where the intense peak for both Pt16Pd16/Carbon-paper is observed at 0.3 keV. Another intense peak is observed at 2 keV which suggests the presence of excess Pt. The histogram image (d) shows a bell-shaped particle distribution on the substrate surface. Therefore, the agglomeration observed in other areas of the carbon

paper also made it challenging to measure accurately the particle size of Pt16Pd16/Carbon-paper. The particle size of Pt16Pd16/Carbon-paper is 16.0 nm as represented in table 4.1.

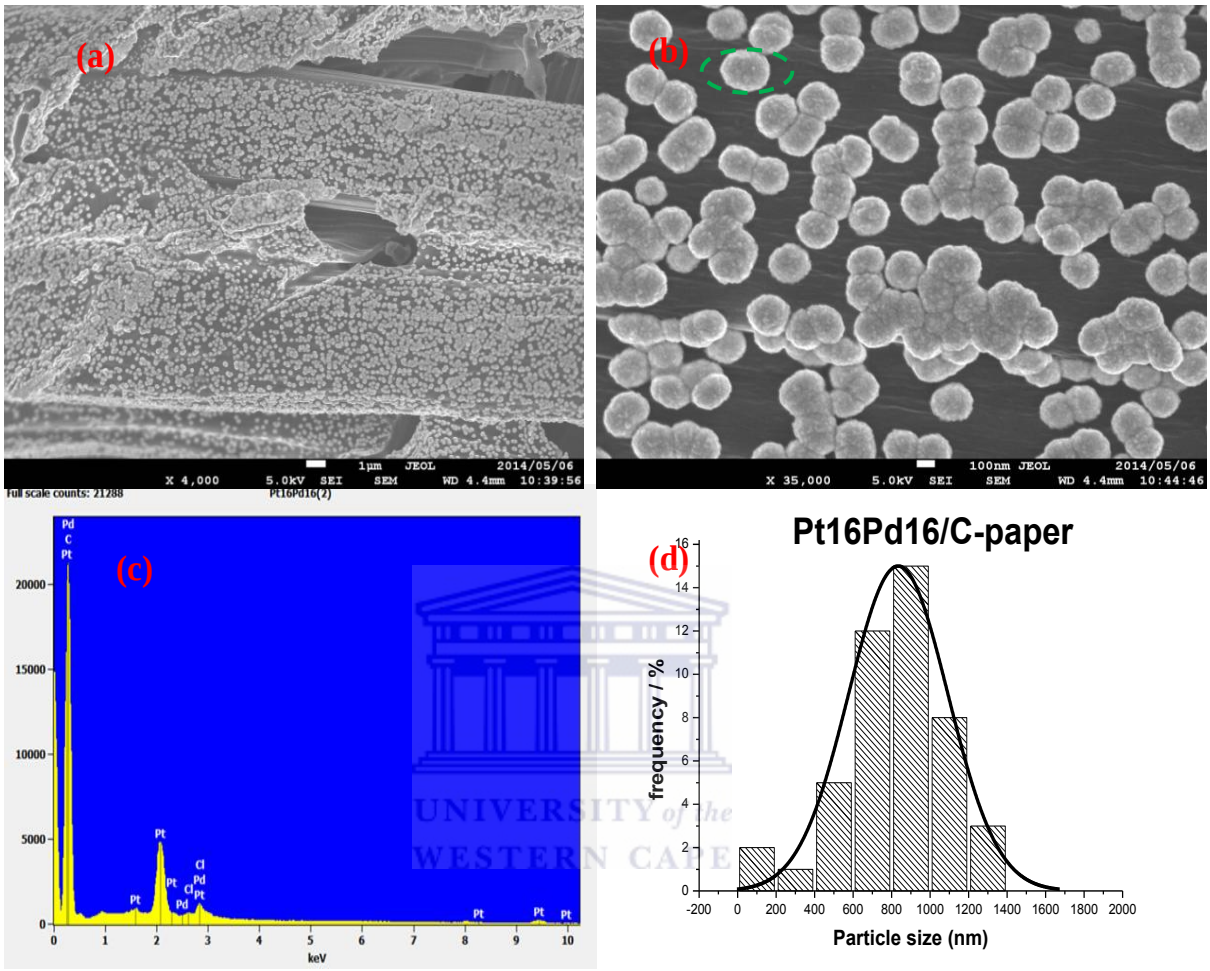

Figure 4.9: SEM morphological structure after 16 cycles of palladium-platinum on carbon paper (Pt16Pd16/Carbon-paper) in (a) low and (b) high magnification and (c) EDX for Pt16Pd16/Carbon-paper and (d) histogram of Pt16Pd16/Carbon-paper.

Figure 4.10 shows codeposition of Pd16Pt16/Carbon-paper in different magnifications. The particles are uniformly distributed and they are of spherical shapes. Agglomeration is also sparsely observed. *Jayashree et al* [167] observed the same morphological structure and agglomeration on the codeposition of Pd: Pt of a ration 1:1. Energy Dispersive X-ray analysis (EDX) shows that the ratio of Pt to Pd in this sample is 1:1. The presence of PdPt is observed at 0.3 keV and 2.8 keV. Pt peak only is observed at 2.1 keV. The image (c)

shows a normal particle distribution. The particle size of Pd16Pt16 codeposition/Carbon-paper is 17.5nm.

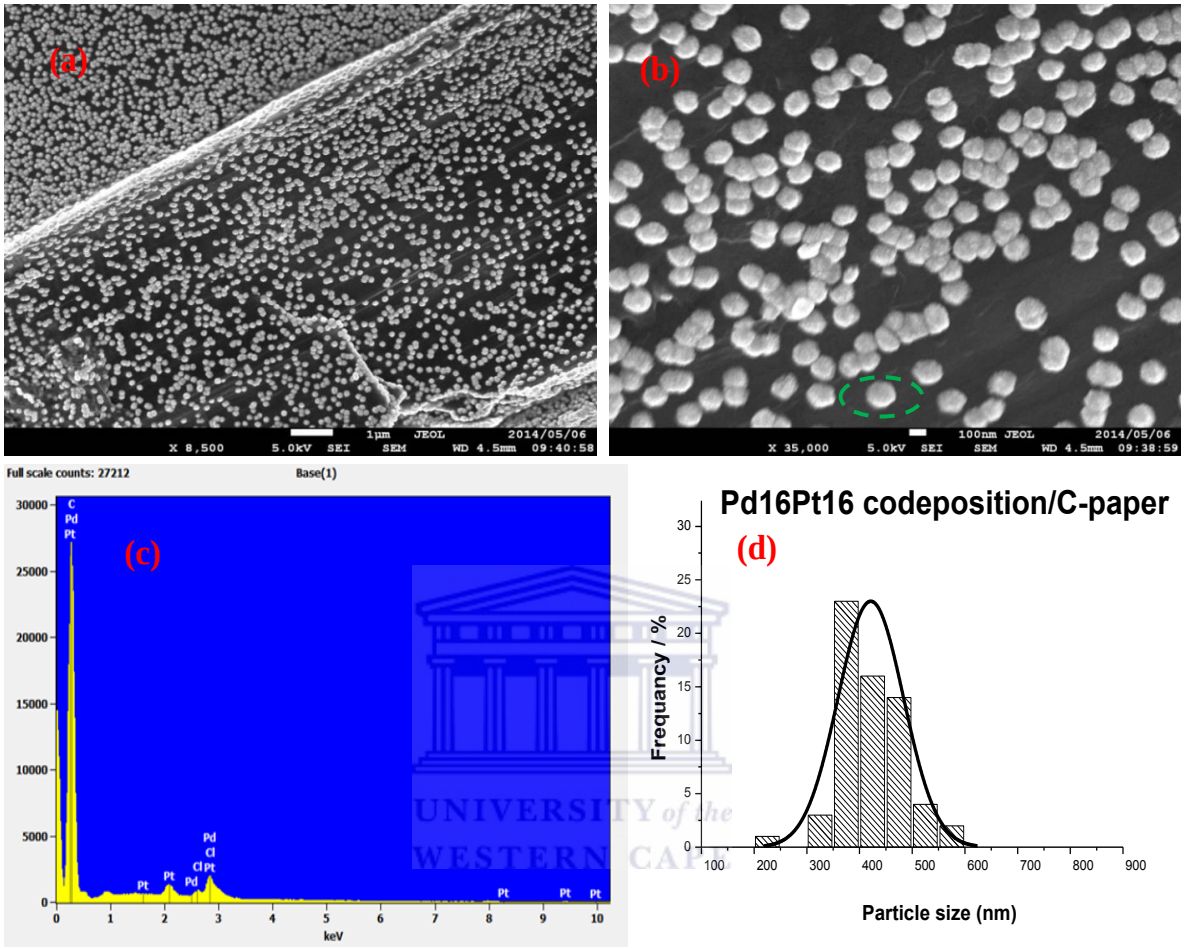

Figure 4.10: SEM morphological structures after 16 codeposition cycles of palladium-platinum on carbon paper (Pd16Pt16 codeposition/Carbon-paper) in (a) low and (b) high and (b) EDX forPd16Pt16codeposition /Carbon-paper and (d) histogram image of Pd16Pt16 codeposition/Carbon-paper.

Figure 4.11 shows Pd16Pt8/Carbon-paper in various magnification. SEM showed good quality deposition and a uniform distribution of particles on carbon paper. The shapes of the particles are not properly defined. Agglomeration is also sparsely observed. The presence of PdPt in (c) is observed at an intense peak at 0.3 keV and 2.9 keV, while a small peak that indicates the presence of Pt is only observed at 2.1 keV. This shows that, in other areas of the substrate there is more Pt present than Pd. A normal distribution of particles is

observed in (d) and a wide spread of the particles on the surface of the substrate. The particle size of Pd16Pt8/Carbon-paper is 0.7 nm.

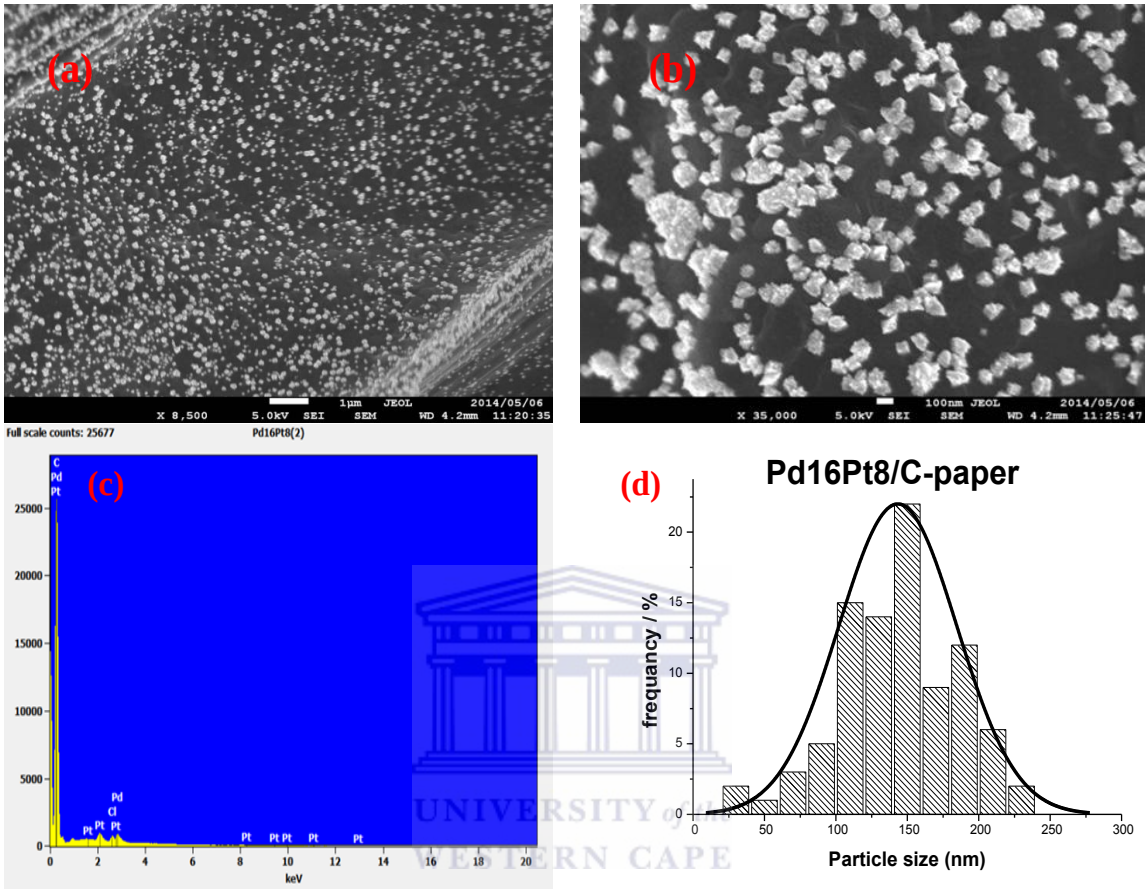

Figure 4.11: SEM morphological structure after 16 and 8 cycles of palladium-platinum on carbon paper (Pd16Pt8/Carbon-paper) in (a) low and (b) high magnification, (c) EDX for Pd16Pt8/Carbon-paper and (d) histogram image of Pd16Pt8/Carbon-paper.

Figure 4.12 (a) and (b) shows Pt24Pd24/Carbon- paper in different magnification. The particles are also agglomerated and they are of spherical shapes. The particles are distributed on carbon paper. The EDX shows the presence of both Pt and Pd at 1.8 keV and 2.3 keV respectively. The analysis of EDX shows an inhomogeneity of the catalyst. An intense peak observed in 2 keV shows an excess Pt in some areas of the carbon paper. It is observed in (c), that the particle distribution is bell-shaped. The gaps that are observed in (c) refer to areas of distribution where there are no observations. The size of Pt24Pd24/Carbon-paper particle is 10 nm as observed in table 4.1.

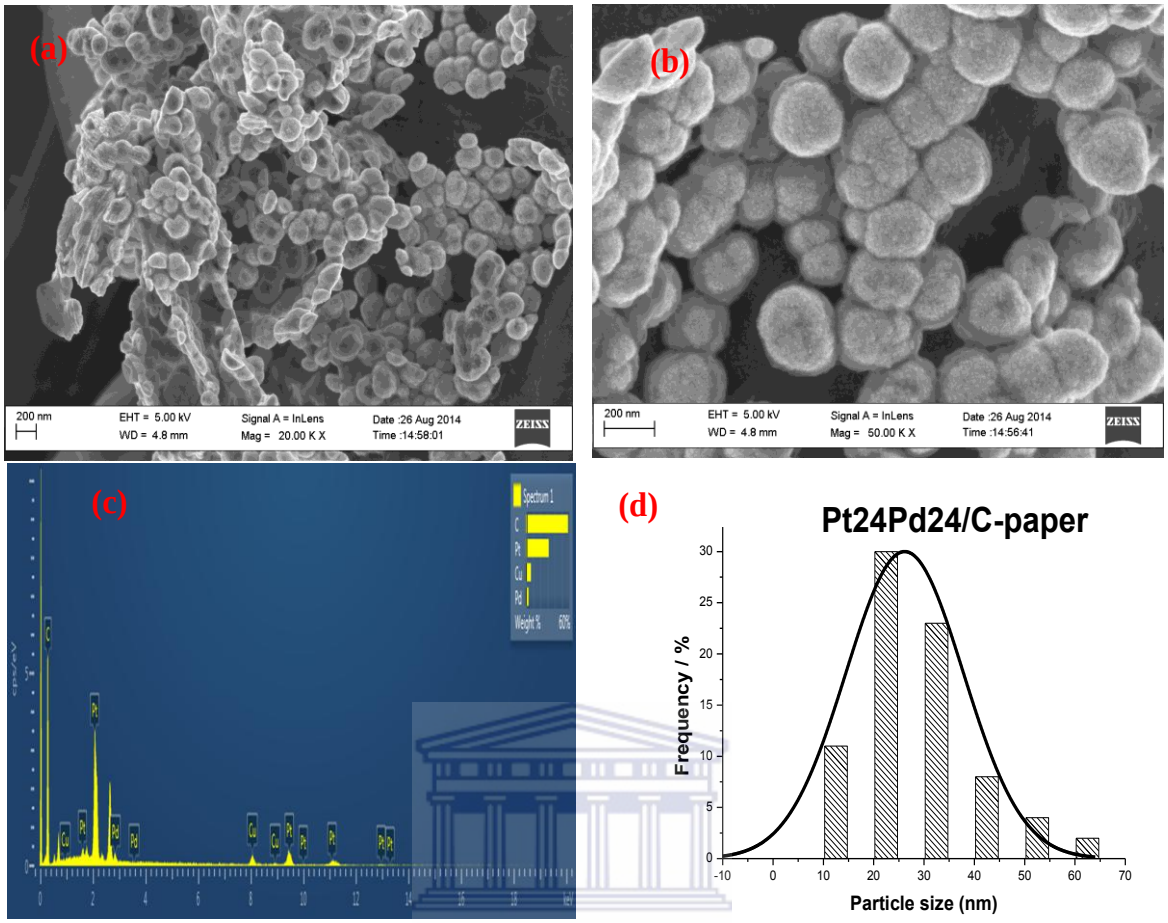

Figure 4.12: HRSEM morphological structure after 24 cycles of platinum-palladium on carbon paper (Pt24Pd24/Carbon-paper) (a) low and (b) high magnification, (c) EDX for Pt24Pd24/Carbon-paper and (d) histogram image of Pt24Pd24/Carbon-paper.

Figure 4.13 (a) and (b) shows Pd24Pt24/Carbon-paper particles various magnifications. The particles are not uniformly distributed and are highly agglomerated. The particle shapes are not properly defined. The EDX shows small peaks of the presence of Pd and Pt at 2.8 keV and 2.9 keV. An intense peak of 2.1 keV is observed in (c), which suggests an excess presence of Pt than Pd on carbon paper. This also indicates that the catalyst is inhomogeneous. As it can be clearly seen in (b), the particles are agglomerated and that made it impossible to use a histogram to analyse and to determine the particle size.

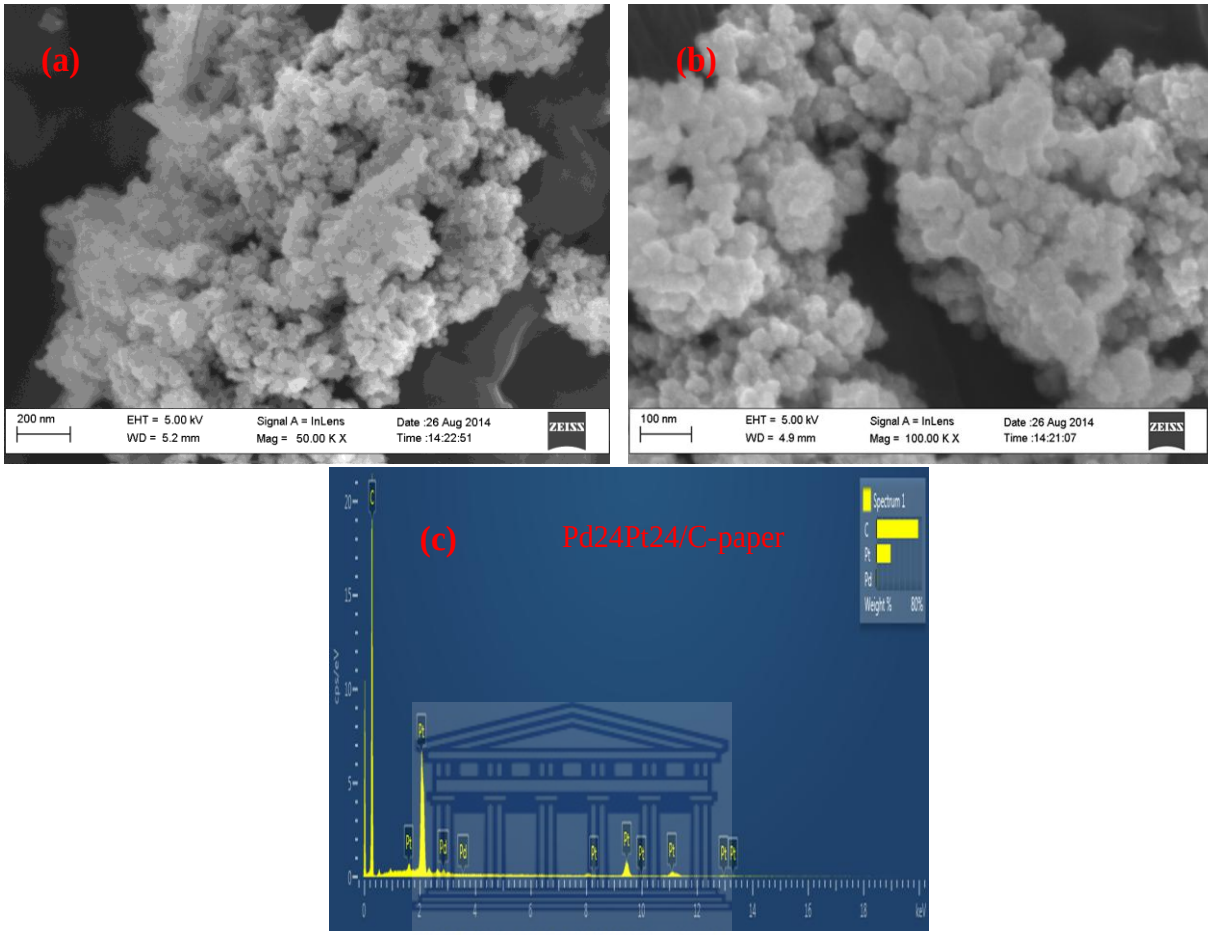

Figure 4.13: HRSEM morphological structure after 24 cycles of palladium-platinum on carbon paper (Pd24Pt24/Carbon-paper) (a) low and (b) high magnification, (c) EDX for Pd24Pt24/Carbon-paper.

Figure 4.14 (a) and (b) shows Pd24Pt24codeposition/Carbon-paper at low and high magnification. The particles are uniformly distributed and are spherical in shape. The EDX shows the presence of Pd and Pt at 1.8 keV and 2.8 keV, respectively. There is no intense peak observed that shows only the presence of Pt or Pd. The Histogram image (c) shows a normal distribution of particles and a wide spread of the particles on the surface of the substrate. The particle size of Pd24Pt24codeposition/Carbon-paper is 11 nm as represented in table 4.1.

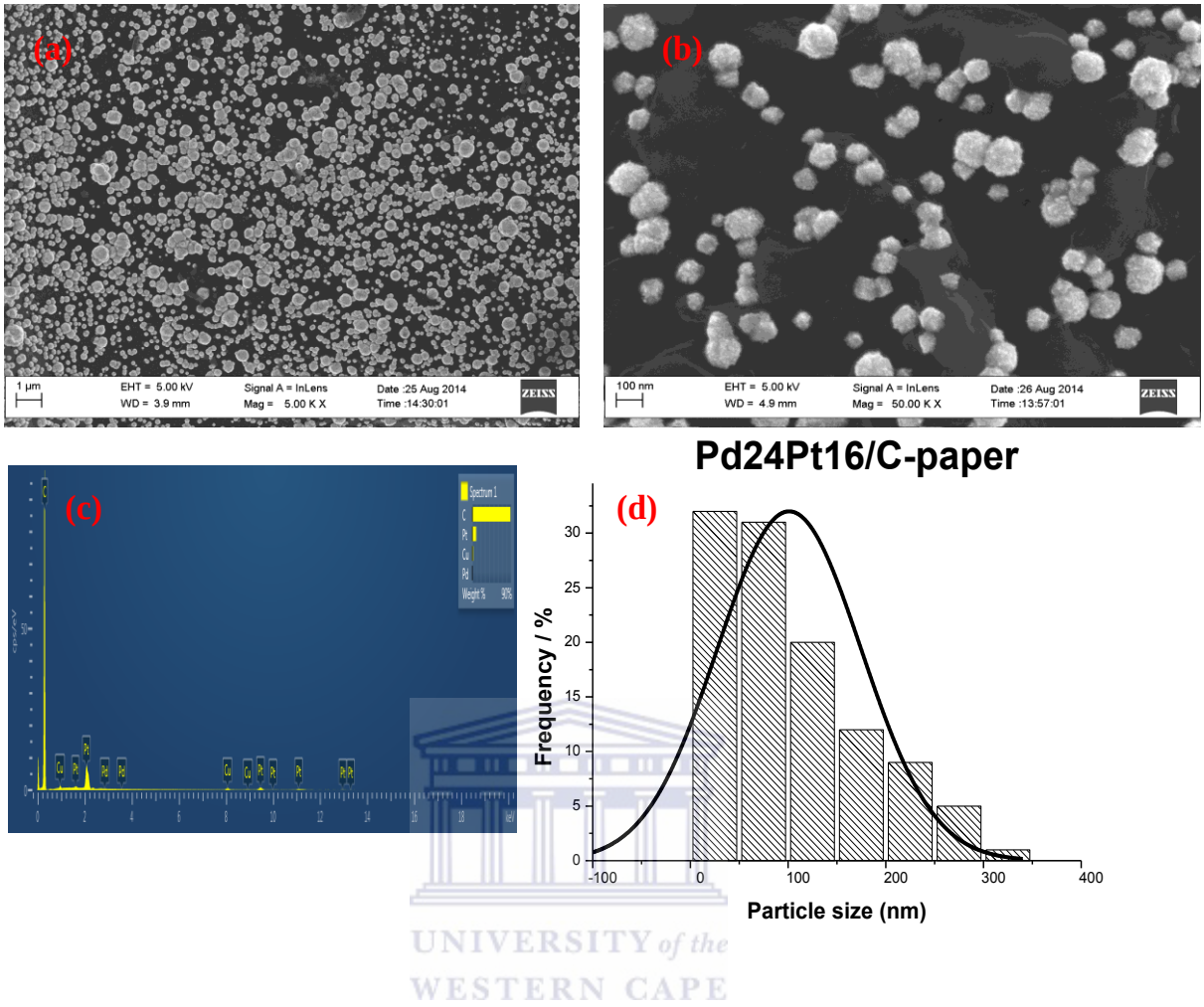

Figure 4.14: HRSEM morphological structure after 24 codeposition cycles of palladium-platinum on carbon paper (Pd24Pt24 codeposition/Carbon-paper) at (a) low and (b) high magnification, (c) EDX for Pd24Pt24 codeposition/Carbon-paper and (d) histogram image of Pd24Pt24 Codeposition/Carbon-paper.

Figure 4.15 (a) low and (b) high magnifications show the distributed particles of Pd24Pt16 on carbon paper. The particles are well distributed on the surface of the substrate. As it can be clearly seen in (a), particles are presented in small and spherical shapes. At high-resolution images, a granular nature of the spherical and dendritic particles is also observed by [167]. The presence of Pd and Pt is confirmed by EDX (c), where Pt is observed at 2.1 keV and Pd at 2.9 keV. A bell-shaped histogram is observed in (d) which shows that most particles are distributed on the substrate. The particles size of 13 nm is observed in table 4.1. A large particle size ranging from 10-20nm was also displayed for the codeposition of Pd: Pt of 1:1 ratio by Jayashree et al [167].

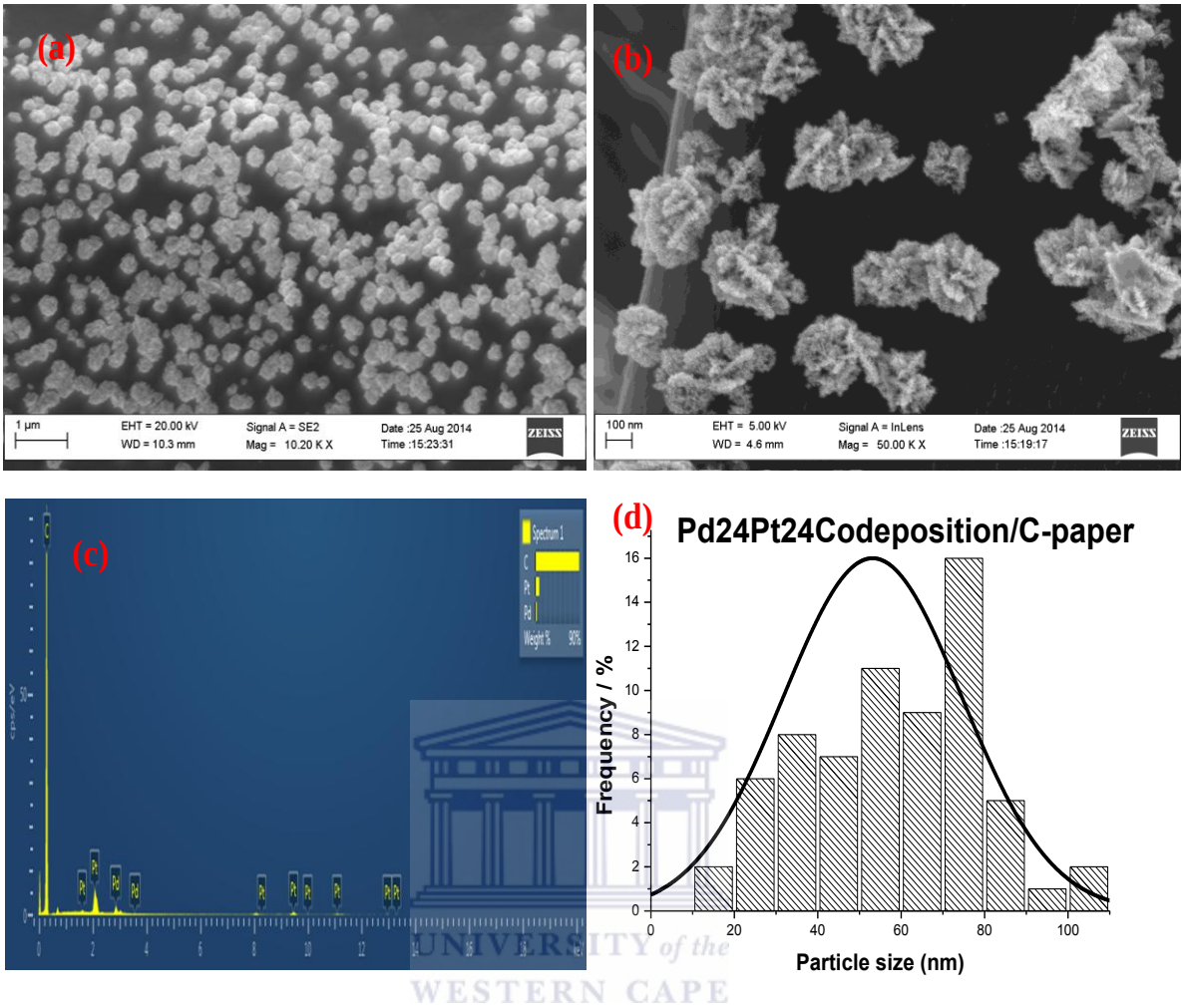

Figure 4.15: HRSEM morphological structure after 24 and 16 cycles of palladium-platinum on carbon paper (Pd24Pt16/Carbon-paper) at low (a) and (b) high magnification, (c) EDX for Pd24Pt16/Carbon-paper and (c) histogram image of Pd24Pt16/Carbon-paper.

Figure 4.16 shows Pd24Pt8/Carbon-paper particles in different magnifications, elementary analysis of Pd:Pt and the particle size. The particles are uniformly distributed. The particles are presented in both small and big spherical-dendrite shapes. Little agglomeration is observed in other areas of the carbon paper. Pt and Pd presence are observed in (c) at the peak of 2.1 keV, while the presence of Pd only is observed at 2.9 keV. The histogram that is observed in (d) shows the well distributed particles, although it was not easy to attain a consistent amount of 100 particles that are used to determine the particle size [167].

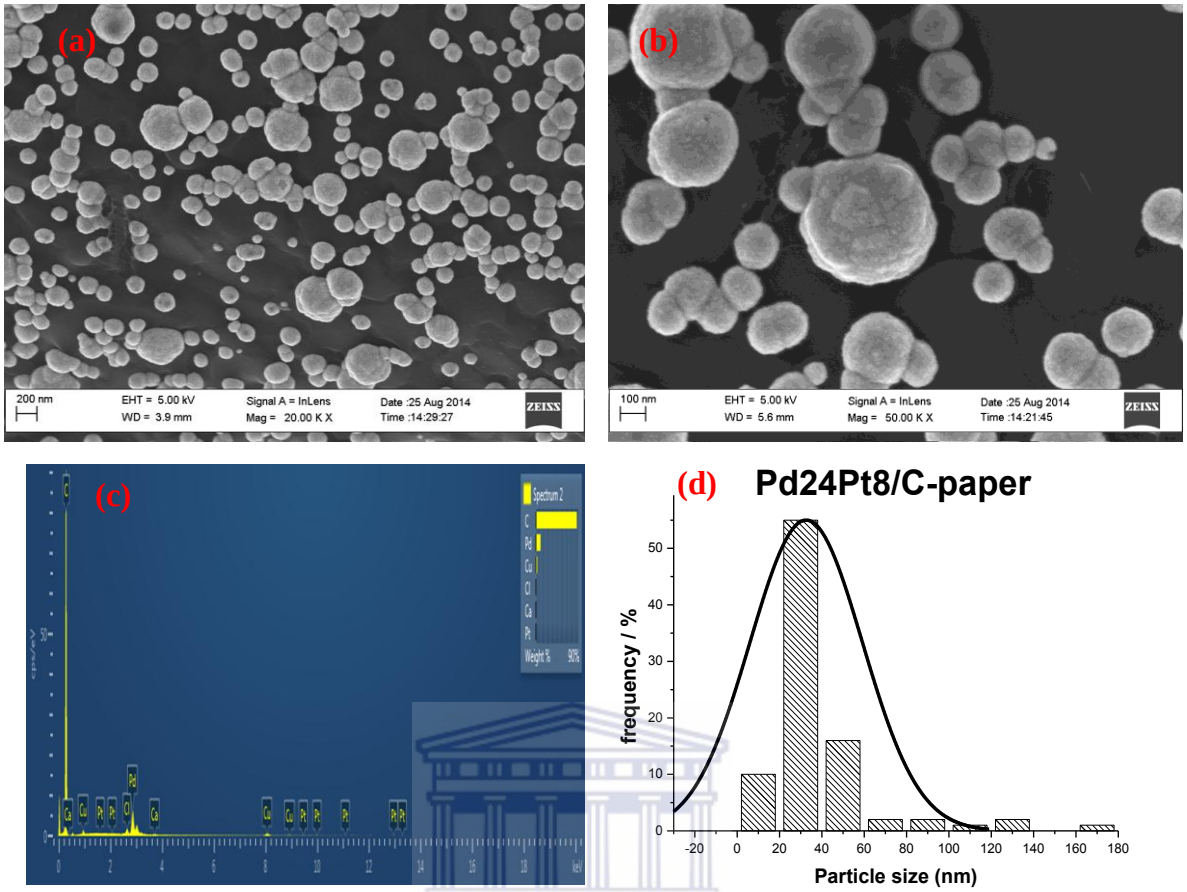

Figure 4.16: HRSEM morphological structure after 16 cycles of palladium-platinum on carbon paper (Pd24Pt8/Carbon-paper) at (a) low and (b) high magnifications, (c) EDX for Pd24Pt8/Carbon-paper and (d) histogram image histogram image of Pd24Pt8/Carbon-paper.

4.1.4 Summary of particle size and particle distribution of the catalyst

From the SEM analysis nanostructured Pt/C-paper have a mean particle size of 4.25nm, followed by Pt24Pd24/Carbon-paper with a mean particle size of 10 nm. The Pd24Pt24/C-paper codeposition also showed a better mean particle size of 11nm. This suggests a good catalyst performance. The EDX agreed with SEM results, although there was an excess Pt shown on the other areas of the carbon paper.

4.2 ELECTROCHEMICAL EVALUATION OF THE PREPARED ELECTROCATALYSTS: ORR ACTIVITY

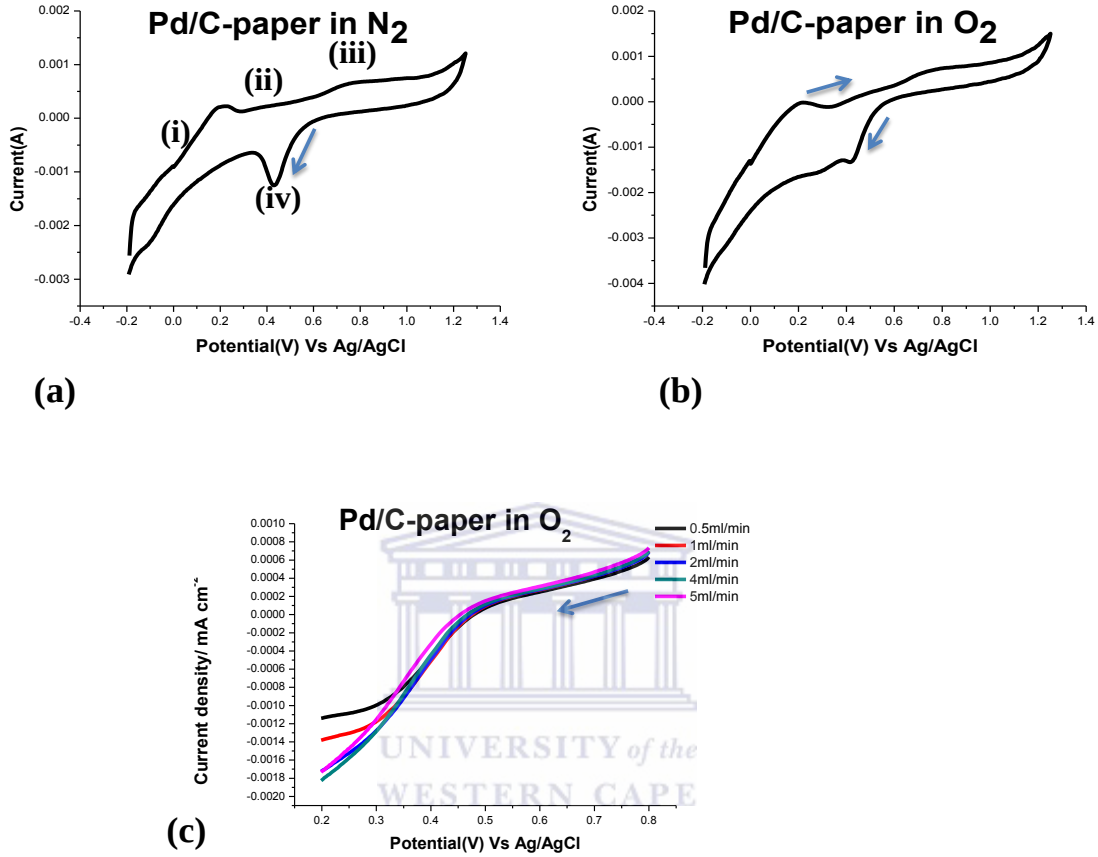

Figure 4.17: Cyclic voltammetry of palladium on carbon paper (Pd/Carbon-paper) in 0.1M $HClO_4$ under (a) N_2 and (b) O_2 saturation, at the scan rate of 50mV/s. linear sweep voltammetry (LSV) (c) of Pd/Carbon-paper in O_2 saturated 0.1M $HClO_4$ at various flow rates. Scan rate = 5mV/s.

The figure 4.17 (a) and (b) shows the typical cyclic voltammetry plots of Pd/Carbon-paper in N_2 and O_2 saturated 0.1M $HClO_4$, respectively. The voltammetry plots were recorded at a fixed scan rate of 50mV/s. In (a), nitrogen indicates plain results of Pd/Carbon-paper and (b) represents the performance of Pd/Carbon-paper in oxygen. As it can be seen in (a) and (b), not all Pd peaks are well defined. The following peaks are observed: (i) hydrogen desorption peak, where hydrogen is desorbed from the Pd surface, (ii) double layer region, (iii) formation of palladium oxide (PdO) and (iv) Pd oxide reduction peak. The hydrogen adsorption peak is not accurately observed on the surface of Pd in (a) and (b), due to the

fact that some hydrogen penetrates into the palladium lattice structure [155]. The Pd-hydride desorption peak appear from -0.2 V to 0.25 V. The double layer region appears from 0.341V to 0.58V, Pd-oxide formation appears from 0.05 V to 0.91 V and Pd-oxide reduction peak appears from 0.66V to 0.30V. The Pd/Carbon-paper has a small electro-active surface (ECSA) area of 14.8 $cm^2g\text{-}^1$, similar to that observed on Pd/Carbon [166].

The figure 4.17 (c) show an LSV for Pd/C-paper, the onset potential and the current density are represented in table 4.2. This is done in order to display the activity of Pd/Carbon-paper in ORR. The optimum flow rate of 5ml/min was chosen for evaluating the ORR activity of all catalysts. The onset potential of 504 V and maximum current density of 0541 mA/cm^2 indicate that Pd/C-paper showed a very weak ORR activity.

Table 4.2: The electrochemical surface area, onset potentials and maximum current densities for the prepared electrocatalysts.

Catalyst	**ECSA ($m^2\ g^{-1}$)**	**Onset Potential (V) vs Ag/AgCl**	**Maximum current density ($mA\ cm^{-2}$)**
Pd/Carbon-paper	14.8	0.504	0.541
Pt/Carbon-paper	78.4	0.548	0.289
Pd8Pt8/Carbon-paper	28.8	0.546	0.612
Pt8Pd8/Carbon-paper	32.4	0.584	0.363
Pd16Pt16/Carbon-paper	40.5	0.582	0.880
Pt16Pd16/Carbon-paper	63.4	0.725	1.353
Pt24Pd24/Carbon-paper	101.2	0.901	1.980
Pd24Pt24/Carbon-paper	48.5	0.701	1.376
Pd16Pt8/Carbon-paper	53.9	0.581	1.243
Pd24Pt16/Carbon-paper	64.1	0.741	1.354
Pd24Pt8/Carbon-paper	37.5	0.582	0.912
Pd16Pt16/Carbon-paper co-deposition	59.9	0.566	1.347
Pd24Pt24/Carbon-paper Co-deposition	83.8	0.591	1.956

The figure 4.18 shows the cyclic voltammetry of Pt/Carbon-paper in (a) N_2 and (b) O_2 saturation. The schematic diagrams represented in (a) shows well defined Pt peak, while in (b) not all peaks are well defined. It is observed in (b) that hydrogen adsorption peak is not accurately defined. This is caused by the technical error that occurred during the deposition. HRSEM images also showed little deposition that occurred on the surface of the carbon paper. The hydrogen desorption peak appears from -0.55V to 0.36V, double layer region appears from 0.41V to 0.54V, Pt-oxide formation appears from 0.59V to 0.75V and Pt reduction peak appears at 0.61V to 0.30V. The large electro-active surface area of 78.4 cm^2 g^{-1} for Pt/Carbon-paper confirms the small particles size that is obtained from HRSEM [166].

The linear sweep voltammetry of Pt/Carbon-paper represented in figure 4.18 (c) shows the activity of Pt in ORR. It is known that Pt/Carbon-paper shows high ORR activity in acid medium [166]. The table 4.2 presented shows less current density (0.289 mA/cm^2) and more onset potential (0.548 V). This means Pt/Carbon-paper showed very weak ORR activity compared to Pd/Carbon-paper (figure 4.17). This is confirmed by HRSEM images which indicated less quality deposition and large particle size than observed in other studies [163].

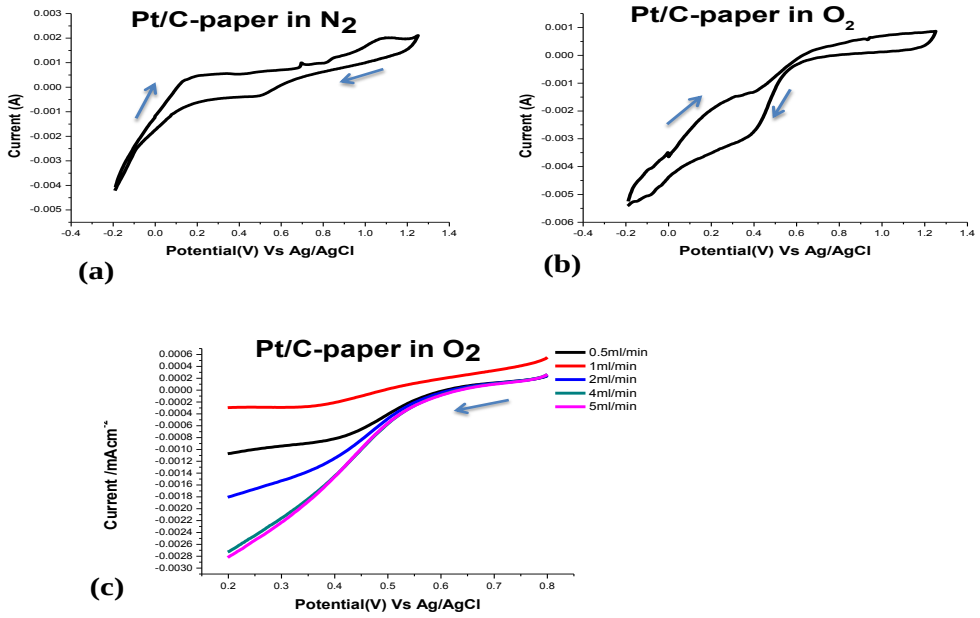

Figure 4.18: Cyclic voltammetry of platinum on carbon paper (Pt/Carbon-paper) under (a) N_2, (b) O_2 and (c) LSV for Pt/Carbon-paper saturated 0.1M $HClO_4$ at the scan rate of 50mV/s.

The figure 4.19 (a) and (b) show the cyclic voltammogram of Pd8Pt8/Carbon-paper respectively in N_2 and O_2 saturation. The peaks of Pd8Pt8/Carbon-paper in (a) and (b) are observed, although not all peaks are well defined, due to less quality deposition as it was shown in SEM images. The potential in oxygen reduction is slightly moving towards the negative side, which indicates a small increase in the reduction of Pd-oxide layer. The Pd-oxide reduction peak appears from 0.6V to 0.21V. The small electro-active surface area of Pd8Pt8/C-paper is 28.8 m^2 g^{-1}.

The LSV's represented in figure 4.19 (c) shows the ORR activity of Pd8Pt8/C-paper in 0.1M $HClO_4$. The flow rate of 2ml/min is not recorded in the LSV, because it was very close to1ml/min. A slight positive onset potential and positive current density is seen in table 4.2. The onset potential of Pd8Pt8 is 0.546 V and the current density is 0.612 mA/cm^2. Although there is a little increase observed in figure 4.19 (c), this indicates that 8 deposition cycles of PdPt/Carbon-paper are not enough to show high ORR activity. The large particle size of Pd8Pt8/Carbon-paper which indicates weak catalytic activity was also displayed by HRSEM.

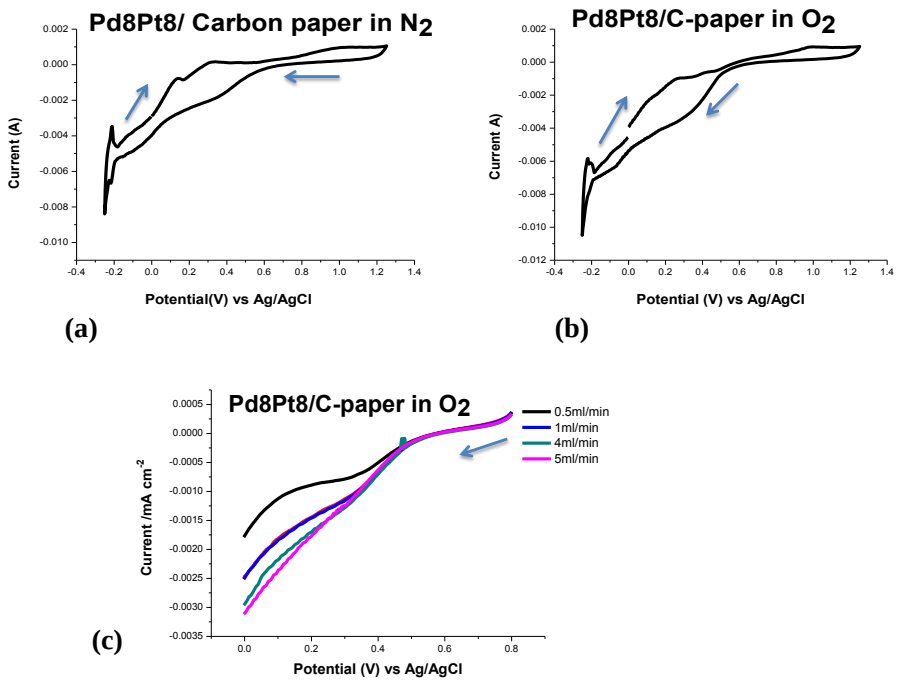

Figure 4.19: Cyclic voltammetry for 8 cycles of palladium- platinum on carbon paper (Pd8Pt8/Carbon-paper) under (a) N_2, (b) O_2 saturation and (c) LSV for Pd8Pt8/Carbon-paper at the scan rate of 50mV/s.

The cyclic voltammogram of P8Pd8/Carbon-paper is represented in figure 4.20 (a) and (b) respectively in N_2 and O_2. As it can be observed in (a) and (b), the peaks are not accurately defined. The reduction peak is observed at 0.36V to 0.20V. This indicates that Pt8Pd8/C-paper is weak in braking the oxygen-oxygen (O—O) bonds. There is a little increase in the electro-active surface area of 32.4 m^2 g^{-1} for Pt8Pd8/Carbon-paper showing that, when Pt is deposited as the first metal there is a uniform deposition than when palladium is deposited as the first metal. This behavior can be explained by the ligand effect, density functional theory (DFT) [169] and bifuntional mechanism [170, 171.].

The figure 4.20 (c) shows a slight increase in Pt8Pd8/C-paper onset potential and current density. The onset potential is 0.584 V and current is 0.636 mA/cm^2 as it is shown in table 4.2. A small flow rate of 1ml/min shows an unknown error that occurred during the analysis. Pt8Pd8/Carbon-paper shows a slight increase towards the positive current density and the onset potential.

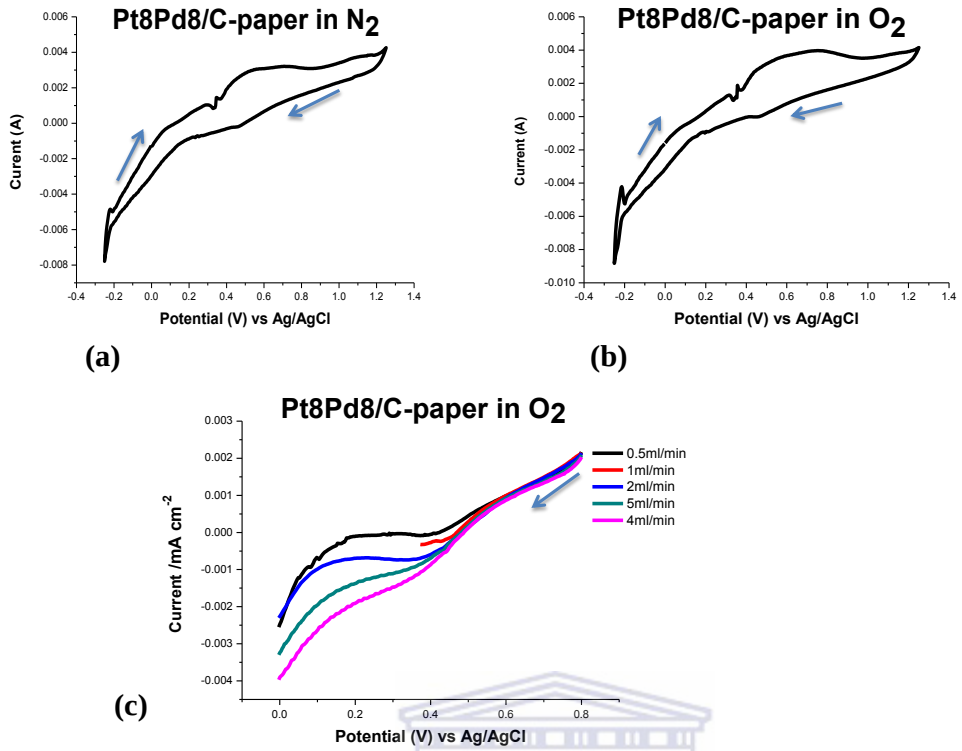

Figure 4.20: Cyclic voltammetry of platinum-palladium on carbon paper (Pt8Pd8/Carbon-paper) under (a) N_2, (b) O_2 condition and (c) LSV for Pt8Pd8/Carbon-paper in 0.1M $HClO_4$ at the scan rate of 50mV/s.

The figure 4.21 shows the cyclic voltammogram of Pd16Pt16/Carbon-paper, respectively in (a) N_2 (plain results) and (b) O_2 saturation. The Pd16Pt16/Carbon-paper show well distinct peaks. The hydrogen desorption, where desorption of hydrogen from the surface of PdPt occurs, double layer region, PdPt-oxide formation, PdPt reduction and hydrogen adsorption on PdPt surface .In (b) the PdPt-hydride peak appears at the potential from-0.24V to 0.065V, double layer region appears from -0.13V to 0.007V, PdPt-oxide formation appear from 0.05V to 0.43V, oxide reduction peak appears from 0.9V to 0.48V and the peak at -0.1V to -0.24V may be attributed to hydrogen adsorbed on PdPt surface. The electro-active surface area of Pd16Pt16 is 40.5 m^2 g^{-1} which is slightly showing an increase compared to the 8 deposition cycles shown in figure 4.19 and figure 4.20 as it is observed in table 4.2.

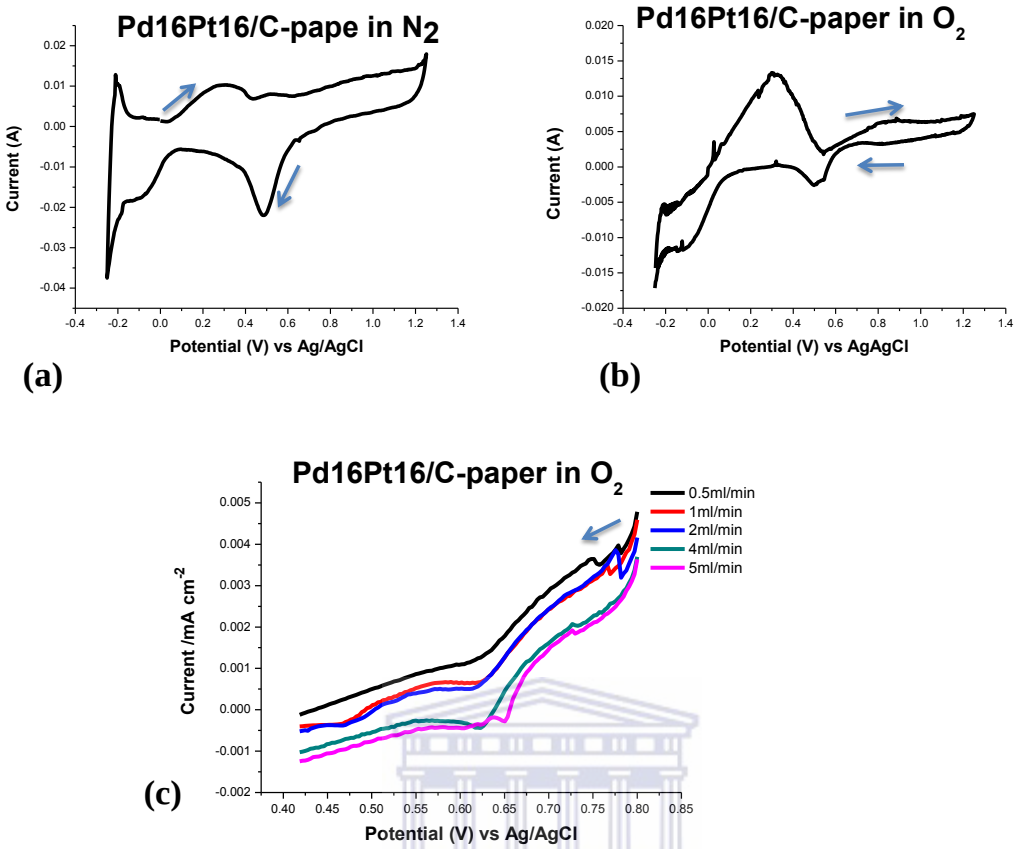

Figure 4.21: Cyclic voltammetry for 16 cycles of palladium- platinum structure on carbon paper (Pd16Pt16/Carbon-paper) under (a) N_2, (b) O_2 and (c) LSV for Pd16Pt16/Carbon-paper saturated 0.1M $HClO_4$, at the scan rate of 50mV/s.

The cyclic voltammetry in figure 4.22 shows Pt16Pd16/Carbon-paper in (a) N_2 and (b) O_2 respectively. A bend increase at -0.05V for anodic oxidation of PdPt/Carbon-paper is observed. *Rikkinen at al* [164] also observed such an increase in the anodic peak for Pd-oxide formation on Pd/Carbon-paper prepared using atomic layer deposition method compared to the commercial Pd/C. The oxide reduction peak of Pt16P16/Carbon-paper appears at the potential from 0.9V to 0.40V. This indicated that Pt16Pd16/Carbon-paper is fast in reducing the oxygen –oxygen (O-O) bonds.

The ORR activity of Pt16Pd16/Carbon-paper is presented in figure 4.22 (c) in 0.1 M $HClO_4$. The LSV's of Pdt16Pd16 shows a good quality ORR activity which is also confirmed by the small particle size obtained in HRSEM [172]. The onset potential of

Pt16Pd16 is 0.725V and the current density is 1.356 mA/cm^2. This suggests that Pt16Pd16/Carbon-paper is a good ORR catalyst.

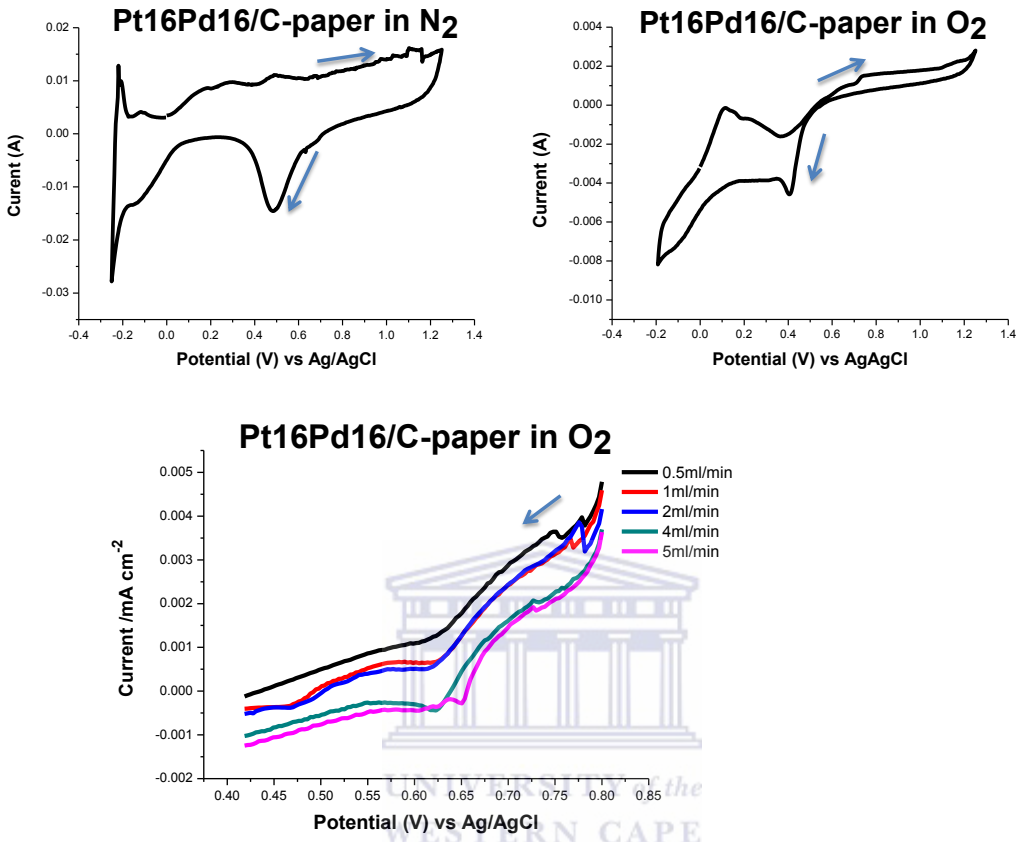

Figure 4.22: Cyclic voltammetry for 16 cycles of platinum-palladium structure on carbon paper (Pd16Pt16/Carbon-paper) in (a) N_2, (b) O_2 conditions and (c) LSV for Pt16Pd16/Carbon-paper, at the scan rate of 50mV/s.

The cyclic voltammetry of Pd16Pd16 codeposition/Carbon-paper is represented in figure 4.23 (a) and (b) respectively in N_2 and O_2. The PdPt-oxide formation is observed at the potential from 0.05V to 0.44V and the PdPt oxide reduction peak appears from 0.8V to 0.43V. The shift in the potential towards the negative side suggests a fast reduction of oxygen bonds on the surface of PtPd [172]. A slight decrease in electrochemical surface area of 59.9 $m^2 g^{-1}$ for Pd16Pt16codeposition/Carbon-paper is seen in table 4.2.

The LSV presented in figure 4.23 shows the ORR activity of Pd16Pt16/Carbon-paper in acid medium. The onset potential of Pd16Pt16codeposition/Carbon-paper is 0.582 V and the current density is 0.880 mA/cm^2. This suggests that the ORR activity of

Pd16Pt16codeposition/Carbon-paper has increased relative to the results in figure 4.21 and 4.22 [167].

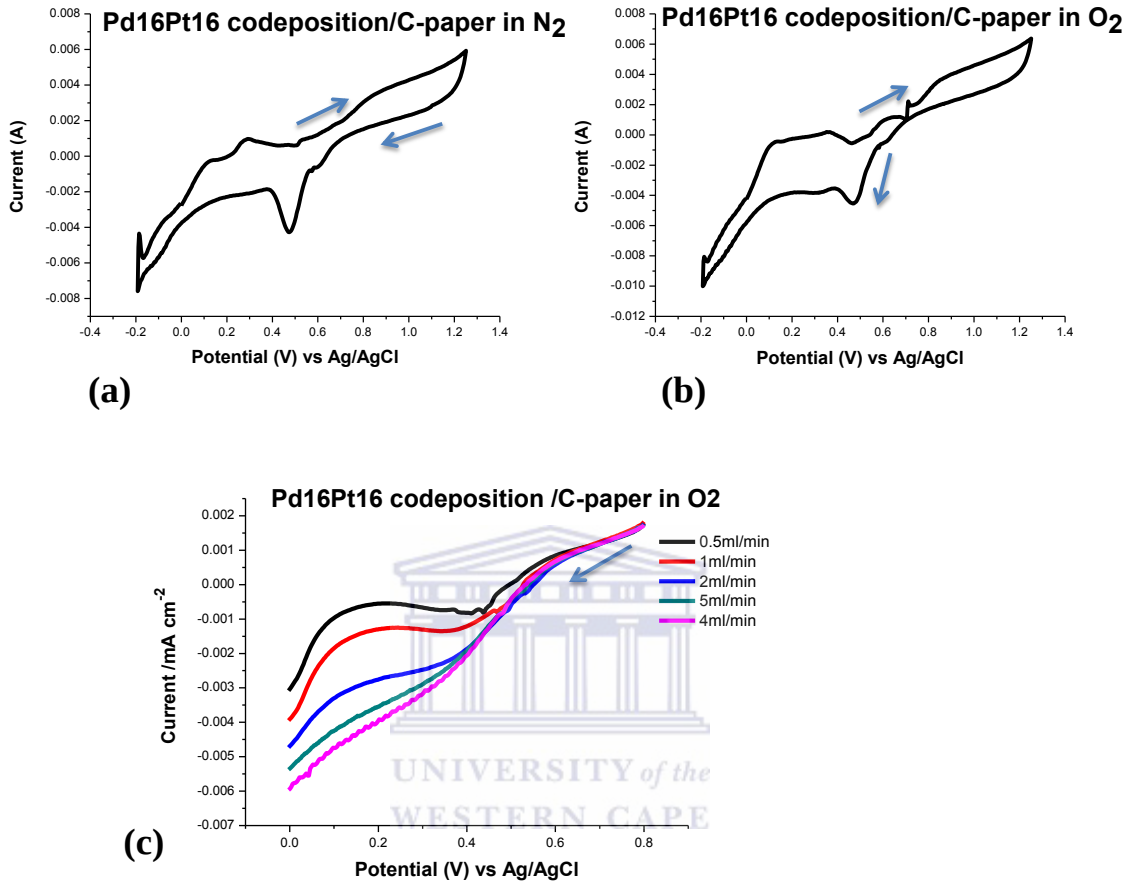

Figure 4.23: Cyclic voltammetry for 16 Codeposition cycles of bimetallic palladium-platinum structure on carbon paper (Pd16Pt16 codeposition/Carbon-paper) under (a) N_2, (b) O_2 and (c) LSV for Pd16Pt16/Carbon-paper in 0.1M $HClO_4$ at the scan rate of 50mV/s.

In figure 4.24 (a) and (b) respectively, the inset illustrates Pd16Pt8/Carbon-paper in N_2 and O_2.The oxide formation of Pd16Pt8/Carbon-paper appears from 0.05V to 0.45V, the Pd16Pt8 oxide reduction peak appears from 0.80V to 0.42V. The Pd16Pt8/Carbon-paper O_2 also shows a move towards the negative potential. The electrochemical surface area of Pd16Pt8 has decreased to the value of 53.9 m^2 g^{-1}. The ORR activity of Pd16Pt8/Carbon-paper is also shown in (c), where the onset potential is 0.581 V and the current density is 1.243 mA/cm^{-2}.

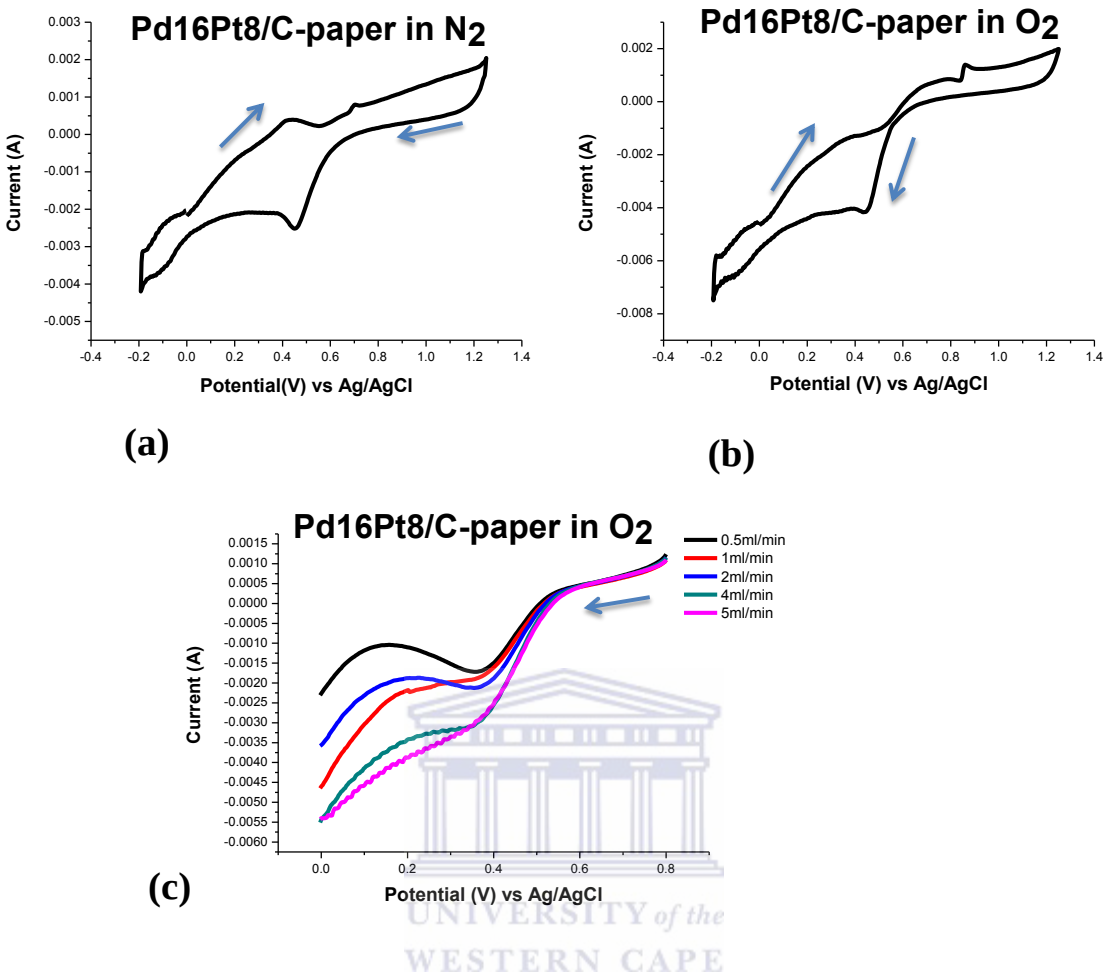

Figure 4.24: Cyclic voltammetry of 16 and 8 cycles for palladium- platinum structure on carbon paper (Pd16Pt8/Carbon-paper) under (a) N_2, (b) O_2 conditions and (c) LSV for Pd16Pt8/Carbon-paper at the scan rate of 50mV/s.

The representative peaks associated with Pd24Pt24/Carbon-paper catalysts are displayed in figure 4.25, respectively in N_2 and O_2 saturation. The anodic peak starting from -0.24V to 0.15V is attributed to the hydrogen that is desorbed on the surface of Pd24Pt24/Carbon-paper, double layer appears from 0.17V to 0.44V. The formation of P24Pt24-oxide appears from 0.49V to 0.85V, oxide reduction peak appears from 0.89V to 0.43V and the peak at 0.1 to -0.2 is attributed to the hydrogen adsorbed on the surface of Pd24Pt24/Carbon-paper. There is a great potential moving to the negative observed in (c) which suggests that oxygen bonds on the surface of Pd24Pt24/Carbon-paper were reduced. A decrease in the electrochemical surface area of 48.5 $m^2\ g^{-1}$ for Pd24Pt24/Carbon-paper is observed which may be attributed to the agglomeration that is indicated by HRSEM [165].

Figure 4.25 (c) shows LSV's for Pd24Pt24/Carbon-paper in O_2 saturated. A slight increase in the ORR activity of Pd24Pt24/Carbon-paper is observed. The onset potential is 0.701V and the current density is 1.376 mA/ cm^2. The weak activity of Pd24Pt24/Carbon-paper is caused by the high agglomeration which also made it difficult to determine the particle size as shown in HRS

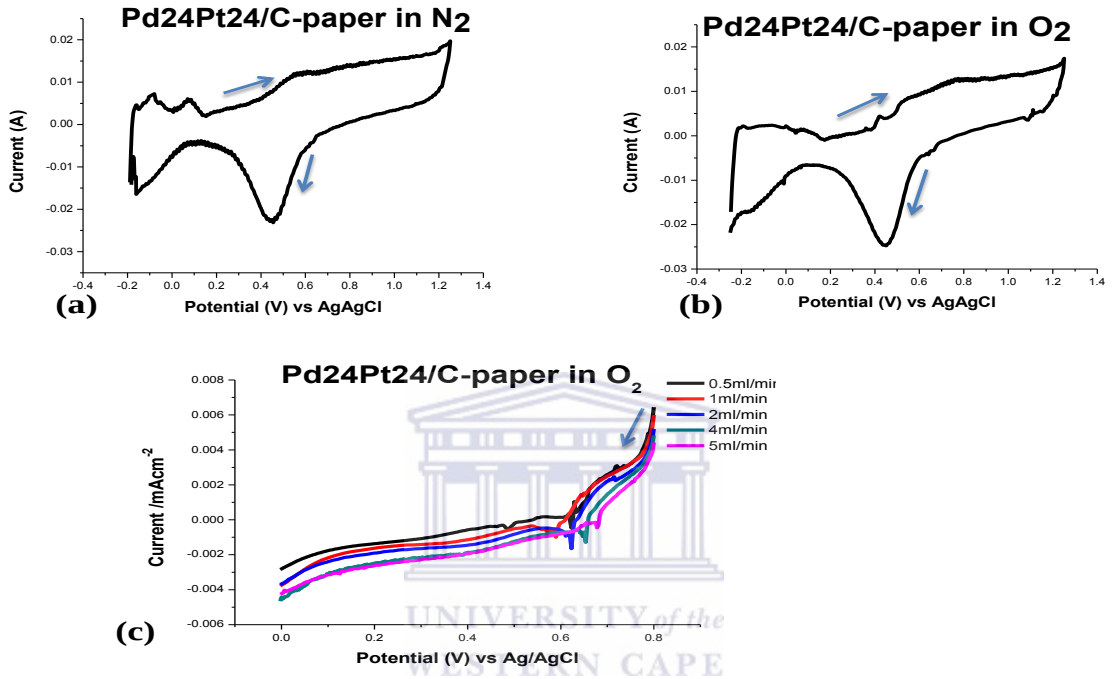

Figure 4.25: Cyclic voltammetry of 24 cycles of bimetallic palladium- platinum structure on carbon paper (Pd24Pt24/Carbon-paper) under (a) N_2 and (b) O_2 saturation 0.1M $HClO_4$, at the scan rate of 50mV/s.

The figure 4.26 shows the cyclic voltammogram of Pt24Pd24/Carbon-paper in (a) N_2 (plain results) and (b) O_2 saturation, respectively. The Pt24Pd24/Carbon-paper display well defined peaks. The hydrogen desorption peak, double layer region, PdPt-oxide formation, PdPt-oxide reduction peak and hydrogen adsorption on PdPt surface. The PdPt-hydride peak appears at the potential from -0.20V to 0.071V, double layer region appears from 0.19V to 0.44V. The formation of PdPt-oxide appears from 0.50V to 1.07V, oxide reduction peak appears from 0.94V to 0.45V and the peak at -0.1V to -0.24V may be attributed to hydrogen adsorbed on PdPt surface. A high increase in electro-active surface area of 101.2 $m^2 g^{-1}$ for Pt24Pd24/Carbon-paper may be attributed to the optimal number of deposition cycles.

Figure 4.26 shows the LSV's of Pt24Pd24/Carbon-paper in O_2 saturated $HClO_4$. The onset potential of Pt24Pd24/Carbon-paper is 0.901V and maximal current density is 1.980 mA/cm^2. This indicates that Pt24Pd24/Carbon-paper is a very good ORR catalyst in acid medium which suggests that Pt24Pd24/Carbon-paper deposited by electrochemical atomic layer deposition (ECALD) is the optimal. The HRSEM also confirmed a strong activity of Pt24Pd24/Carbon-paper with small particles size.

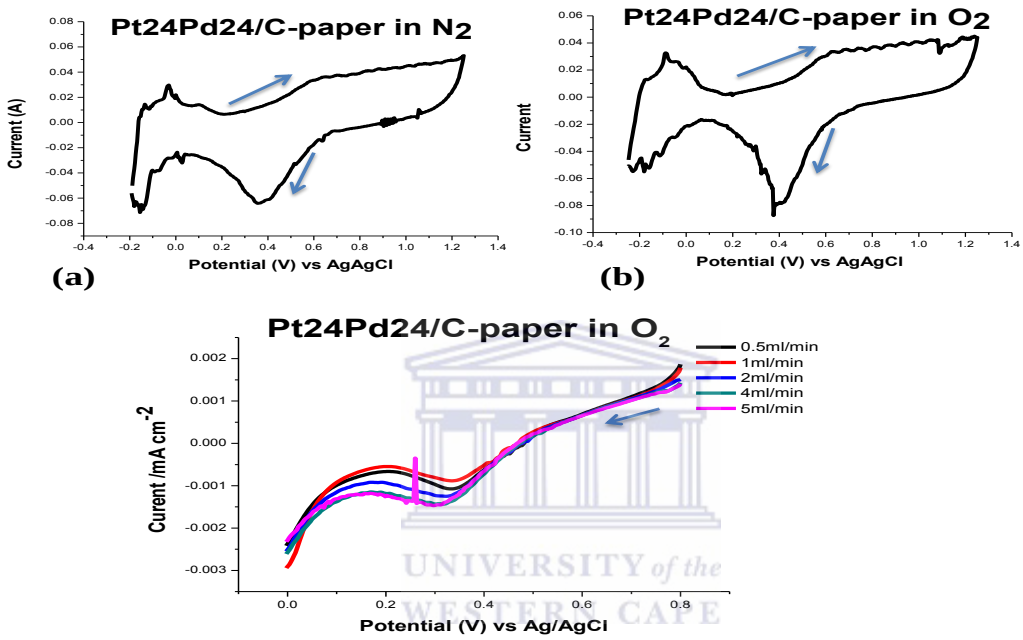

Figure 4.26: Cyclic voltammetry for 24 cycles of platinum- palladium structure on carbon paper (Pt24Pd24/Carbon-paper) under (a) N_2 and (b) O_2 conditions in 0.1 M $HClO_4$ at the scan rate of 50mV/s.

The cyclic voltammetry showed in figure 4.27 display Pd24Pt24codeposition/Carbon-paper in (a) N_2 and (b) O_2, respectively. The peaks are all defined. The Pd24Pt24 codeposition shows great performance as it can be observed in (b). A strong oxide peak is also observed in the potential range from 0.49V to 0.81V and the reduction peak appears from 0.94V to 0.50V. The reduction peak moves towards the negative potential. This indicates that Pd24Pt24 codeposition shows good performance under oxygen saturation. The electro-active surface area of Pd24Pt24 codeposition/Carbon-paper is 83.8 $m^2 g^{-1}$.

The figure 4.27 (c) shows the LSV's of Pd24Pt24codeposition/Carbon-paper in O2 saturated 0.1M $HClO_4$. The onset potential of Pd24Pt24/Carbon-paper appears at 0.591 V

and maximum current density appears at 1.956 mA/cm^2. This indicated that Pd24Pt24codeposition/Carbon-paper has higher ORR activity compared to Pd16Pt16 codeposition/Carbon-paper (figure 4.23).

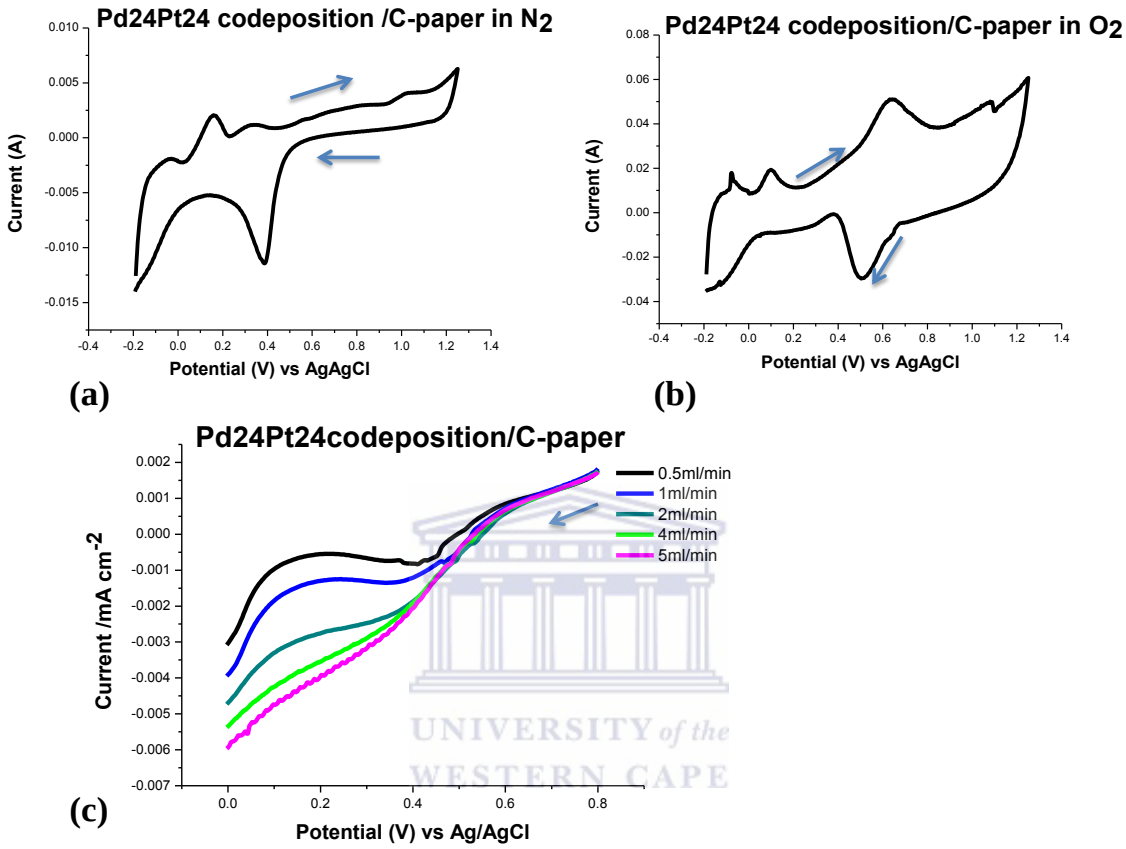

Figure 4.27: Cyclic voltammetry for 24 codeposition cycles of palladium- platinum structure on carbon paper (Pd24Pt24 codeposition/Carbon-paper) under (a) N_2 and (b) O_2 saturation in 0.1M $HClO_4$ at the scan rate of 50mV/s.

The figure 4.28 shows the CV's of Pd24Pt16/Carbon-paper in (a) N_2 and (b) O_2. An increase in the anodic oxide formation peak is observed in (b) from 0.05V to 0.44V. A broad peak is formed during the reverse scan starting from 0.94V to 0.44V, which indicates the reduction of Pd24Pt16-oxide layer. The Pd24Pt16/Carbon-paper showed good activity in reducing oxygen. The electro-active surface area of Pd24Pt8/Carbon-paper is 64.1 $m^2\ g^{-1}$ which is much better compared to the codeposition of Pd16Pt16/Carbon-paper figure 4.24. In addition figure 4.28 also shows the LSV's for Pd24Pt16/Carbon-paper in O_2. The onset potential for Pd24Pt16 and current density has increased to 0.741V and

1.354 mA/ cm^2 compared to Pd16Pt8/Carbon-paper (figure 4.24) due to the fact the their ratios are the same (2:1). However, this is not the optimal deposition cycles for ORR activity.

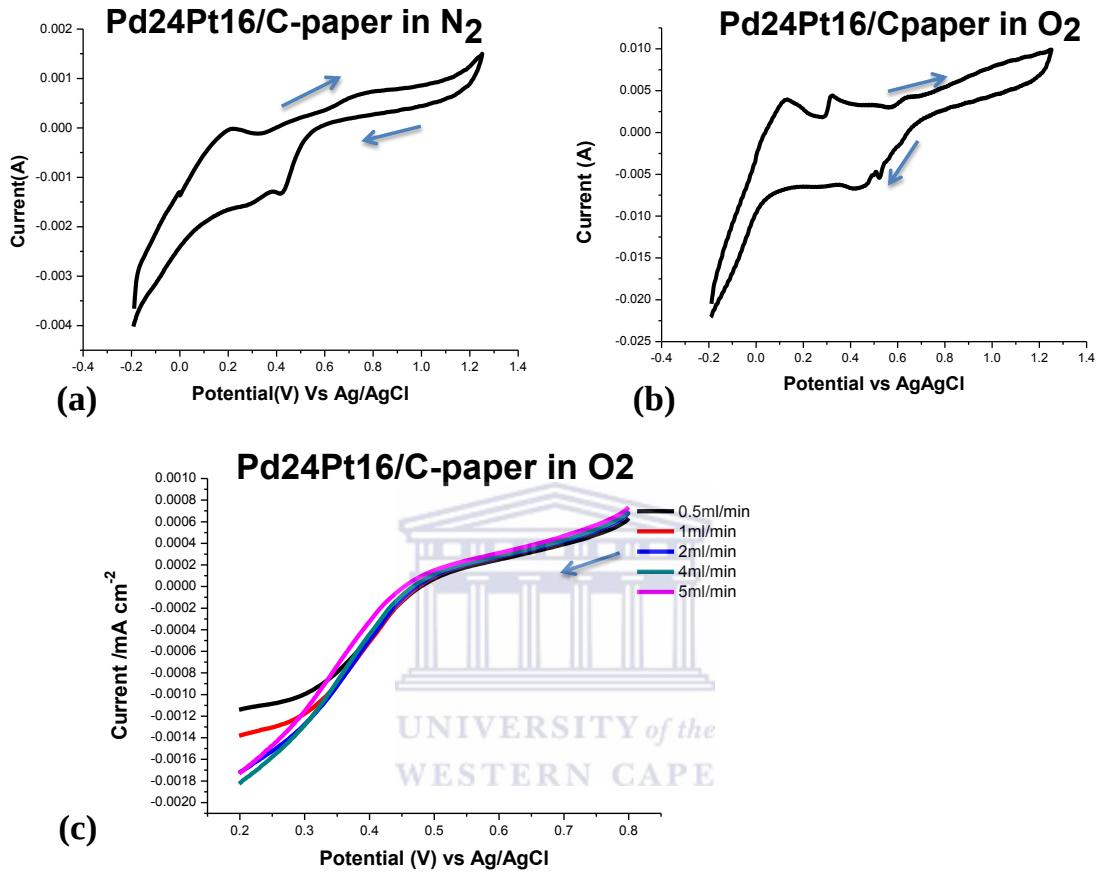

Figure 4.28: Cyclic voltammetry for 24 and 16 cycles of palladium- platinum structure on carbon paper (Pd24Pt16 /Carbon-paper) under (a) N_2 and (b) O_2 saturation in 0.1M $HClO_4$, at the scan rate of 50mV/s.

The cyclic voltammetry for 3:1 of Pd-Pt is shown in figure 4.29 respectively in N_2 and O_2. The reduction peak is observed from 0.73V to 0.45V. This indicates the poor activity of Pd24Pt8/C-paper in reducing the oxygen bonds. A decrease of 37.5 m^2 g^{-1} for Pd24Pt8/C-paper confirms the large particle side that was observed in HRSEM.

Figure 4.29 represents the LSV's for Pd24Pt8/Carbon-paper in O_2, only four LSV's are shown due to technical problems. The onset potential and current density has decreased to

0.582V and 0.912mA/cm^2 which suggests that Pd24Pt8/Carbon-paper is not a good ORR catalyst.

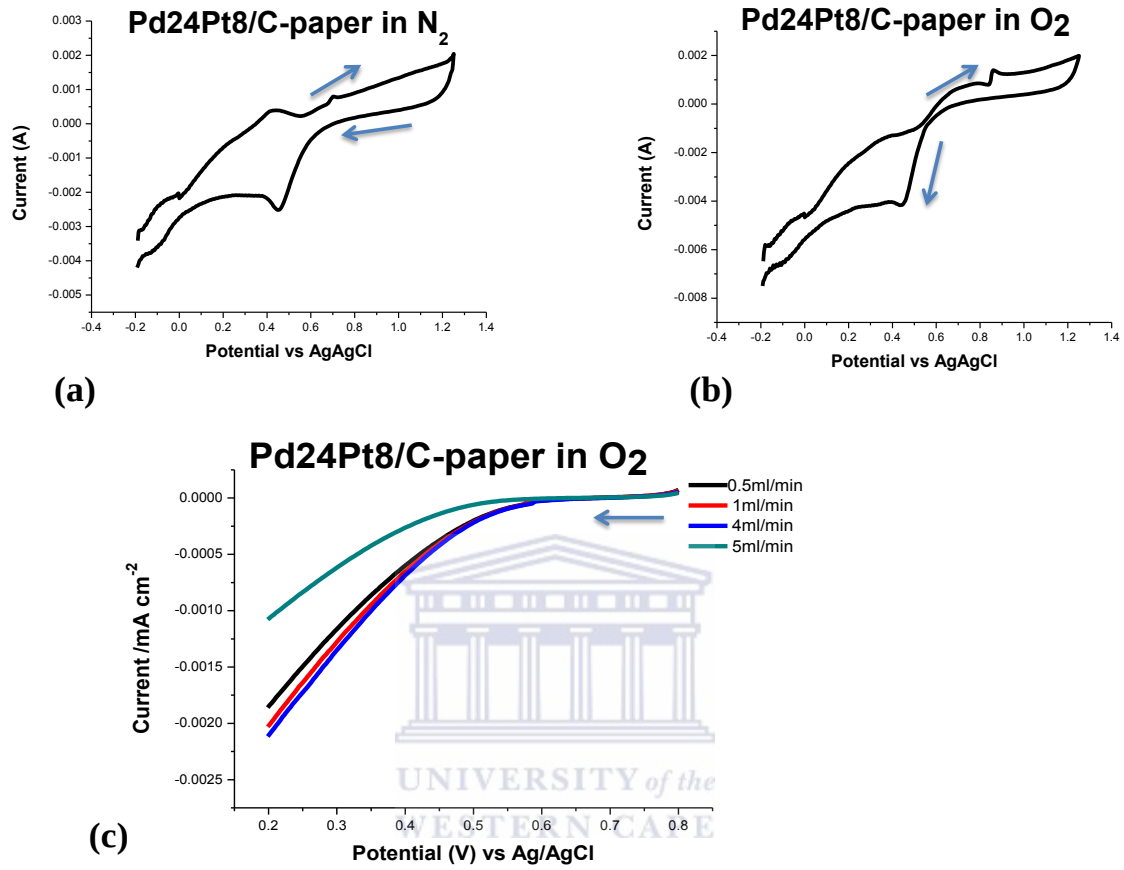

Figure 4.29: Cyclic voltammetry for 24 and 8 cycles of palladium- platinum structure on carbon paper (Pd24Pt8 /Carbon-paper) under (a) N_2 and (b) O_2 saturated 0.1M $HClO_4$ at the scan rate of 50mV/s.

4.3 Summary of ORR activities in the presence of methanol for the prepared catalysts.

The cyclic voltammetry (CV) and linear sweep voltammetry LVS) study shows that Pt24Pd24/Carbon-paper has a large surface area (101.2 m^2 g^{-1}), high onset potential (0.9V) and high current density (1.980 mA cm^{-2}). This indicated that Pt24Pd24/Carbon-paper is the best ORR binary catalyst which is in good agreement with the small particle size (10nm) that is observed in HRSEM.

4.3 ORR ACTIVITY IN THE PRESENCE OF METHANOL (POISONING STUDIES)

In this study the cathode catalysts that are methanol tolerant will be discussed according to their decreasing order of activity towards methanol. This is done in order to know which catalyst will not be affected by the cross-over process of methanol. Only five Pd based binary catalyst will be discussed, because they have shown improved ORR activities.

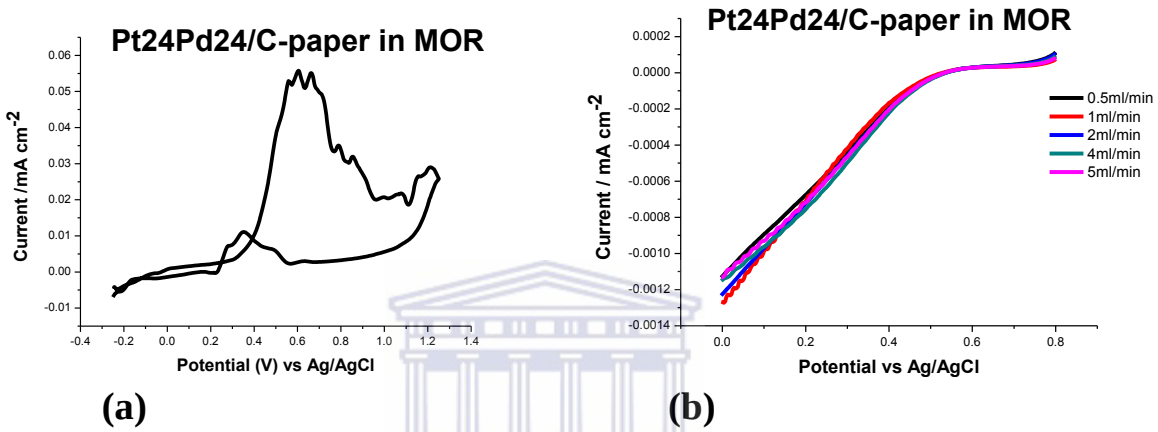

Figure 4.30: (a) Cyclic voltammetry of Pt24Pd24/Carbon-paper in 0.1M $HClO_4$ and 0.1M CH_3OH saturation and (b) is Linear sweep voltammetry (LVS) of Pt24Pd24/Carbon-paper.

The cyclic voltammetry of methanol oxidation reduction (MOR) for 1:1 of Pt-Pd is shown at 24 cycles figure 4.30 (a). The methanol oxidation peak and oxidation reduction peak of Pt24Pd24/Carbon-paper are clearly observed. The LSV's in (b) shows the activity of Pt24Pd24/Carbon-paper in methanol oxidation reactions. The optimal flow rate of 5ml/min is the one chosen to measure the methanol oxidation peak in all catalyst. The more positive onset potential appear at 0.576 V as seen in table 4.4 which shows that Pt24P24/Carbon-paper is a better catalyst for methanol oxidation reactions. There is no high methanol oxidation peak for Pt24Pd24/Carbon-paper observed as shown in table 4.4 which suggests the good activity of Pt24Pd24/Carbon-paper in methanol oxidation reaction. This means that Pt24Pd24/Carbon-paper is the best ORR catalyst for direct methanol fuel cell [174].

Table 4.4: The onset potentials for ORR electrocatalysts in methanol

Catalysts	Onset Potential (V) vs Ag/AgCl ORR in MOR	Onset Potential (V) vs Ag/AgCl ORR without MOR	Voltage difference (mV)
Pt24Pd24/C-paper	0.576	0.9	324
Pd24Pt24codeposition/C-paper	0.563	0.591	28
Pd24Pt16/C-paper	0.537	0.741	204
Pt16Pd16/C-paper	0.534	0.725	191
Pd16Pt16codeposition/C-paper	0.496	0.582	86

The cyclic voltammetry of methanol oxidation reactions for Pd24Pt24 codeposition/Cabon-paper is shown in figure 4.31(a). As compared to figure 4.30, it is observed from figure 4.31 (a) that there is a small observed methanol oxidation peak of Pd24Pt24codeposition/Carbon-paper. However, Pd24Pt24codeposition/Carbon-paper also showed good activity under methanol. The LSV shown in (b) also display the activity of Pd24Pt24 codeposition in MOR where the methanol oxidation peak is indicated by the onset potential of 0.563 V. This shows a little appearance of the methanol oxidation peak of Pd24Pt24 codeposition. However, Pd24Pt24 codeposition/Carbon-paper seems to have less activity than Pt24Pd24/Carbon-paper (figure 4.30) in methanol, which suggests that it is less affected by the presence of methanol crossing over to the cathode.

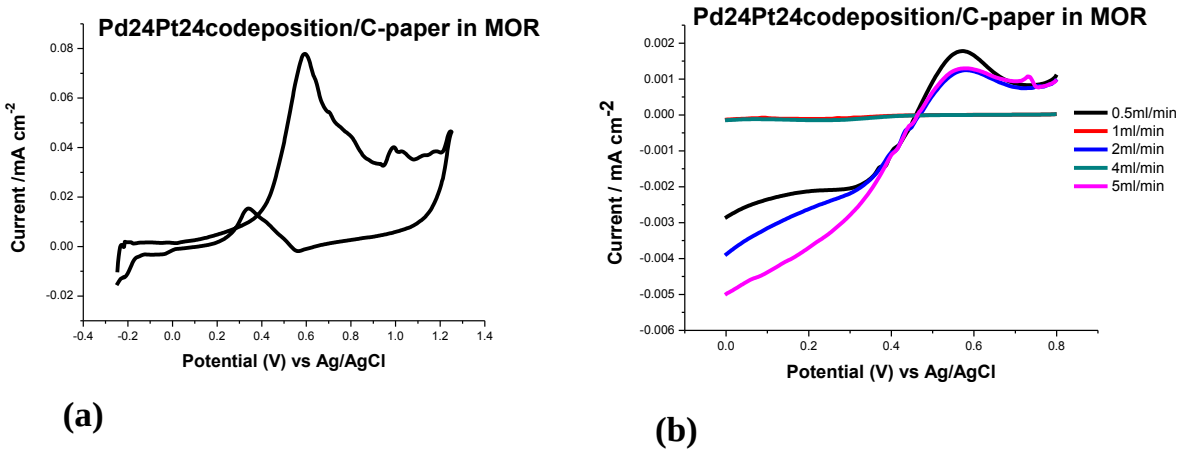

Figure 4.31: (a) Cyclic voltammetry (b) LSV's of Pd24Pt24codeposition/Carbon-paper in 0.1M $HClO_4$ and 0.1M CH_3OH saturation.

The methanol oxidation reaction of Pd24Pt16/Carbon-paper is shown in figure 4.32 (a) and (b) where the activity of Pd24Pt16/Carbon-paper in methanol seems to be decreasing. As it can be seen from (a), the methanol oxidation peak of Pd24Pt16/Carbon-paper is very broad and that shows a weak activity towards methanol. The figure 4.32 (b) shows the LSV's of Pd24Pt16/Carbon-paper where the methanol oxidation peaks at 1ml/min and 4ml/min cannot be clearly observed. The activity of Pd24Pt16/Carbon-paper is indicated by the methanol oxidation peak. The onset potential is 0.537 V which suggests that the activity of Pd24Pt16/Carbon-paper in methanol is decreasing.

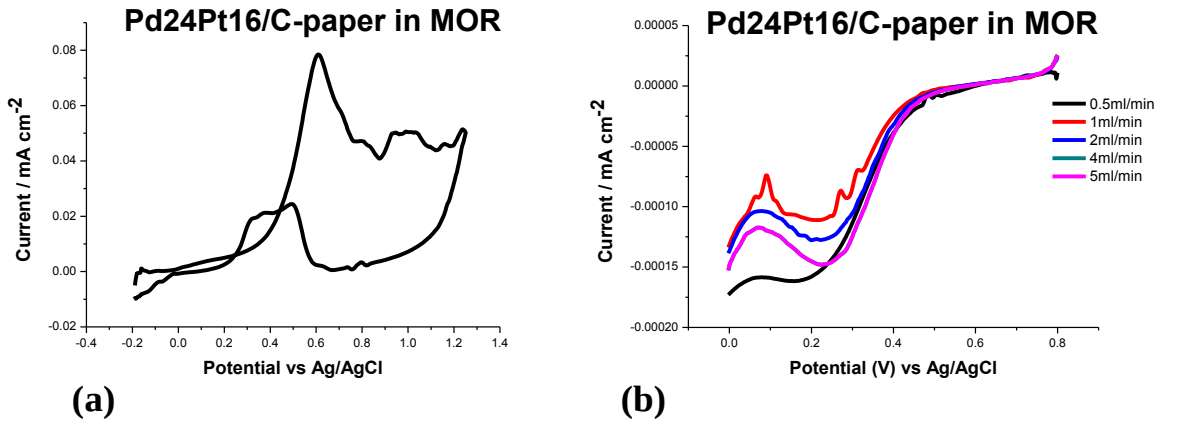

Figure 4.32: (a) Cyclic voltammetry and (b) LSV of Pd24Pt16/Carbon-paper 0.1M $HClO_4$ and 0.1M CH_3OH saturation.

The figure 4.33 shows a cyclic voltammetry for methanol oxidation reactions of Pt16Pd16/Carbon-paper. There is a high methanol oxidation peak of Pt16Pd16/Carbon-paper observed in (a) which indicates that Pt16Pd16/Carbon-paper is less active in methanol. The figure 4.32 (b) shows the LSV's of Pt16Pd16/Carbon-paper which are more towards the negative side. The onset potential of Pt16Pd16/Carbon-paper is 0.534 V. This suggests that Pt16Pd16/Carbon-paper has an increase in methanol oxidation peak which implies that the ORR of Pt16Pd16/Carbon-paper catalyst in the presence of methanol will be affected. The activity of this catalyst is less the same as that of Pd24Pt16/Carbon-paper in methanol.

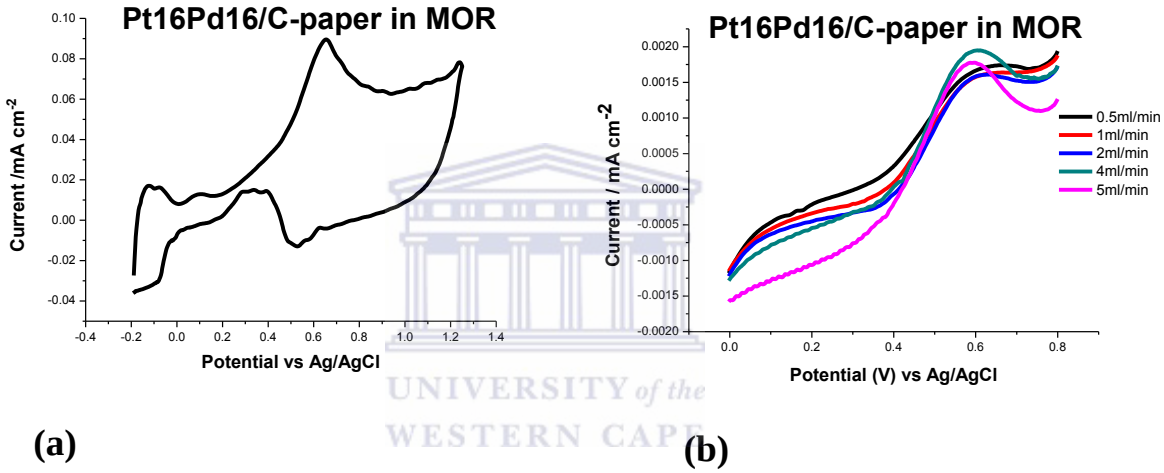

Figure 4.33: (a) Cyclic voltammetry and (b) LSV of Pt16Pd16/Carbon-paper 0.1M $HClO_4$ and 0.1M CH_3OH saturation.

The activity of Pd16Pt16codeposition/C-paper in methanol oxidation reactions is shown in figure 4.34 (a) and (b), respectively. The methanol oxidation peak observed in (a) is indicated by the onset potential of Pd16Pt16codeposition/C-paper which is 0.496 V. This suggests a good activity of Pd16Pt16codeposition/C-paper under methanol.

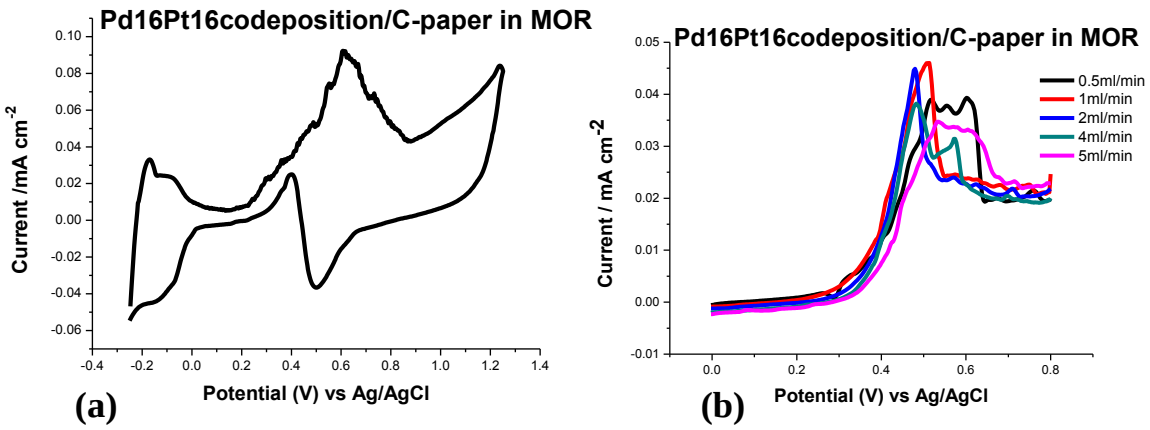

Figure 4.34: (a) Cyclic voltammetry (b) LSV of Pd16Pt16codeposition/C-paper 0.1M $HClO_4$ and 0.1M CH_3OH saturation.

4.4 THE ORR STUDIES: CALCULATION OF THE NUMBER OF ELECTRONS TRANSFERED

To number of electrons (Koutecky – Levich plot), which is represented as 1/i vs. $1/v^{-1/3}$ plot for oxygen reduction reaction at different potentials. The analysis was performed from the LSV's at potential 0.39V, 0.36V, 0.35V, 0.32V, and 0.30V. The K-L plots at E= 0.30V were taken for each catalyst and compared according to their ratios and first deposited metal. This potential was consistent for all catalysts. Analysis of the LSV curves to extract kinetic parameters related to ORR involved the following expression [155].

$$\frac{-1}{i} = \frac{1}{k} + \frac{1}{nAFZ_{O2}C_{O2}v^{-1/3}} \qquad (11)$$

The current kinetics were computerised using equation (11) where *i* is the current measure at the applied potential *E*, *v* it the linear velocity (m s^{-1}), C_O is the saturation concentration of O_2 (1.22 $x10^{-6}$ mol cm^{-3}), *n* is the number of electrons transferred and A is the surface area of the electrode. The experimental curves show a linear relation between 1/i and $1/ v^{-1/3}$ which indicates that Pt/C-paper and Pd/C-paper follow *n* = 4 as described in the literature [70].

Figure 4.36 illustrate that (a) Pd/Carbon-paper and (b) Pt/Carbon-paper, follows the direct four electron path-way for ORR at different potentials. This phenomenon was also observed by *Mkwizu et al* [155] for the reaction path of different catalysts and in the case of monometallic Pt nanoclusters, the four-electron direct reduction of O_2 to water (H_2O) occurred.

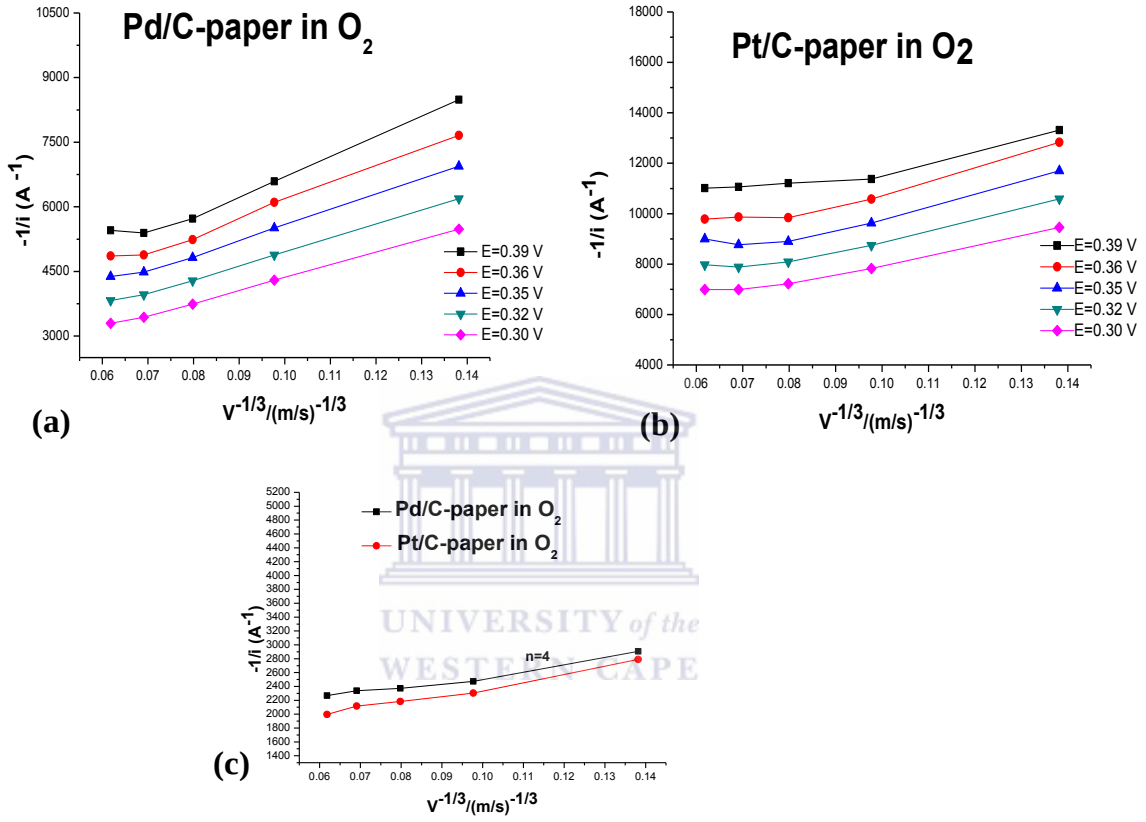

Figure 4.36: K-L plots of 1/i versus $1/v^{-1/3}$ for (a) Pd/Carbon-paper and (b) Pt/Carbon-paper, generated from LSV's recorded on 0.1M $HClO_4$ in different potentials (0.39V, 0.36V, 0.35V, 0.32V, 0.30V) respectively and (c) the K-L plot for 4-electron direction.

Figure 4.37 presents the K-L plots of Pd8Pt8/Carbon and Pt8Pd8/Carbon. The difference between the catalytic activities Pt8Pd8/Carbon-paper and Pd8Pt8/Carbon-paper (1:1) is shown in figures 4.37 (a), (b) and (c). The performance of Pd8Pd8/Carbon-paper in breaking the O_2 bonds to H_2O is better compared to Pd8Pt8/Carbon-paper. This suggests that Pd8Pt8/Carbon-paper and Pt8Pd8/Carbon-paper can used as a two-electron direct catalyst, which lowers the activity of hydrogen peroxide(H_2O_2) direct to H_2O [175, 176].

However CV and LSV confirmed the weak activity of Pd8Pt8/Carbon-paper and Pt8Pd8/Carbon-paper.

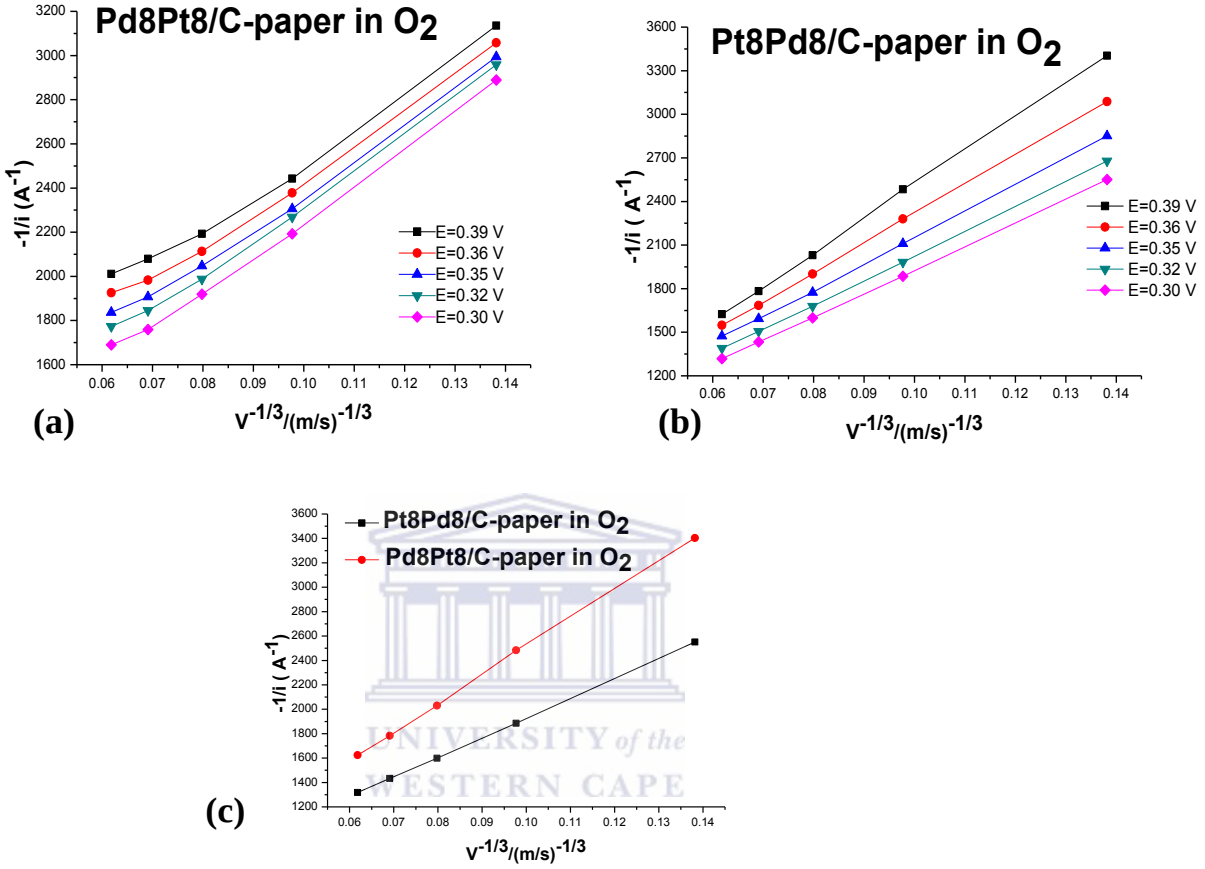

Figure 4.37: K-L plots of 1/i versus $1/v^{-1/3}$ for (a) Pd8Pt8/Carbon-paper and (b) Pt8Pd8/Carbon-paper, generated from LSV's recorded in 0.1 M $HClO_4$ in different potentials (0.39V, 0.36V, 0.35V, 0.32V, 0.30V) and (c) the K-L plot for 4-electron direction.

The figure 4.38 presents the K-L plots of 1:1, Pd-Pt and Pt-Pd/C at 16 cycles. The Pt16Pd16/Carbon-paper follows the 4-electron direct reduction of O_2 to H_2O as described in [155], whilst Pd16Pt16/Carbon-paper shows the catalytic activity of a 2-electron direct reduction of O_2 to H_2O_2. The CV and LSV of Pd16Pt16/Carbon-paper also showed less ORR activity and HRSEM confirmed a lot of particle agglomeration [166].

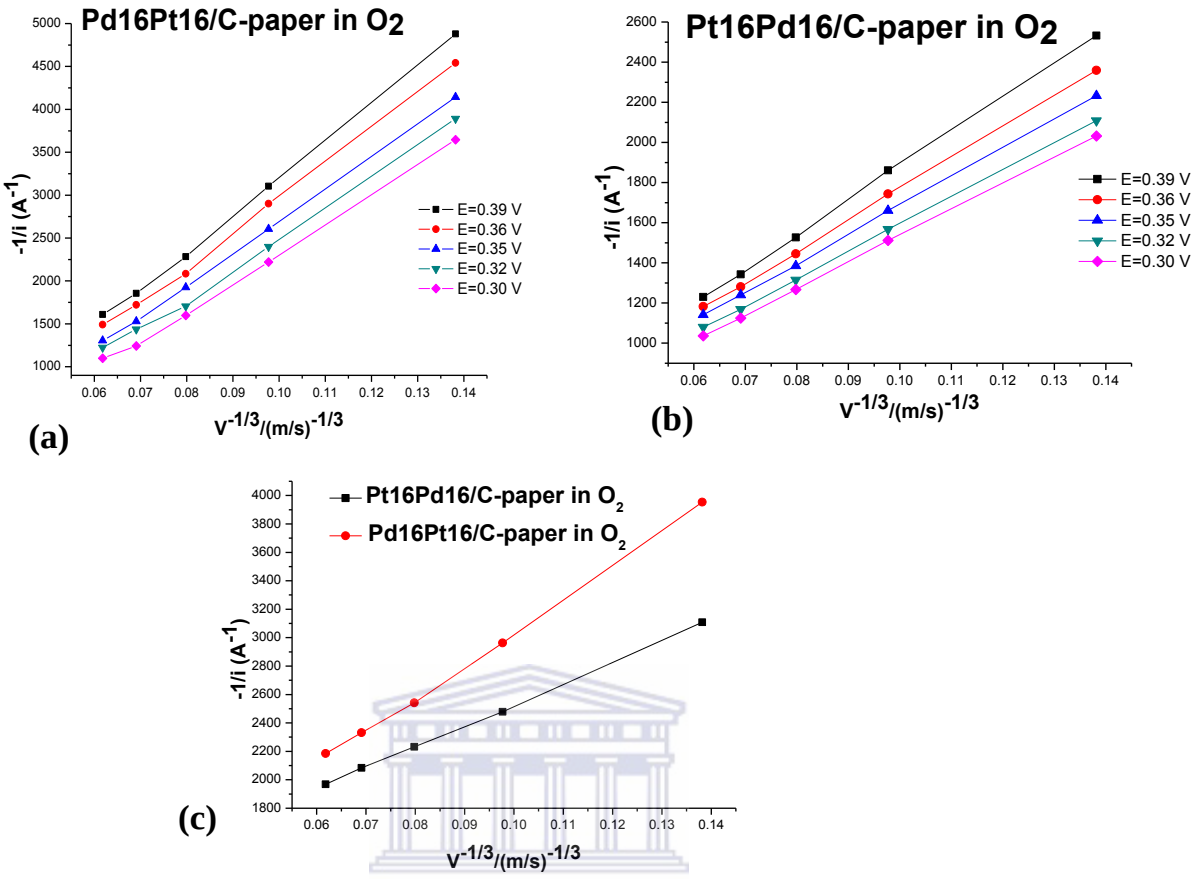

Figure 4.38: K-L plots of 1/i versus $1/v^{-1/3}$ for (a) Pd16Pt16/Carbon-paper and (b) Pt16Pd16/Carbon-paper, generated from LSV's recorded on 0.1 M $HClO_4$ in different potentials (0.39V, 0.36V, 0.35V, 0.32V, 0.30V) and (c) the K-L plot for 4-electron direction.

Figure 4.39 presents the difference between the K-L plots of 1:1, Pd-Pt and Pt-Pd. The K-L plot of Pt24Pd24/Carbon-paper is more likely the same as the K-L Plot of Pt/Carbon-paper, Pd/C-paper (figure 4.32) and Pt/Carbon described *Mkhwizu et al* and *Zhang et al* [155 & [177]. This implies that the reaction occurring in Pt24Pd24/Carbon-paper follows the four-electron transfer pathway. The reaction occurring in Pd24Pt24/Carbon-paper catalyst is a two-electron transfer pathway, which is not a good cathode catalyst as it follows the electro-reduction of oxygen to hydrogen peroxide that can lead to a low efficiency and corrosion. This may be attributed to the agglomeration of the particles that are observed by HRSEM.

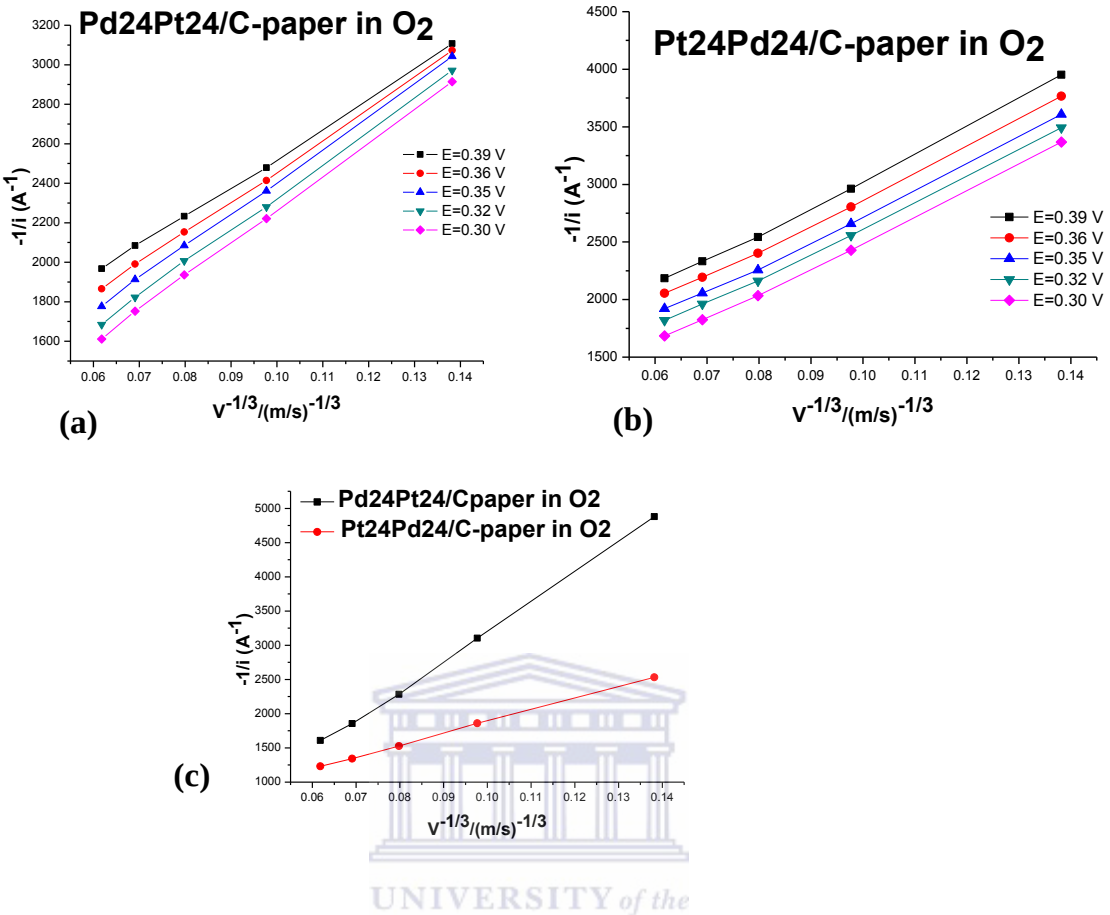

Figure 4.39: K-L plots of 1/i versus $1/v^{-1/3}$ for (a) Pd24Pt24/Carbon-paper and (b) Pt24Pd24/Carbon-paper, generated from LSV's recorded on 0.1 $HClO_4$ in different potentials (0.39V, 0.36V, 0.35V, 0.32V, 0.30V) and (c) the K-L plot for 4-electron direction.

The different performance of the two codeposition are shown in figure 4.40 above, as to which catalyst follow the 4-electrode reduction of O_2 to water and 2-electrode reduction of O_2 to peroxide. As it can be seen from figure 4.40 (c) Pd24Pt24codeposition/Carbon-paper appears to follow the 4-electron reduction of O_2 to water, which is the preferred ORR reaction. The performance of Pd16Pt16codeposition/C-carbon paper is surpassed by that of Pd24Pt24codeposition/Carbon-paper. This implies that Pd24Pt24 codeposition/Carbon-paper is the better ORR catalyst.

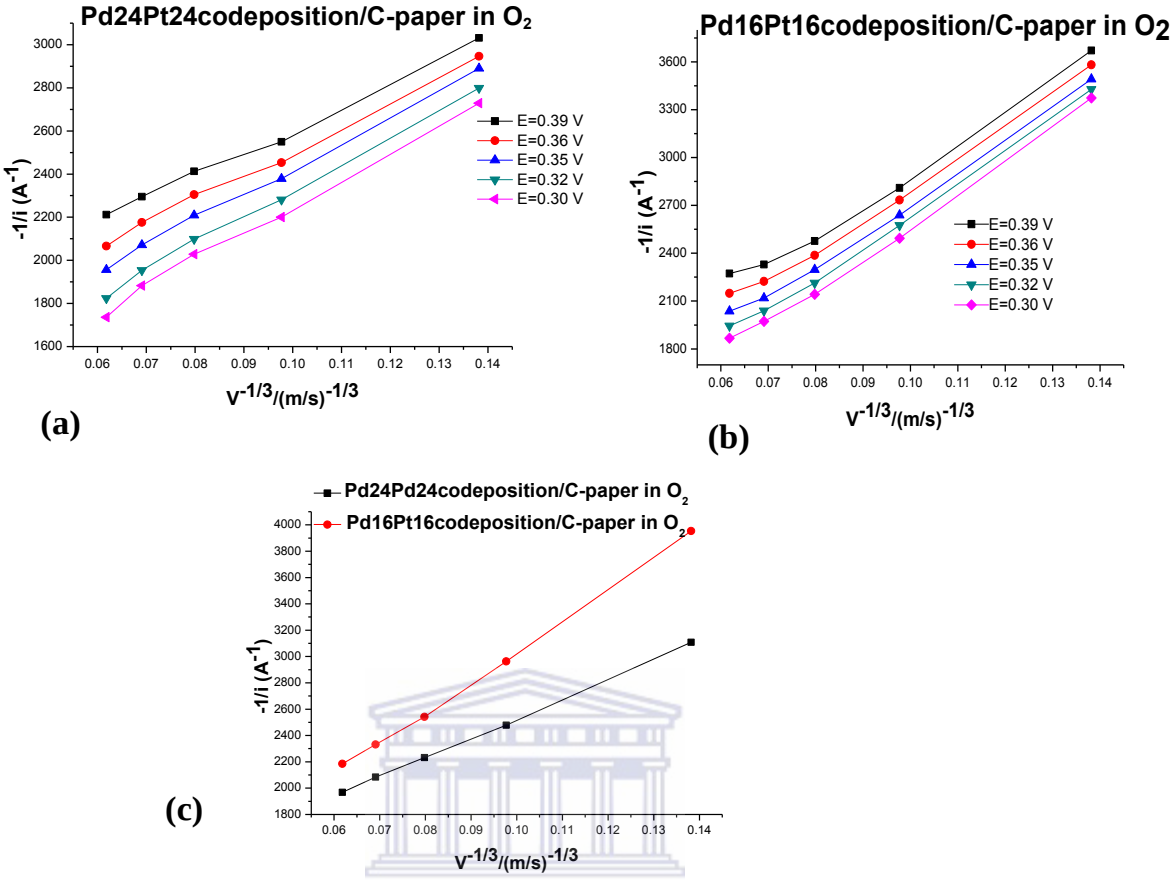

Figure 4.40: K-L plots of 1/i versus $1/v^{-1/3}$ for (a) Pd24Pt24codeposition/Carbon-paper and (b) Pt16Pd16codeposition/Carbon-paper, generated from LSV's recorded on 0.1 $HClO_4$ in different potentials (0.39V, 0.36V, 0.35V, 0.32V, 0.30V) and (c) the K-L plot for 4-electron direction.

The K-L plot of Pd24Pt16/Carbon-paper and Pd16Pt8/Carbon-paper shows parallel linear plots that suggest the similar activity of these two catalysts in reducing O_2 bonds to H_2O [177]. However, the CV and LSV (ECSA, onset potential and current density) of Pd24Pt16/Carbon-paper in O_2 saturation shows better catalytic activity due to multiple deposition cycles than Pd16Pt8/Carbon-paper.

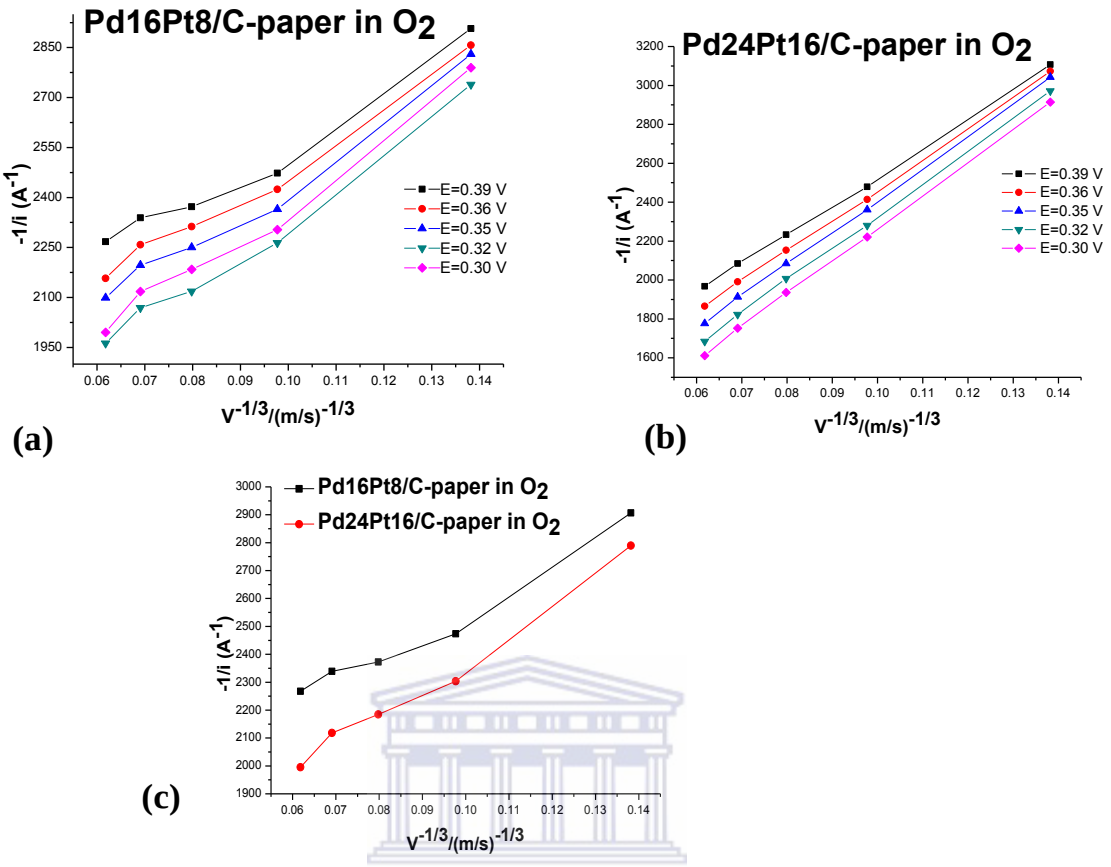

Figure 4.41: K-L plots of 1/i versus $1/v^{-1/3}$ for (a) Pd16Pt8/Carbon-paper and (b) Pd24Pt16/Carbon-paper, generated from LSV's recorded on 0.1 $HClO_4$ in different potentials (0.39V, 0.36V, 0.35V, 0.32V, 0.30V) and (c) the K-L plot for 4-electron direction.

CHAPTER 5
CONCLUSION AND RECOMMENDATIONS

5.1 Conclusion

Pd, Pt and Pd based binary catalyst were deposited on carbon paper substrate via surface limited redox replacement reaction (SLRR) of Cu overpotential deposition (OPD). The deposition of Cu was optimized to 90s. The deposition cycle of 8 was used for Pt/C-paper and Pd/C-paper. Multiples of eight in different ratios (1:1, 2:1, and 3:1) were used to deposit Pt: Pd binary catalyst. The CV, LSV and K-L plots of Pt24Pd24/C-paper catalyst showed a comparative ORR activity with the Pt/C in 0.1 M $HClO_4$ electrolyte. Moreover, the Pd:Pt/C-paper catalysts showed weak ORR activities in the presence of methanol in acid medium, Pt:Pd/C-paper catalyst exhibits much higher ORR activity. The high methanol tolerance of the Pt24Pd24/C-paper catalysts during the ORR can be explained by the low activity for methanol oxidation, which could originate from the composition effect, from the presence of Pd atoms and from the formation of Pd-based alloys. SEM and HRSEM confirmed the narrower distribution and particle size of Pt24Pd24/C-paper. The use of a complexing agent (Cl^-) reduced the exchange rate of Pd for Cu relative to the rate of Pd^{2+} ions solution that was introduced into the cell. Slowing down the exchange rate of Pd^{2+} ions improved the film uniformity through the deposit.

5.2 Recommendations for further work

Although this work may be considered as successful, it still leaves a scope for further investigation. Some of the recommendations for future research include:

- Development of Ternary catalysts

- Best performing ORR and best tolerant deposit on carbon paper modified with microporous (carbon black and PtFe) for MEA fabrication.

References

1. C.A. Amann, *Technical Options for Energy Conservation and Controlling Environmental Impact in Highway Vehicles*, Energy and the Environment in the 21st Century, Massachusetts Institute of Technology, (1990): p. 41-60.

2. P.H. Abelson, *J.Science*, **247**, (1990): p.1529.

3. G. Hoogers, Editor, *Fuel Cell Technology Handbook*, CRC Press, Boca Raton, FL, **5**.(2003):p.8.

4. J. Larminie, A. Dicks, *Fuel cell system explained 2nd Edition*, John Wiley, New York. **23,** (2003): p.14-20.

5. P.Pillay, *Hydrogen Economy and alternative fuels*, originally published on the IEEE Emerging Technology portal, (2006-2012). *http://www.ieee.org/go/emergingtech.*

6. C. Rayment and S. Sherwin, *Introduction to fuel cell* University of Norte Dame, Notre Dame, IN 46556, USA. **14,** (2003): p. 12-13.

7. P. Costamagna, S. Srinivasan, *J. Power Sources*. **102**, (2001): p.242-252.

8. S.Wasmus, A. Kuver, *J.Electroanal.Chem*.**461**, (1999): p. 14-31.

9. E. Antolini, *J. Power Sources*. **170**, (2007): p.1-12.

10. *Advantages and benefits of hydrogen and fuel cell technologies*, Fuel cell Markets. (2002-2012). www.fuelcellmarkets.com/fuel_cell_markets/5, 1, 1,663.html.

11. R. W. Reeve, P. A. Christensen, A. J. Dickinson, A. Hamnett, and K. Scott, *Electrochem Acta*. **45**, (2000):p. 4237-4250.

12. H. Cheng, W. Yuan, and K. Scott, *Electrochem Acta.* **52**, (2006): p.466-473.

13. M. Hilgendorff, K. Diesner, H. Schulenburg, P. Bogdanoff, M.Bron, and S. Fiechter, *J. Materials for Electrochem Syst*. **5**, (2002):p.71-81.

14. H. Schulenburg, M. Hilgendorff, I. Dorbandt, *J.Power Sources*. **155**, (2006):p.47-51.

15. A. Heinzela, V. M. Barrag, *J. Power Sources*, **84**, (1999):p.70-74.

16. C. Pu, W. Huang, K. L. Ley and E. S. Smotkin, *J. Electrochem Soc.* **142**, (1995):p.19-20.

17. D.M. Dobkin and M.K. Zuraw, *Kluwer Academic Publishers*. **13**, (2003): p.288.

18. R. Fischer, *J Materials Science*. **9,** (2005): p.214.

19. Li, Zhengwen, Rahtu, Antti; Roy. G .Gordon, *J Electrochem Soc.* **153** (2006): P.787-794.

20. S.K. Young's, *Material Matters*. **1**, (2006): p. 29-47.

21 R.S. Khurmi and R.S. Sedha, *Material Science. 4th Ed,* (2008): p. 18.

22. W.Z. Nerst, *J. Electrochem*. **6**, (1899): p.41-43.

23. E. Baur, H.Z. Preis, *J. Electrochem*. **43** (1937): p.727-32.

24. W.R. Grove, *Philosophical magazine and journal of science*. **101**, (1842): p.417-420.

25. Energy Efficiency and Renewable Energy: *Fuel Cell Technologies Program*. http://www1.eere.energy.gov/hydrogenandfuelcells.

26. World energy council. *Survey of energy resources 18th Ed*. London. (1998).

27. International energy agency (IEA) *J.Transport Economics and Policy*. **31**, (1997):277-292.

28. Fuel Cells 2000, Fuel Cell Basics. www.fuel cell.org/basics/types.

29. B. Walsh and R. Wichet, *National Institute of Building Sciences*. (2010.).www.climatetechwiki.org.

30. R. L. Busby, *Hydrogen and fuel cells-A comprehensive guide*. **37**, (2005): p.100.

31. F. Barbir, M. Nadal, M. Fuchs, *Fuel Cell Powered Utility Vehicles*, proc. Portable Fuel Cell Conference, **20**, (1999): p.113-126.

32. A.B. Stambouli and E. Traversa, *Renewable and Sustainable Energy Reviews*. **6**, (2002): p.433-455.

33. H. Bonnemann, R.M. Richards, *Eur. J. Inorg. Chem*. **10**, (2001): p.2455.

34 A. Roucoux, J. Schulz, H. Patin, *Chem. Rev*. **102**, (2002): p.3757.

35. A. Verma, S. Basu, *J.Power Sources*. **174**, (2007): p180–185.

36. K. Kordesch, V. Hacker, J. Gsellmann, M. Cifrain, G. Faleschini, P. Enzinger, R. Fankhauser, M. Ortner, M. Muhr, Robert R. Aronson. *J. Power Sources*. **86**, (2000): p.162–165.

37. V. H. Ramani, K. Russell and J.M. Fenton, Electrochem Acta, **47**, (2002): p.77.

38. K. Kordesch, J. Gsellmann, , M. Cifrain, S. Voss, V. Hacker, R.R. Aronson, C. Fabjan, T. Hejze, , J. Daniel-Ivad, *J.Power Sources*, **80**, (1999): p.190-197.

39. K. Kordesch, V. Hacker, J. Gsellmann, P. Enzinger, M. Cifrain, R. Aronson, G. Faleschini, M. Muhr, K. Friedrich, *J.Power Sources*, **86**, (2000): p. 163-166.

40. A.J. Appleby, F.R. Folkes, *Fuel cell handbook*, Van Nostrand Reinhold, New York, (1989): p. 264.

41. Johnsson-Matthey, *ETSU Direct Methanol Fuel Cell Review*, Tech. rep.UK Department of Trade & Industry. (1995)

42. M. Winter, R. J. Brodd, *Chemical Reviews*. **104,** (2004): p.4245–4269.

43. J. R. Varcoe, R. C. T. Slade, *Fuel Cells*. **5**, (2005): p.187–200.

44. P. K. Shen, C. Xu, Adv. *Fuel Cells*. **5**, (2005): p.149–179.

45. E. Agel, J. Bouet, *J.Power Sources*. **101**, (2001): p.267–274.

46. J. Zhang, *PEM fuel cell electrocatalysts and catalyst layers-Fundamentals and applications*. **20**, (2008): p.50.

47 M. Wilson, S. Gottesfeld, *J. Appl. Electrochem*. **22**, (1992): p.1-7.

48 A. Appleby, F. Foulkes, *Fuel cell handbook*, Van Nostrand Reinhold, New York. **3**, (1989): p.762.

49. J.E. Larminie, A. Dicks, *Fuel Cell Systems Explained. 2nd Ed.* John Willey **37**, (2000): p. 428.

50 F. Maillard, G. Lu, A. Wieckowski and U. Stimming, *J. Phys Chem*. **B 109**, (2005): p.16230-16243.

51. M. Cell, MCEL. Technology/Technology advantages. *J. Material Science*. **181**, (2005):p.547.

52. Johnsson-Matthey, ETSU *Direct Methanol Fuel Cell Review*, Tech. rep.UK Department of Trade & Industry. **12**, (1995):p.455.

53. K. Ley, R. Liu, C. Pu, Q. Fan, N. Leyarovska, C. Segre and E. Smotkin, *Electrochem. Acta*. **144**, (1997): p.1543-1548.

54. D. Lee, S. Hwang and I. Lee, *J.Power Sources*. **145**, (2005): p.147-153.

55. Natural gas and technology, *Natural.org*. (2004-2011). www.naturalgas.org/environment/technology.asp

56. N. Munichandraiah, K. McGrath, G.K. Prakash, S. Aniszfeld, R. George and A. Olah, *J.Power Sources*. **117**, (2003):p.98–101.

57. L. Zhang, J. Zhang, DP. Wilkinson, H. Wang, *J. Power Sources*. **156**, (2006):p.171–82.

58. C. Song, Y. Tang, J. Zhang, J. Zhang, H. Wang, J. Shen, *Electrochem Acta*. **52**, (2007): p.2552–2561.

59. A. Damjanovic, *J Electroanal Chem*. **355**, (1993): p.57–77.

60. V.P. Zhdanov, B. Kasemo, *Electrochem Commun*. **8**, (2006): p.1132–6.

61. J.K. Norskov, J. Rossmeisl, A. Logadotir, L. Lindqvist, J.R. Kitchin, T. Bligaard, *J Phys Chem*. **108**, (2004): p.86–92.

62. Z. Shi, J. Zhang, Z. Liu, H. Wang, D.P .Wilkinson, *Electrochim Acta*. **51**, (2006): p.1905–16.

63. E.V. Anslyn and D.A. Dougherty, *Modern Physical organic chemistry*. **490**, (2006):p. 612.

64. A. Fullick and P. Fullick. *Chemistry for AQA.* ISBN 0 435 583913 (2001): p.9.3.

65. H. Knözinger and K. Kochloefl, Hetergeneous Catalysis and Solid Catalysts, in *Ullmann's Encyclopedia of Industrial Chemistry*, 6th Edn., Wiley-VCH Verlag GmbH & Co KGaA, Weinheim, Germany, **17**, (2002):p.5-13.

66. J. K. Nørskov, J. Rossmeisl, A. Logadottir, L. Lindqvist, J. R. Kitchin, T. Bligaard and H. Jónsson, *J. Phys. Chem*. **108**, (2004): p.17886.

67. R. Borup, J. Meyers, B. Pivovar, Y. S. Kim, R. Mukundan, N. Garland, D. Myers, M. Wilson, F. Garzon, D. Wood, P. Zelenay, K. More, K. Stroh, T. Zawodzinski, J. Boncella,

J. E. McGrath, M. Inaba, K. Miyatake, M. Hori, K. Ota, Z. Ogumi, S. Miyata, A. Nishikata, Z. Siroma, Y. Uchimoto, K. Yasuda, K.-i. Kimijima and N. Iwashita, *Chem. Rev*. **107**, (2007): p.3904.

68. M. Pourbaix, *Atlas of Electrochemical Equilibria in Aqueous Solutions, 2nd Ed*. . John Wiley, New. York, (1974): P. 392.

69. K. Kinoshita and Electrochemical Society, *J. Electrochem Soc*, **431** (1992): p.431.

70. K. Lee, O. Savadogo, A. Ishihara, S. Mitsushima, N. Kamiya, and K. I. Ota, *J. Electrochem Soc*. **153**, (2006): p. 20–24.

71. H. Cheng, W. Yuan, and K. Scott, *Electrochem Acta*. **52**, (2006): p. 466– 473.

72. M. Hilgendorff, K. Diesner, H. Schulenburg, P. Bogdanoff, M. Bron, and S. Fiechter, *J. New Materials for Electrochem Syst* **5**, (2002):p.71–81.

73. H. Schulenburg, M. Hilgendorff, I. Dorbandt, *J.Power Sources*. **155**, (2006): p.47–51.

74. F. Maillard, M. Martin, F. Gloaguen, J. M. Leger, *Electrochem Acta*. **47**, (2002): p.3431.

75. A. K. Shukla, R. K. Raman, N. A. Choundhuri, K. R. Priolkar, P. R. Serode, S. Emura, R. Kumashiro, *J.Electroanal chem*. **563**, (2004): p.181.

76. J. Zhang, J *Electroanal Chem* **611,** (2010):p.87–95.

77. A. Tsivadze, M. R. Tarasevich, V. A. Bogdanovskaya, L. N. Kuznetsova, N. K. Modestov, A. D. Doklady, *J. Chemistry*. **410**, (2006): p.154-157.

78. I.E. Santiago, C.L. Varanda, and H. Mercedes Villullas, *J. Phys. Chem*. **111**, (2007): p.3146-3151.

79. S. Song, Y. Wang, P. Tsiakaras, P.K. Shen, *Appl. Catal*. **78**, (2008): p 381.

80. R. W. Reeve, P. A. Christensen, A. J. Dickinson, A. Hamnett, and K. Scott, *Electrochem Acta*. **45**, (2000): p.4237–4250.

81. H. Cheng, W. Yuan, and K. Scott, *Electrochem Acta*. **52**, (2006): p.466–473.

82. M. Hilgendorff, K. Diesner, H. Schulenburg, P. Bogdanoff, M. Bron, and S. Fiechter, *Journal of New Materials for Electrochemical Systems*. **5**, (2002): p.71–81.

83. W.E. Mustain, K. Kepler, J. Prakash, *Electrochem. Commun*. **8**, (2006): p.406.

84. W. Wang, G. Huang, J. Liu, Z. Zou, Z. Li, H. Yang, *Electrochem Commun*. **10**, (2008); p.1396.

85. Jong-Ho Choi, Kyung-Won Park, In-Su Park, Woo-Hyun Nam, Yung-Eun Sung *Electrochimica Acta*. **50**, (2004): p.787–790.

86. L. B. Sheridan, J. Czerwiniski; N. Jayaraju, D. K. Gebregziabiher, J. L. Stickney, D. B. Robinson, M. P. Soriaga, *J. Electrochem Soc*. **3**, (2012): p.96−107.

87. C. Gebregziabiher, D. K. Liang, X. H. Zhang, Q. H. Ivanova, V. Haumesser, P. H. Stickney, *J. Electrochem. Soc.* **157**, (2010): p.466−471.

88. V. Bambagioni, C. Bianchini, A. Marchionni, J. Filippi, F. Vizza, J. Teddy, P. Serp, M. Zhiani, *J. Power Sourc*. **190**, (2009); p.241-251.

89. C. Bianchini, P.K. Shen, *Chem. Rev*. **109**, (2009): p.4183-4206.

90. Y.-. Lee, S.-. Han, K.-. Park, *Electrochem. Commun*. **11**, (2009): p.1968-1971.

91. R. Pattabiraman, *J.Appl. electrochem: General*. **153**, (1997): p.9-20.

92. W. Zhang, P. Sherrell, A.I. Minett, J.M. Razal, *J. Chen, Energy Environ. Sci.* **3**, (2010); p.1286-1293.

93. C.E. Banks, R.G. Compton, *Analyst.* **131**, (2006): p.15-21.

94. E. Antolini and E. R. Gonzalez, *Solid State Ionics*. **180**, (2009): p.745-769.

95. Y. Takasu, T. Kawaguchi, W. Sugimito, Y. Murakami, *Electrochim. Acta*. **48**, (2003): p.3861.

96. A.S. Arico, S. Srinivasan and V. Antonucci, *J. new material for elecrochem Syst*. **2**, (2001): p.133.

97 P. V. Shanahana, L. Xua, C. Liang, M. Waje, S. Daic, Y.S. Yan, *J.Power Sources*. **185**, (2008): p.423–427.

98. G. Wu, L. Li, J.H. Li, B.Q. Xu, *J. new material for elecrochem Syst*. **43**, (2005): p.2579.

99. M. Uchida, Y. Fukuoka, Y. Sugawara, H. Ohara, A. Ohta, *J. Electrochem. Soc*. **145**, (1998): p.3708.

100. M.L. Anderson, R.M. Stroud, D.R. Rolison, *J.electrochem Soc* **2**, (2002): p.235.

101. M. Mastragostino, A. Mossiroli, F. Soavi, *J. Electrochem. Soc*. **151**, (2004): p.1919.

102. Y.H. Pai, J.H. Ke, C.C. Chou, J.J. Lin,J.M. Zen, F.S. Shieu, *J. Power source*. **163** (2006): p. 398-402

103. Foley M. A practical guide to understanding Carbon nanotubes, Production Methods, Markets and Utilities. **4,** (2006): p.1.

104. Hirsch, Angewandte, Ch*emistry*. **114,** (2002): p.1933-1939.

105 A.J. Zarbin, J.*Material Research*. **30**, (2007): p 1469-1479.

106 H. Nalwa (Ed), *Nanostructured Materials and Nanotechnology, Concise Edition ed*. Academic Press, San Diego, (2002):p.970.

107. A.Y. Kasumov, H. Bouchiat, B. Reulet, O. Stephan, I.I. Khodos, Y.B. Gorbatov, C. Colliex, *Europhys. Lett*, **43**, (1998): p 89-94.

108. D. Chu, J. Wang, S. Wang, L. Zha, J. He, Y. Hou, Y. Yan, H. Lin, Z. Tian, *Catal. Commun*, **10**, (2009): p 955-958.

109. S. Yin, P.K. Shen, S. Song, S.P. Jiang, *Electrochim. Acta*. **54**, (2009): p 6954-6958.

110. M.P. Siswana, K.I. Ozoemena, T. Nyokong, *Electrochem. Acta*. **52**, (2006): p 114-122.

111. Z.Q. Tian, Y.M. Liang, P.K. Shens, *J. Phys. Chem*. **110**, (2006): p 5343-5350.

112. Z. Sun, X. Zhang, Y. Liang, H. Li, *J. Power Sources*, **191** (2009):p. 366-370.

113. T. Kim, H. K. Lee, and J. Shim, *J.Nanosci and Nanotech*. **8**, (2008): p. 5302–5305.

114. B.R. Pamplin, *Progress in Crystal Growth and Characterization of Materials*, **1**, (1979): p 395.

115. R. Castellano, *Solar Panel Processing hand book,* Philadelphia, USA, (2010): p 50.

116. T. Teranishi, M. Hosoe, T. Tanaka and M. Mayaka, *J. Phys. Chem.* **103**, (1999): p.3818.

117. H.B. Suffredini, V. Tricoli, L.A. Avaca, N. Vatistas, *Electrochem Commun*. **6**, (2004): p 1025-1028

118. Hu. Linjie, K. A. Boateng, J. M. Hill, *J.Mol Catalysis A: Chemical*. **259**, (2006): p 51-60.

119. M.L. Calegaro, H.B. Suffredini, S.A.S. Machado, L.A. Avaca, *J.Power Sources.* **156**, (2006): p 300–305.

120. M. Wilson and S. Gottesfeld, *J. Appl. Electrochem*. **22**, (1992): p.7.

121. Y. Takasu, T. Fujiwara and Y. Murakami, *J. Electrochem. Soc*. **147**, (2000): p.421.

122. A.J. Dickinson, L.P.L. Carrette, J.A. Collins, K.A. Friedrich, U. Stimming, *Electrochem.Acta*. **47**, (2002): p.3733.

123. K.A. Friedrich, K.P. Geyzers, A.J. Dickinson, U. Stimming, *J. Electroanal. Chem.* **261**, (2002): p.524–525.

124. H. Li, Q. Xin, W. Li et al, *Chem Commun*. **23**, (2004): p 2776–2777.

125. J.I. B. Joo, Y. J. Kim, W. Kim et al, *Korean J.Chemical Engineering*. **25**, (2008): p. 770–774.

126. C. F Powell, J. H. Oxley, Jr. J. M. Blocher. *High temperature vapors handkook*, Wiley, New York, *J.Sci*, (1967):p.191.

127. W. D. Westwood, *Sputter Deposition;* AVS Education Committee book series, New York: Education Committee, **2** (2003): p.3-5.

128. D. M. Mattox, *Handbook of Physical Vapor Deposition (PVD) Processing*, Noyes Publications, New Jersey, (1998), p. 482.

129. L. George, E. Trigg, H. Immergut, *Encyclopedia of Applied Physics – EAP,* **23**. (1997): p.428.

130. U. Helmersson; M. Lattemann, J. Bohlmark, A. P. Ehiasarian, J. T. Gudmundsson, *Thin Solid Films*. **1**, (2006): p 513.

131. S, Donald, *Thin-Film Deposition: Principles and Practice*. MacGraw-Hill. New York. **1**. (1995): P. 15-129.

132. M. Dobkin and K. Zuraw. *Principles of chemical vapor Book*. (2003): 273.

133. K. Okada, *J. Adv. Mater*. **8**, (2007): p 624.

134. C. Wild, CVD Diamond Properties and Useful Formula CVD Diamond Booklet (2008). www.diamond-materials.com/download.

135. T. Aaltonen, Ph.D. thesis, University of Helsinki, Finland. Available from (2005) http://ethesis.helsinki.fi/en/.

136. B. W Gregory, M. L Norton, J. L Stickney, *J Electroanal Chem*. **293**, (1990): p 85–101.

137. B.W Gregory, J.L Stickney, *J Electroanal Chem*. **300**, (1991): p 543–561.

138. D.M Kolb *Advances in electrochemistry and electrochemical engineering Tobias, Eds*. John Wiley, New York. **11**, (1978): p 125.

139. J. L Stickney, S.D Rosasco, D Song, M.P Soriaga, A.T Hubbard. *Surf Sci*. **130**, (1983): p 326–347.

140. E. Antolini, *J.Power Sources*. **170**, (2007) 1-12.

141. L. P. Colletti, Jr. B. H Flowers, J. L. Stickney, *Journal of the Electrochemical Society*, **145**, (1998): p.1442-1449.

142. B. H. Jr. Flowers, T. L. Wade, J. W. Garvey, M. Lay, U. Happek, and J. L. Stickney, *J.Electroanal Chem*, (2002): p. 524-525.

143. D. McMullan, *Europian Physical Journal*.**175**, (2006): p. 1928–1965.

144. D. McMullan, An improved scanning electron microscope for opaque specimens. J. *Electronics Control*, **7**. (1953):p.97.

145. C. W Oatley, W.C Nixon, Pease RFW Scanning electron microscopy. *Adv. Electronics Electron Phys.* **21**, (1965) 181–247.

146. Smith KCA, Oatley, CW. The scanning electron microscope and its fields of application. *British Journal of Applied Physics*. **6**, (1955): p 391.

147. Ahmed, H. and, Beck, A.H.W. Thermionic emission from dispenser cathodes. *J. Appl. Phys*. **34**. (1963):p. 997-998.

148. E. Suzuki. *J. Microscopy*. **208**, (2002): p.153–157.

149. P.S. Kounaves, Voltammetric techniques In: Settle FA, (Ed), *Handbook of instrumental techniques for analytical chemistry, illustrated ed*, (1997): p 712-713.

150. A. Huxley, K S. Cole, Bio graphical Memoirs, *National Academy of Science, Washington*, DC, **4**,(1996): p 3.

151. A. J. Bard and L. R. Faulkner, Electrochemical Methods, 2nd ed., *J. Wiley*, New York, (2000):p.448.

152. A.J. Bard, L.R. Faulkner, Electrochemical methods: fundamentals and applications. New York: *Wiley*, (1980). 67.

153. Khurmi and R.S. sedha, Material Science, Ed. *4*, ISBN 8121901464. (*2008*): *p*. 18.

154. A. koichi, T.koichi, M. hiroaki, *Electroanal. Chem*, **146** (1983): p 417-424.

155. T.S. Mkwizu, M.K. Mathe, and I. Cukrowski, *Langmuir*. **26**, (2010): p 570.

156. Remegia M. Modibedi, Mkhulu K. Mathe, Rapelang G. Motsoeneng, Lindiwe E. Khotseng, Kenneth I. Ozoemena, Eldah K. Louw, *Electrochimica Acta*. **128**, (2014): p 406-411.

157. T.S Mkwizu, M.K Mathe, I. Cukrowski, *Langmuir*. **26**, (2010):p. 570-580.

158. M. W. Breiter, *Journal of Electroanalytical Chemistry*, **81**, (1977): p 275–284.

159. T. Mall´at, E. Poly´anszky, and J. Petr ´ o, *Journal of Catalysis*, **44**, (1976): p. 345–351.

160. Modibedi, R. M.; Masombuka, T.; Mathe, M. K. *Int. J. Hydrogen Energy*. **36**, (2011):p.4664–4672.

161. A. A. Michri, A. G. Pshchenicknikov, R. Kh. Burshtein, *Electrochim Acta* **8**, (1972): p 364–366.

162. T. Chierchie, C. Mayer, W. J Lorenz, *J. Electroanal. Chem*. **135**, (1982): p 211–220.

163. Remegia M. Modibedi, Eldah K. Louw, Kenneth I. Ozoemena, Mkhulu K. Mathe, *ECS Transactions*. **50**, (2013): p 9.

164.4 J. L. Stickney, Y.G. Kim, J. Y. Kim, D. Vairavapandian, *J.Phys Chem*. **110**, (2006):p 17998-18006.

165. Y. Kim, J. Kim, D. Vairavapandia, J. Stickney, *J.Phys Chem*. **110**, (2006): p 17998-18006.

166. G. F. Álvarez, M. Mamlouk, and K. Scott, *Int. J Electrochem.* **2011**, (2011): p 12.

167. R.S. Jayashree a, J.S. Spendelowa, J. Yeomb, C. Rastogi a, M.A. Shannon b, P.J.A. Kenis, *Electrochem Acta.* **50**, (2005): p 4674–4682.

168. W. Wenming, H. Qinghong, L. Juanyin, Zhiqing, Z. L Zhilin, Y. Hui, *Electrochem commun*. **10**, (2008): p 1396.

169.170 T.Y Jeon, K.S Lee, S. J Yoo, Y.H Cho, S.H Kang, Y.E Sung, *Langmuir*. **26**, (2010): p 91239.

170. M. Watanabe, S. Motoo, *J.Electroanal.Chem*. **60**, (1975): p 259.

171. H. Wang, L.R Alden, F. J DiSalvo, Abrun˜ a HcD, *Langmuir*. **25**, (2009): p 7725.

172. W. Xing, G. Yin, J. Zhang, *Rotating Electrode Methods and Oxygen Reduction Electrocatalysts*. (2014): p. 86.

173. S.C Chang L.W.H Leung and M.J Weaver, *J. Phys*. Chem. **94**, (1990): p 6013.

174. G. Andreadis, P. Tsiakaras, *Chem Eng Sci*. **61**, (2006): p 7497.

175. Van Brussel, M. Kokkinidis, G. Vandendael, I. Buess-Herman, C. *Electrochem. Commun.*, **4**, (2002): p 808.

176. J.-W. Lee, B. N. Popov, *J. Solid State Electrochem*. **11**, (2007): p 1355.

177. L. Zhang, C. Song, J. Zhang, H. Wang, D.P. Wilkinson, *J Electrochem Soc*.**152**, (2005): p 2421.